SIAM J. Applied Dynamical Systems
Vol. 10, No. 1, pp. 278–324

The Frequency Map for Billiards inside Ellipsoids*

Pablo S. Casas† and Rafael Ramírez-Ros†

Abstract. The billiard motion inside an ellipsoid $Q \subset \mathbb{R}^{n+1}$ is completely integrable. Its phase space is a symplectic manifold of dimension $2n$, which is mostly foliated with Liouville tori of dimension n. The motion on each Liouville torus becomes just a parallel translation with some frequency ω that varies with the torus. Further, any billiard trajectory inside Q is tangent to n caustics $Q_{\lambda_1}, \ldots, Q_{\lambda_n}$, so the caustic parameters $\lambda = (\lambda_1, \ldots, \lambda_n)$ are integrals of the billiard map. The frequency map $\lambda \mapsto \omega$ is a key tool for understanding the structure of periodic billiard trajectories. In principle, it is well-defined only for nonsingular values of the caustic parameters. We present two conjectures, fully supported by numerical experiments. We obtain, from one of the conjectures, some lower bounds on the periods. These bounds depend only on the type of the n caustics. We describe the geometric meaning, domain, and range of ω. The map ω can be continuously extended to singular values of the caustic parameters, although it becomes "exponentially sharp" at some of them. Finally, we study triaxial ellipsoids of $\mathbb{R}^3$. We numerically compute the bifurcation curves in the parameter space on which the Liouville tori with a fixed frequency disappear. We determine which ellipsoids have more periodic trajectories. We check that the previous lower bounds on the periods are optimal, by displaying periodic trajectories with periods four, five, and six whose caustics have the right types. We also give some new insights for ellipses of $\mathbb{R}^2$.

Key words. billiards, integrability, frequency map, periodic orbits, bifurcations

AMS subject classifications. 37J20, 37J35, 37J45, 70H06, 14H99

DOI. 10.1137/10079389X

1. Introduction.

Birkhoff [7] introduced the problem of *convex billiard tables* more than 80 years ago as a way to describe the motion of a free particle inside a closed convex curve such that it reflects at the boundary according to the law "angle of incidence equals angle of reflection." He also realized that this billiard motion can be modeled by an area preserving map defined on an annulus. There exists a tight relation between the invariant curves of this billiard map and the caustics of the billiard trajectories. Caustics are curves with the property that a trajectory, once tangent to one, stays tangent after every reflection. Good starting points in the literature of the billiard problem are [29, 40, 27]. We also refer the reader to [28] for some nice figures of caustics.

When the billiard curve is an ellipse, any billiard trajectory has a caustic. The caustics are the conics confocal to the original ellipse: confocal ellipses, confocal hyperbolas, and the foci. The foci are the singular elements of the family of confocal conics. In this case, the billiard map is integrable in the sense of Liouville, so the annulus is foliated by its invariant

*Received by the editors April 30, 2010; accepted for publication (in revised form) by V. Rom-Kedar January 18, 2011; published electronically March 24, 2011.
http://www.siam.org/journals/siads/10-1/79389.html
†Departament de Matemàtica Aplicada I, Universitat Politècnica de Catalunya, Diagonal 647, 08028 Barcelona, Spain (pablo@casas.upc.edu, Rafael.Ramirez@upc.edu). The first author was supported in part by MCyT-FEDER grant MTM2006-00478 (Spain). The second author was supported in part by MICINN-FEDER grant MTM2009-06973 (Spain) and CUR-DIUE grant 2009SGR859 (Catalonia).

curves, the billiard map becomes just a rigid rotation on its regular invariant curves, and the rotation number varies analytically with the curve.

The billiard dynamics inside an ellipse is known. We stress just three key results related to the search of periodic trajectories. First, Poncelet showed that if a billiard trajectory is periodic, then all the trajectories sharing its caustic conic are also periodic [34]. Second, Cayley gave some algebraic conditions for determining the caustic conics whose trajectories are periodic [9]. Third, the rotation number can be expressed as a quotient of elliptic integrals [32, 41, 44]. We note that the search of periodic trajectories inside an ellipse can be reduced to the search of rational rotation numbers.

A rather natural generalization of this problem is to consider the motion of the particle inside an ellipsoid of $\mathbb{R}^{n+1}$. Then the phase space is no longer an annulus, but a symplectic manifold of dimension $2n$. Many of the previous results have been extended to ellipsoids, although those extensions are far from being trivial. For instance, any billiard trajectory inside an ellipsoid has n caustics, which are quadrics confocal to the original ellipsoid. This situation is fairly exceptional, since quadrics are the only smooth hypersurfaces of $\mathbb{R}^{n+1}$, $n \geq 2$, that can have caustics [6]. Then the billiard map is still completely integrable in the sense of Liouville, the caustics being a geometric manifestation of its integrability. In particular, the phase space is mostly foliated with Liouville tori of dimension n. The motion on each Liouville torus becomes just a parallel translation with some frequency that varies with the torus. Some extensions of the Poncelet theorem can be found in [11, 12, 13, 36]. Several generalized Cayley-like conditions were stated in [15, 16, 17, 18]. Finally, the frequency map can be expressed in terms of hyperelliptic integrals; see [13, 35]. The setup of these last two works is $\mathbb{R}^3$, but their formulae can be effortlessly extended to $\mathbb{R}^{n+1}$.

From Jacobi and Darboux it is known that hyperelliptic functions play a role in the description of the billiard motion inside ellipsoids and the geodesic flow on ellipsoids. Nevertheless, we skip the algebro-geometric approach (the interested reader is referred to [33, 30, 31, 2, 3]) in this paper, in order to emphasize the dynamical point of view. Here, we just mention that the billiard dynamics inside an ellipsoid can be expressed in terms of some Riemann theta-functions associated with a hyperelliptic curve, and so one can write down explicitly the parameterizations of the invariant tori that foliate the phase space; see [42, 23].

Periodic orbits are the most distinctive special class of orbits. Therefore, the first task to carry out in any dynamical system should be their study, and one of the simplest questions about them is to look for minimal periods. In the framework of smooth convex billiards the minimal period is always two. Nevertheless, since all the two-periodic billiard trajectories inside ellipsoids are *singular*—in the sense that some of their caustics are singular elements of the family of confocal quadrics—two questions arise. Which is the minimal period among *nonsingular* billiard trajectories? Which ellipsoids display such trajectories?

In order to get a flavor of the kind of results obtained in this paper, let us consider the three-dimensional problem. Let Q be the triaxial ellipsoid given by $x^2/a + y^2/b + z^2/c = 1$, with $0 < c < b < a$. We assume that $a = 1$ without loss of generality. Any billiard trajectory inside Q has as caustics two elements of the family of confocal quadrics given by

$$Q_\lambda = \left\{ (x, y, z) \in \mathbb{R}^3 : \frac{x^2}{a-\lambda} + \frac{y^2}{b-\lambda} + \frac{z^2}{c-\lambda} = 1 \right\}.$$

We restrict our attention to nonsingular trajectories, that is, trajectories whose caustics are ellipsoids, $0 < \lambda < c$; one-sheet hyperboloids, $c < \lambda < b$; or two-sheet hyperboloids, $b < \lambda < a$. The singular values $\lambda \in \{a, b, c\}$ are discarded. It is known that there are only four types of pairs of nonsingular caustics: EH1, H1H1, EH2, and H1H2. (The notation is self-explanatory.) It is also known that any nonsingular periodic billiard trajectory inside Q has three so-called *winding numbers* $m_0, m_1, m_2 \in \mathbb{N}$ which describe how the trajectory folds in $\mathbb{R}^3$. For instance, m_0 is the period. The geometric meanings of m_1 and m_2 depend on the type of the pair of caustics; see section 5. We note two key observations about winding numbers. First, some of them must be even, namely, the ones that can be interpreted as the number of crossings with some coordinate plane. Second, we conjecture that they are ordered as follows: $m_2 < m_1 < m_0$. This unexpected behavior is supported by extensive numerical experiments. In fact, we believe that it holds in any dimension. The combination of both observations crystallizes in the following lower bounds.

Theorem 1. *If the previous conjecture on the winding numbers holds, any periodic billiard trajectory inside a triaxial ellipsoid of* $\mathbb{R}^3$ *whose caustics are of type EH*1*, H*1*H*1*, EH*2*, and H*1*H*2 *has period at least five, four, five, and six, respectively.*

All the billiard trajectories of periods two and three are singular. The two-periodic ones are contained in some coordinate axis, so they have two singular caustics. The three-periodic ones are contained in some coordinate plane, so they have one singular caustic.

We shall prove in section 3 the generalization of these lower bounds to any dimension; see Theorem 9. Samples of periodic trajectories with minimal periods are shown in Figure 13. Hence, these lower bounds are optimal. Next, we look for ellipsoids with minimal periodic trajectories. We recall that $a = 1$, so each ellipsoid Q is represented by a point in the triangle $P = \{(b, c) \in \mathbb{R}^2 : 0 < c < b < 1\}$. Let P_1^*, P_2^*, P_3^*, and P_4^* be the four regions of P that correspond to ellipsoids with minimal periodic trajectories of type EH1, H1H1, EH2, and H1H2, respectively. They are shown in Figure 1, and their shapes are described below.

Numerical Result 1. *Let* $r = \frac{3-\sqrt{5}}{2} \approx 0.382$*,* $b_1^* = b_2^* = 1$*, and* $b_3^* = b_4^* = \frac{1}{2}$*. Then*

$$P_j^* = \left\{(b, c) \in P : b < b_j^*,\ c < g_j^*(b)\right\}, \quad 1 \le j \le 4,$$

for some continuous functions $g_j^* : [0, b_j^*] \to \mathbb{R}$ *such that*

(i) g_1^* *is concave increasing in* $[0, 1]$*,* $0 < g_1^*(b) < b$ *for all* $b \in (0, 1)$*, and* $g_1^*(1) = r$*;*

(ii) g_2^* *is concave increasing in* $[0, 1]$*,* $g_1^*(b) < g_2^*(b) < b$ *for all* $b \in (0, 1)$*,* $g_2^*(1) = \frac{1}{2}$*;*

(iii) g_3^* *is the identity in* $[0, r]$*, concave decreasing in* $[r, \frac{1}{2}]$*, and* $g_3^*(\frac{1}{2}) = 0$*; and*

(iv) g_4^* *is increasing in* $[0, \frac{1}{3}]$*, concave decreasing in* $[\frac{1}{3}, \frac{1}{2}]$*,* $3b/4 < g_4^*(b) < b$ *for all* $b \in (0, \frac{1}{3})$*,* $0 < g_4^*(b) < g_3^*(b)$ *for all* $b \in (\frac{1}{3}, \frac{1}{2})$*,* $g_4^*(\frac{1}{3}) = \frac{1}{4}$*, and* $g_4^*(\frac{1}{2}) = 0$*.*

The functions g_j^* can be explicitly expressed by means of algebraic formulae. We shall prove that $g_2^*(b) = b/(1 + b)$ in Proposition 18. We shall study the other three functions in another paper [38], because the techniques change drastically. A generalized Cayley-like condition is the main tool. For instance,

$$g_4^*(b) = \begin{cases} \left(1 - b/2 - \sqrt{b(1 - 3b/4)}\right) b/(1 - b)^2 & \text{for } 0 \le b \le 1/3, \\ (1 - 2b)b/(1 - b)^2 & \text{for } 1/3 \le b \le 1/2. \end{cases}$$

This function g_4^* is not concave in the interval $[0, 1/3]$.

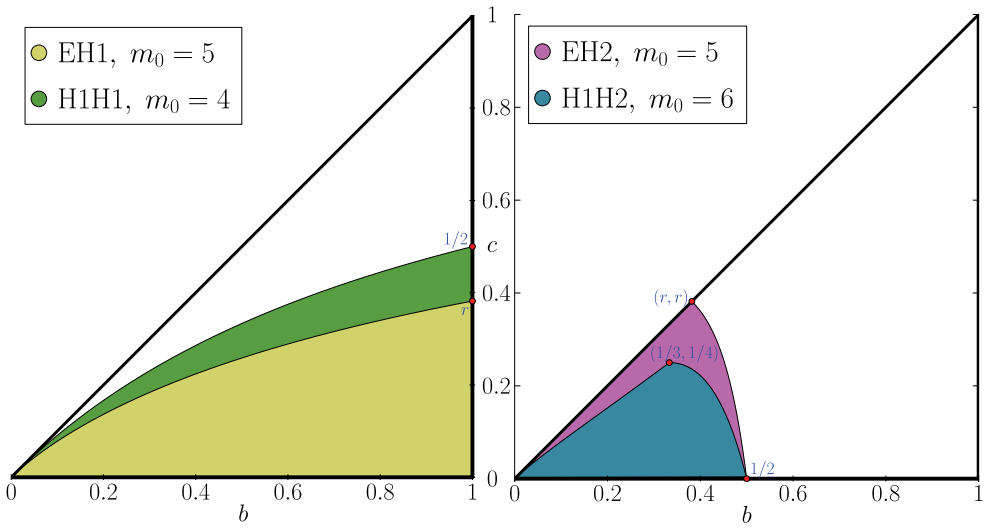

Figure 1. *The four regions of ellipsoids with minimal periodic trajectories. Left: The yellow region (type EH1, period 5) is contained in the green one (type H1H1, period 4). Right: The blue region (type H1H2, period 6) is contained in the magenta one (type EH2, period 5).*

We shall describe in section 5 the regions corresponding to ellipsoids that have periodic trajectories with given winding numbers (or quasi-periodic trajectories with given frequencies) for the four caustic types. Those general regions have the same shape as these "minimal" regions. That is, they are below the graphs of some functions with properties similar to the ones stated previously. Therefore, we discover a general principle: *The more spheric is an ellipsoid, the poorer are its four types of billiard dynamics.* Here, spheric means $(b, c) \approx (1, 1)$. We quantify this principle in Propositions 15 and 17.

The key step for the numerical computation of these regions is to explicitly extend the frequency map for singular values of the caustic parameters. The extension is "exponentially sharp" at some points, which implies another general principle. *The billiard trajectories with some almost singular caustic are ubiquitous.* We shall enlighten this general principle in section 5.7 by giving a quantitative sample, and we reinforce it with the minimal periodic trajectories shown in Figure 13.

Finally, we want to mention that there exist many remarkable results about periodic trajectories in other billiard and geodesic problems. For instance, several nice algebraic closed geodesics on a triaxial ellipsoid can be seen in [24], and a Cayley-like condition for billiards *on* quadrics was established in [1]. Some results stray from any integrable setup. For example, some general lower bounds on the number of periodic billiard trajectories inside strictly convex smooth hypersurfaces can be found in [4, 20, 21, 22]. The planar case was already solved by Birkhoff [7]. Of course, these lower bounds are useless for integrable systems where the periodic trajectories are organized in continuous families.

We complete this introduction with a note on the organization of the paper. In section 2 we briefly review some well-known results about billiards inside ellipsoids in order to fix notation that will be used throughout the rest of the paper. Next, the frequency map is introduced and interpreted in section 3. This section, concerning ellipsoids of $\mathbb{R}^{n+1}$, also contains two

conjectures and the lower bounds on the periods. Billiards inside ellipses of $\mathbb{R}^2$ and inside triaxial ellipsoids of $\mathbb{R}^3$ are thoroughly studied in sections 4 and 5, respectively. Billiards inside nondegenerate ellipsoids of $\mathbb{R}^{n+1}$ are revisited in section 6. Some technical lemmas have been relegated to the appendices.

2. Preliminaries.

In this section, details are scarce and technicalities are avoided. Experts can simply browse this section. We will list several basic references for the more novice reader.

2.1. Confocal quadrics and elliptic billiards.

The following results go back to Jacobi, Chasles, Poncelet, and Darboux.

The starting point of our discussion is the n-dimensional nondegenerate ellipsoid

$$Q = \left\{ x = (x_1, \dots, x_{n+1}) \in \mathbb{R}^{n+1} : \sum_{i=1}^{n+1} \frac{x_i^2}{a_i} = 1 \right\}, \tag{1}$$

where $a_1, \dots, a_{n+1}$ are some fixed real constants such that $0 < a_1 < \cdots < a_{n+1}$. The degenerate cases in which the ellipsoid has some symmetry of revolution are not considered here. This ellipsoid is an element of the family of *confocal quadrics* given by

$$Q_\mu = \left\{ x = (x_1, \dots, x_{n+1}) \in \mathbb{R}^{n+1} : \sum_{i=1}^{n+1} \frac{x_i^2}{a_i - \mu} = 1 \right\}, \qquad \mu \in \mathbb{R}.$$

The meaning of Q_μ is unclear in the singular cases $\mu \in \{a_1, \dots, a_{n+1}\}$. In fact, there are two natural choices for the singular confocal quadric Q_μ when $\mu = a_j$. The first choice is to define it as the n-dimensional coordinate hyperplane,

$$H_j = \left\{ x = (x_1, \dots, x_{n+1}) \in \mathbb{R}^{n+1} : x_j = 0 \right\},$$

but it also makes sense to define it as the $(n-1)$-dimensional *focal quadric*,

$$F_j = \left\{ x = (x_1, \dots, x_{n+1}) \in \mathbb{R}^{n+1} : x_j = 0 \text{ and } \sum_{i \neq j} \frac{x_i^2}{a_i - a_j} = 1 \right\},$$

which is contained in the hyperplane H_j. Both choices fit in the framework of elliptic billiards, but we shall use the notation $Q_{a_j} = H_j$ in this paper.

Theorem 2 (see [33, 29, 2, 40]). *Given a fixed nondegenerate ellipsoid Q, a generic line $\ell \subset \mathbb{R}^{n+1}$ is tangent to exactly n distinct nonsingular confocal quadrics $Q_{\lambda_1}, \dots, Q_{\lambda_n}$ such that $\lambda_1 < \lambda_2 < \cdots < \lambda_n$, $\lambda_1 \in (-\infty, a_1) \cup (a_1, a_2)$, and $\lambda_i \in (a_{i-1}, a_i) \cup (a_i, a_{i+1})$, for $i = 2, \dots, n$.*

Set $a_0 = 0$. If a generic line ℓ has a transverse intersection with the ellipsoid Q, then $\lambda_1 > 0$, so $\lambda_1 \in (a_0, a_1) \cup (a_1, a_2)$. The value $\lambda_1 = 0$ is attained just when ℓ is tangent to Q. A line is generic in the sense of the theorem if and only if it is neither tangent to a singular confocal quadric[1] nor contained in a nonsingular confocal quadric.

[1] By abuse of notation, it is said that a line is tangent to the singular confocal quadric Q_{a_j} when it is contained in the coordinate hyperplane H_j or when it passes through the focal quadric F_j.

If two lines obey the reflection law at a point $x \in Q$, then both lines are tangent to the same confocal quadrics [40]. This shows a tight relation between elliptic billiards and confocal quadrics: all lines of a billiard trajectory inside the ellipsoid Q are tangent to exactly n confocal quadrics $Q_{\lambda_1}, \dots, Q_{\lambda_n}$, which are called *caustics* of the trajectory. We will say that $\lambda = (\lambda_1, \dots, \lambda_n) \in \mathbb{R}^n$ are the *caustic parameters* of the trajectory.

Definition 1. *A billiard trajectory inside a nondegenerate ellipsoid of the Euclidean space* $\mathbb{R}^{n+1}$ *is* nonsingular *when it has* n *distinct nonsingular caustics, that is, when its caustic parameter belongs to the* nonsingular caustic space

$$\Lambda = \left\{ (\lambda_1, \dots, \lambda_n) \in \mathbb{R}^n : \begin{array}{l} 0 < \lambda_1 < \lambda_2 < \cdots < \lambda_n \\ \lambda_i \in (a_{i-1}, a_i) \cup (a_i, a_{i+1}) \text{ for } 1 \le i \le n \end{array} \right\}. \tag{2}$$

We will deal only with nonsingular billiard trajectories along this paper. We denote the 2^n open connected components of the nonsingular caustic space as follows:

$$\Lambda_\sigma = \left\{ (\lambda_1, \dots, \lambda_n) \in \mathbb{R}^n : \begin{array}{l} 0 < \lambda_1 < \lambda_2 < \cdots < \lambda_n \\ \lambda_i \in (a_{i+\sigma_i - 1}, a_{i+\sigma_i}) \text{ for } 1 \le i \le n \end{array} \right\}$$

for $\sigma = (\sigma_1, \dots, \sigma_n) \in \{0,1\}^n$. For instance, the first caustic Q_{λ_1} is an ellipsoid if and only if $\lambda_1 \in (a_0, a_1)$, that is, if and only if $\lambda \in \Lambda_\sigma$ with $\sigma_1 = 0$. We will draw the space Λ for ellipses and triaxial ellipsoids of $\mathbb{R}^3$ in sections 4 and 5, respectively.

Theorem 3. *If a nonsingular billiard trajectory closes after* m_0 *bounces, all trajectories sharing the same caustics close after* m_0 *bounces.*

Poncelet proved this theorem for conics [34]. Darboux generalized it to triaxial ellipsoids of $\mathbb{R}^3$. Later on, this result was generalized to any dimension in [11, 12, 13, 36].

Theorem 4. *The nonsingular billiard trajectories sharing the caustics* $Q_{\lambda_1}, \dots, Q_{\lambda_n}$ *close after* m *bounces—up to the action of the group of symmetries* $G = (\mathbb{Z}/2\mathbb{Z})^{n+1}$ *of* Q*—if and only if* $m \ge n+1$ *and*

$$\operatorname{rank} \begin{pmatrix} h_{m+1} & \cdots & h_{n+2} \\ \vdots & & \vdots \\ h_{2m-1} & \cdots & h_{n+m} \end{pmatrix} < m - n, \tag{3}$$

where $\sqrt{(a_1 - s) \cdots (a_{n+1} - s)(\lambda_1 - s) \cdots (\lambda_n - s)} = h_0 + h_1 s + h_2 s^2 + \cdots$.

The group G is formed by the 2^{n+1} reflections—involutive linear transformations—with regard to coordinate subspaces. The phrase "a billiard trajectory closes after m bounces up to the action of G" means that if $(q_k)_{k \in \mathbb{Z}}$ is the sequence of impact points of the trajectory, then there exists a reflection $g \in G$ such that $q_{k+m} = g(q_k)$ for all $k \in \mathbb{Z}$. Hence, billiard trajectories that close after m bounces up to the action of the group G close after $m_0 = m$ or $m_0 = 2m$ bounces, because $q_{k+2m} = g(q_{k+m}) = g^2(q_k) = q_k$.

Cayley proved this theorem for conics [9]. Later on, this result was generalized to any dimension by Dragović and Radnović in [15, 16].

2.2. Complete integrability of elliptic billiards. We recall some results obtained by Liouville, Arnold, Moser, and Knörrer.

A symplectic map $f : M \to M$ defined on a $2n$-dimensional symplectic manifold is *completely integrable* if there exist some smooth f-invariant functions $I_1, \dots, I_n : M \to \mathbb{R}$ (the *integrals*) that are in involution—that is, whose pairwise Poisson brackets vanish—and that are functionally independent almost everywhere on the phase space M. In this context, the map $I = (I_1, \dots, I_n) : M \to \mathbb{R}^n$ is called the *momentum map*. A point $m \in M$ is a *regular point* of the momentum map when the n-form $\mathrm{d}I_1 \wedge \cdots \wedge \mathrm{d}I_n$ does not vanish at m. A vector $\lambda \in \mathbb{R}^n$ is a *regular value* of the momentum map when every point in the level set $I^{-1}(\lambda)$ is regular, in which case the level set is a Lagrangian submanifold of M and we say that $I^{-1}(\lambda)$ is a *regular level set*.

The following result is a discrete version of the Liouville–Arnold theorem.

Theorem 5 (see [43]). *Any compact connected component of a regular level set $I^{-1}(\lambda)$ is diffeomorphic to $\mathbb{T}^n$, where $\mathbb{T} = \mathbb{R}/\mathbb{Z}$. In appropriate coordinates the restrictions of the map to this torus becomes a parallel translation $\theta \mapsto \theta + \omega$. The map $\lambda \mapsto \omega$ is smooth at the regular values of the momentum map.*

Thus the phase space M is almost foliated by Lagrangian invariant tori, and the map on each torus is simply a parallel translation. These tori are called *Liouville tori*, the shift ω is the *frequency* of the torus, and the map $\lambda \mapsto \omega$ is the *frequency map*. The dynamics on a Liouville torus with frequency ω is m_0-periodic if and only if $m_0\omega \in \mathbb{Z}^n$. Liouville tori become just invariant curves when $n = 1$, in which case the shift is usually called the *rotation number* of the invariant curve, and denoted by ρ instead of ω.

Now, let Q be a (strictly) convex smooth hypersurface of $\mathbb{R}^{n+1}$ diffeomorphic to the sphere $\mathbb{S}^n$, not necessarily an ellipsoid. The billiard motion inside Q can be modelled by means of a symplectic diffeomorphism defined on the $2n$-dimensional phase space

$$M = \{(q,p) \in Q \times \mathbb{S}^n : p \text{ is directed outward } Q \text{ at } q\}. \tag{4}$$

We define the billiard map $f : M \to M$, $f(q,p) = (q',p')$, as follows. The new velocity p' is the reflection of the old velocity p with respect to the tangent plane T_qQ. That is, if we decompose the old velocity as the sum of its tangent and normal components at the surface, $p = p_{\mathrm{t}} + p_{\mathrm{n}}$ with $p_{\mathrm{t}} \in T_qQ$ and $p_{\mathrm{n}} \in N_qQ$, then $p' = p_{\mathrm{t}} - p_{\mathrm{n}} = p - 2p_{\mathrm{n}}$. The new impact point q' is the intersection of the ray $\{q + \mu p' : \mu > 0\}$ with the surface Q. This intersection is unique and transverse by convexity.

Elliptic billiards fit within the frame of the Liouville–Arnold theorem.

Theorem 6 (see [33, 31, 42, 2]). *The billiard map associated with the nondegenerate ellipsoid (1) is completely integrable, and the caustic parameters $\lambda_1, \dots, \lambda_n$ are the integrals. The set of regular values of the corresponding momentum map is given by (2).*

3. The frequency map.

3.1. Definition and interpretation. The rotation number for the billiard inside an ellipse is a quotient of elliptic integrals; see [32, 11]. Explicit formulae for the frequency map of the billiard inside a triaxial ellipsoid of $\mathbb{R}^3$ can be found in [13, sect. III.C]. An equivalent formula is given in [35, sect. 5]. Both formulae contain hyperelliptic integrals, and they can be effortlessly generalized to any dimension. Since we want to avoid as many technicalities as possible, we will not talk about Riemann surfaces, basis of holomorphic differential forms,

basis of homology groups, period matrices, or other objects that arise in the theory of algebraic curves.

The following notation is required to define the frequency map. Once we have fixed the parameters $a_1, \dots, a_{n+1}$ of the ellipsoid, and the caustic parameters $\lambda_1, \dots, \lambda_n$, we set

$$T(s) = \prod_{i=1}^{2n+1} (c_i - s), \quad \{c_1, \dots, c_{2n+1}\} = \{a_1, \dots, a_{n+1}\} \bigcup \{\lambda_1, \dots, \lambda_n\}.$$

If $\lambda \in \Lambda$, then $c_1, \dots, c_{2n+1}$ are pairwise distinct and positive, so we can assume that

$$c_0 := 0 < c_1 < \cdots < c_{2n+1}. \tag{5}$$

Hence, $T(s)$ is positive in the $n+1$ open intervals (c_{2j}, c_{2j+1}), and the improper integrals

$$K_{ij} = \int_{c_{2j}}^{c_{2j+1}} \frac{s^i \mathrm{d}s}{\sqrt{T(s)}}, \qquad i = 0, \dots, n-1, \quad j = 0, \dots, n, \tag{6}$$

are absolutely convergent, real, and positive. We also consider the $n+1$ column vectors

$$K_j = (K_{0j}, \dots, K_{n-1,j})^t \in \mathbb{R}^n.$$

It is known that vectors $K_1, \dots, K_n$ are linearly independent; see [26, sect. III.3].

Definition 2. *The* frequency map $\omega : \Lambda \to \mathbb{R}^n$ *of the billiard inside the nondegenerate ellipsoid Q is the unique solution of the system of n linear equations*

$$K_0 + 2\sum_{j=1}^{n} (-1)^j \omega_j K_j = 0. \tag{7}$$

Remark 1. Sometimes it is useful to think that the frequency ω depends on the parameter $c = (c_1, \dots, c_{2n+1}) \in \mathbb{R}_+^{2n+1}$ and not only on the caustic parameter $\lambda = (\lambda_1, \dots, \lambda_n) \in \Lambda$. In such situations, we will write $\omega = \varpi(c)$. This map $c \mapsto \varpi(c)$ is homogeneous of degree zero and analytic in the domain defined by inequalities (5). Homogeneity is deduced by performing a change of scale in the integrals (6). Hence, we can assume without loss of generality that $c_{2n+1} = a_{n+1} = 1$. Analyticity follows from the fact that the integrands in (6) are analytic with respect to the variable of integration in all the intervals of integration and with respect to c, as long as condition (5) takes place.

This definition coincides with the formulae contained in [13, 35] for $n = 2$. It is motivated by the characterization of periodic billiard trajectories contained in the next theorem. The factor 2 has been added to simplify the interpretation of the components of the frequency map, which are all positive, due to the factors $(-1)^j$.

Theorem 7 (see [17, 18]). *The nonsingular billiard trajectories inside the nondegenerate ellipsoid Q are periodic with exactly m_j points at $Q_{c_{2j}}$ and m_j points at $Q_{c_{2j+1}}$ if and only if $m_0 K_0 + \sum_{j=1}^{n} (-1)^j m_j K_j = 0$.*

The numbers $m_0, m_1, \dots, m_n$ that appear in Theorem 7 are called *winding numbers*. The nonsingular billiard trajectories with caustic parameter λ are periodic with winding numbers $m_0, m_1, \dots, m_n$ if and only if

$$\omega_j(\lambda) = \frac{m_j}{2m_0} \in \mathbb{Q}_+, \qquad j = 1, \dots, n. \tag{8}$$

We note that m_0 is the number of bounces in the ellipsoid $Q = Q_{c_0}$, so it is the period.

Remark 2. The sequence of winding numbers of a nonsingular periodic billiard trajectory contains information about how the trajectory folds in the space $\mathbb{R}^{n+1}$. The following properties can be deduced from results contained in [17, sect. 4.1]. Here, "number of __" means "number of times that any periodic billiard trajectory with those caustic parameters does __ along one period." The intervals (c_{2j}, c_{2j+1}) with $j \neq 0$ can adopt exactly four different forms, each one giving rise to its own geometric picture:

1. If $(c_{2j}, c_{2j+1}) = (a_j, \lambda_{j+1})$, then m_j is the number of crossings with H_j, so it is even, and $m_j/2$ is the number of oscillations around the hyperplane H_j.
2. If $(c_{2j}, c_{2j+1}) = (\lambda_j, a_{j+1})$, then m_j is the number of crossings with H_{j+1}, so it is even, and $m_j/2$ is the number of oscillations around the hyperplane H_{j+1}.
3. If $(c_{2j}, c_{2j+1}) = (a_j, a_{j+1})$, then m_j is the number of (alternate) crossings with H_j and H_{j+1}, so it is even, and $m_j/2$ is the number of rotations that the trajectory performs when projected onto the (x_j, x_{j+1})-coordinate plane π_j.
4. If $(c_{2j}, c_{2j+1}) = (\lambda_j, \lambda_{j+1})$, then m_j is the number of (alternate) tangential touches with Q_{λ_j} and $Q_{\lambda_{j+1}}$, so it can be even or odd, and it is the number of oscillations between both caustics.

These four properties suggest to us the following definitions, which establish the geometric meaning of the components of the frequency map. They change with the open connected components of the nonsingular caustic space.

Definition 3. *Let $\omega = (\omega_1, \dots, \omega_n) : \Lambda \to \mathbb{R}^n$ be the frequency map.*

1. *If $(c_{2j}, c_{2j+1}) = (a_j, \lambda_{j+1})$, then $\omega_j = m_j/2m_0$ is the* H_j-oscillation number.
2. *If $(c_{2j}, c_{2j+1}) = (\lambda_j, a_{j+1})$, then $\omega_j = m_j/2m_0$ is the* H_{j+1}-oscillation number.
3. *If $(c_{2j}, c_{2j+1}) = (a_j, a_{j+1})$, then $\omega_j = m_j/2m_0$ is the* π_j-rotation number.
4. *If $(c_{2j}, c_{2j+1}) = (\lambda_j, \lambda_{j+1})$, then $2\omega_j = m_j/m_0$ is the* $(Q_{\lambda_j}, Q_{\lambda_{j+1}})$-oscillation number.

Remark 3. It is important to notice that (only) when a m_0-periodic billiard trajectory has two caustics of the same type—that is, when some interval (c_{2j}, c_{2j+1}) falls into the fourth case—is it possible that $m_0\omega \notin \mathbb{Z}^n$, although then $2m_0\omega \in \mathbb{Z}^n$. This is due to the factor 2 that we have added in the definition of the frequency map.

Finally, if Q_{λ_1} is not an ellipsoid—that is, if $\lambda_1 > a_1$—then $c_1 = a_1$, and m_0 is the number of crossings with H_1, so it is even. Therefore, the following corollary holds.

Corollary 8. *Among all the nonsingular billiard trajectories inside a nondegenerate ellipsoid, only those with an ellipsoid as caustic can have odd period.*

3.2. Two conjectures.

We believe that the following properties hold.

Conjecture 1. *The frequency map is a local diffeomorphism; i.e.,*

$$\det\left(\frac{\partial \omega_j}{\partial \lambda_i}(\lambda)\right)_{1\leq i,j\leq n} \neq 0 \qquad \forall \lambda \in \Lambda.$$

This conjecture has several relevant consequences throughout the paper. Popov and Topalov [35] have shown that the frequency map is *almost everywhere* nondegenerate when Q is a triaxial ellipsoid of $\mathbb{R}^3$, although they consider only the components Λ_σ such that $\sigma_1 = 0$. The nondegeneracy of the frequency map is important because it is an essential hypothesis—although we acknowledge that it can be replaced by some weaker Rüssmann-like

nondegeneracy conditions [39, sect. 2]—in most KAM-like theorems, which are the standard tool for proving the persistence of Liouville tori under small smooth perturbations of completely integrable maps. Therefore, if Conjecture 1 holds, we can conclude that most of the Liouville tori of the billiard phase space persist under small smooth perturbations of the ellipsoid. We shall present evidence for this conjecture in sections 4 and 5.

Conjecture 2. *Winding numbers of nonsingular periodic billiard trajectories are ordered in a strictly decreasing way. More concretely,* $2 \le m_n < \cdots < m_1 < m_0 =$ period.

Inequality $m_n \ge 2$ is immediate, because $c_{2n+1} = a_{n+1}$, so m_n is even. Inequalities $m_j \le m_0$ for $j \ge 1$ are also immediate, because the number of crossings with any fixed hyperplane or the number of tangential touches with any fixed caustic can not exceed the number of segments of the periodic billiard trajectory. The strict inequalities $m_j < m_0$ could be also established (using the symmetries of the ellipsoid), but we skip the details, since such a small improvement is not worth the effort.

If both conjectures hold, the components of the frequency map are also ordered in a strictly decreasing way and lie in the range $(0, 1/2)$; that is,

$$0 < \omega_n(\lambda) < \cdots < \omega_1(\lambda) < 1/2 \qquad \forall \lambda \in \Lambda. \tag{9}$$

To prove this, we note that Conjecture 1 implies that $\omega(\Lambda)$ is open in $\mathbb{R}^n$ and $\omega^{-1}(\mathbb{Q}^n)$ is dense in Λ, whereas Conjecture 2 and relation (8) imply that the strict inequalities $0 < \omega_n < \cdots < \omega_1 < 1/2$ hold for rational frequencies. Therefore, $0 \le \omega_n(\lambda) \le \cdots \le \omega_1(\lambda) \le 1/2$ for any $\lambda \in \Lambda$, but these inequalities must be strict because $\omega(\Lambda)$ is open. We have numerically checked that inequalities (9) hold for thousands of random choices of $a_1, \ldots, a_{n+1}, \lambda_1, \ldots, \lambda_n$ in "dimensions" $n \le 5$. The details of the experiments for $n = 2$ are presented in section 5.

3.3. Lower bounds on the periods. We know from Theorem 4 that the period m_0 of any nonsingular periodic billiard trajectory inside a nondegenerate ellipsoid $Q \subset \mathbb{R}^{n+1}$ verifies that $m_0 \ge n + 1$. This result can be improved in several ways using the ordering of the winding numbers stated in Conjecture 2. For instance, the global lower bound $m_0 \ge n + 2$ follows directly. We present below more refined semiglobal lower bounds, holding each one on a different open connected component of the nonsingular caustic space. They are obtained by realizing that some winding numbers must be even, in agreement with the first items in Remark 2. The lower bound associated with some connected component reaches the value $2n + 2$, which doubles the original lower bound given in Theorem 4.

Theorem 9. *Given any* $\sigma = (\sigma_1, \ldots, \sigma_n) \in \{0,1\}^n$, *let* $E_\sigma \subset \{0, 1, \ldots, n\}$ *be such that* (a) $0 \in E_\sigma \Leftrightarrow \sigma_1 = 1$, (b) $j \in E_\sigma \Leftrightarrow (\sigma_j, \sigma_{j+1}) \ne (1, 0)$, *and* (c) $n \in E_\sigma$.

(i) *If* $m_0, \ldots, m_n$ *are the winding numbers of a periodic trajectory with caustic parameter in* Λ_σ, *then* m_j *is even for all* $j \in E_\sigma$.

(ii) *If Conjecture 2 holds, any periodic billiard trajectory inside a nondegenerate ellipsoid of* $\mathbb{R}^{n+1}$ *whose caustic parameter is in* Λ_σ *has period at least*

$$\varkappa(\sigma) := \min \left\{ m_0 : \begin{array}{l} \exists\, 2 \le m_n < \cdots < m_0 \text{ sequence of integers} \\ \text{such that } m_j \text{ is even for any } j \in E_\sigma \end{array} \right\}.$$

(iii) *Let* $\mathbf{1} = (1, \ldots, 1) \in \{0,1\}^n$, $\varsigma = (\ldots, 0, 1, 0, 1, 0) \in \{0,1\}^n$, $\sigma \in \{0,1\}^n$. *Then*

$$n + 2 = \varkappa(\varsigma) < \varkappa(\sigma) < \varkappa(\mathbf{1}) = 2n + 2 \qquad \forall\, \sigma \ne \mathbf{1}, \varsigma.$$

Proof. (i) We recall that m_j must be even in the three first cases listed in Remark 2. This is the key property. For instance, m_n is always even because $c_{2n+1} = a_{n+1}$. If $\sigma_1 = 1$, then $\lambda_1 \in (a_1, a_2)$ and $c_1 = a_1$, so m_0 is even. If m_j is odd, then $(c_{2j}, c_{2j+1}) = (\lambda_j, \lambda_{j+1})$ and $\lambda_j, \lambda_{j+1} \in (a_j, a_{j+1})$, so $(\sigma_j, \sigma_{j+1}) = (1, 0)$. Hence, we have seen that $(\sigma_j, \sigma_{j+1}) \neq (1, 0) \Rightarrow m_j$ is even.

(ii) This follows directly from the previous item and the definition of $\varkappa(\sigma)$.

(iii) First, we note that $E_{\mathbf{1}} = \{0, \dots, n\}$ and $E_\varsigma = \{\dots, n-4, n-2, n\}$. Therefore, $\varkappa(\mathbf{1}) = \min\{m_0 : \exists\, 2 \leq m_n < \cdots < m_0$ sequence of even numbers$\} = 2n + 2$, and

$$\varkappa(\varsigma) = \min\left\{ m_0 : \begin{array}{l} \exists\, 2 \leq m_n < \cdots < m_0 \text{ sequence of} \\ \text{integers s.t. } m_n, m_{n-2}, \dots \text{ are even} \end{array} \right\} = n + 2.$$

The minimum value of m_0 among all integer sequences such that $2 \leq m_n < \cdots < m_0$ is attained at the sequence $m_j = n + 2 - j$, $0 \leq j \leq n$. Thus, $\varkappa(\sigma) \geq n + 2$ for all $\sigma \in \{0, 1\}^n$, and $\varkappa(\sigma) = n + 2 \Rightarrow E_\sigma = E_\varsigma \Rightarrow \sigma = \varsigma$.

On the other hand, $E_\sigma \subset E_{\sigma'} \Rightarrow \varkappa(\sigma) \leq \varkappa(\sigma')$. Hence, $\varkappa(\sigma) \leq \varkappa(\mathbf{1}) = 2n + 2$ for all $\sigma \in \{0, 1\}^n$. Finally, $\varkappa(\sigma) = 2n + 2 \Rightarrow E_\sigma = \{0, \dots, n\} \Rightarrow \sigma_j \neq 0$ for all $j \Rightarrow \sigma = \mathbf{1}$. ∎

Remark 4. Let $\mathbf{0} = (0, \dots, 0)$ and $\bar{\varsigma} = (\dots, 1, 0, 1, 0, 1)$. Then $E_{\mathbf{0}} = \{1, \dots, n\}$ and $E_{\bar{\varsigma}} = \{\dots, n-5, n-3, n-1, n\}$, so $\varkappa(\mathbf{0}) = 2n + 1$ and $\varkappa(\bar{\varsigma}) = n + 3$.

Remark 5. All these lower bounds can be explicitly computed when $n = 2$. In that case,

$$4 = \varkappa(\varsigma) < \varkappa(\mathbf{0}) = 5 = \varkappa(\bar{\varsigma}) < \varkappa(\mathbf{1}) = 6,$$

where $\varsigma = (1, 0)$, $\mathbf{0} = (0, 0)$, $\bar{\varsigma} = (0, 1)$, and $\mathbf{1} = (1, 1)$. Therefore, Theorem 1 about triaxial ellipsoids of $\mathbb{R}^3$ is just a particular case of Theorem 9. It suffices to realize that $\sigma = \mathbf{0}$, $\sigma = \varsigma$, $\sigma = \bar{\varsigma}$, and $\sigma = \mathbf{1}$ correspond to the cases EH1, H1H1, EH2, and H1H2, respectively.

Remark 6. The function $\varkappa : \{0, 1\}^n \to \{n + 2, \dots, 2n + 2\}$ is surjective and has average

$$\bar{\varkappa} := 2^{-n} \sum_{\sigma \in \{0,1\}^n} \varkappa(\sigma) = \frac{3n}{2} + 2.$$

We skip the details; the proof is by induction over n. Thus, these semiglobal lower bounds improve the global lower bound $n + 2$ by, on average, almost 50%.

Now, a natural question arises: Are these semiglobal lower bounds optimal? Optimal does not mean that there exists a $\varkappa(\sigma)$-periodic billiard trajectory whose caustic parameter is in Λ_σ inside *all* nondegenerate ellipsoids, but just inside *some* of them. And we ask another question: Which are the ellipsoids with such "minimal" periodic billiard trajectories? Both questions become almost trivial for ellipses; see section 4.6. The case of triaxial ellipsoids of $\mathbb{R}^3$ was numerically answered in the introduction. The general case remains open, but we conjecture that all these semiglobal lower bounds are optimal.

4. Billiard inside an ellipse. In this section we describe the main properties of the frequency map when $n = 1$, in which case it is called rotation number and denoted by ρ. Many of these properties are old, but the observation that the rotation number is exponentially sharp at the singular caustic parameter seems to be new. The known results can be found in the monographs [29, 40] and the papers [32, 11, 41, 44].

4.1. Confocal caustics. To simplify the exposition, we write the ellipse as

$$Q = \left\{ (x, y) \in \mathbb{R}^2 : \frac{x^2}{a} + \frac{y^2}{b} = 1 \right\}, \qquad a > b > 0,$$

where we could assume, without loss of generality, that $a = 1$; see Remark 1. Then any nonsingular billiard trajectory inside Q is tangent to one confocal caustic of the form

$$Q_\lambda = \left\{ (x, y) \in \mathbb{R}^2 : \frac{x^2}{a - \lambda} + \frac{y^2}{b - \lambda} = 1 \right\},$$

where the caustic parameter λ belongs to the nonsingular caustic space[2]

$$\Lambda = E \cup H, \qquad E = (0, b), \qquad H = (b, a). \tag{10}$$

We have chosen those names for the connected components of Λ because then Q_λ is an ellipse for $\lambda \in E$ and a hyperbola for $\lambda \in H$.

4.2. Phase portrait. We now describe the billiard dynamics inside an ellipse. This description goes back to Birkhoff [7, sect. VIII.12], so it is rather old and we just list the results. Concretely, we want to know how the phase space is foliated by Liouville tori (invariant curves on which the motion becomes a rigid rotation) and separatrices (invariant curves on which the motion tends to some hyperbolic periodic trajectories).

Let us put some global coordinates (φ, r) over the billiard phase space M defined in (4), just for visualization purposes. First, following Birkhoff, we parameterize the impact points on the ellipse by means of an angular coordinate $\varphi \in \mathbb{T}$. We take, for instance, $q = \gamma(\varphi) = (a^{1/2} \cos \varphi, b^{1/2} \sin \varphi)$. Second, given an outward unitary velocity $p \in \mathbb{S}$, we set $r = \langle \gamma'(\varphi), p \rangle$, and so $|r| < |\gamma'(\varphi)| = (a \sin^2 \varphi + b \cos^2 \varphi)^{1/2}$. Then the correspondence $(q, p) \mapsto (\varphi, r)$ allows us to identify the phase space M with the annulus

$$\mathbb{A} = \left\{ (\varphi, r) \in \mathbb{T} \times \mathbb{R} : r^2 < a \sin^2 \varphi + b \cos^2 \varphi \right\}. \tag{11}$$

In these coordinates, the caustic parameter becomes $\lambda(\varphi, r) = (a - b) \sin^2 \varphi + b - r^2$. The partition of the annulus into invariant level curves of λ is shown in Figure 2.

Each regular level set contains *two* Liouville curves and represents the family of tangent lines to a fixed nonsingular caustic Q_λ. If Q_λ is an ellipse, each Liouville curve has a one-to-one projection onto the φ coordinate and corresponds to rotations around Q_λ in opposite directions, so they are invariant under f. If Q_λ is a hyperbola, then each Liouville curve corresponds to the impacts on *one* of the two pieces of the ellipse between the branches of Q_λ, so they are exchanged under f and invariant under f^2.

The singular level set $\{(\varphi, r) \in \mathbb{A} : \lambda(\varphi, r) = b\}$ gives rise to the ∞-shaped curve

$$\lambda^{-1}(b) = \left\{ (\varphi, r) \in \mathbb{A} : r = \pm (a - b)^{1/2} \sin \varphi \right\},$$

[2]When $\lambda \to b^-$ (resp., $\lambda \to b^+$) the caustic Q_λ flattens into the region of the x-axis enclosed by (resp., outside) the foci of the ellipse Q. When $\lambda \to a^-$, the caustic flattens into the whole y-axis.

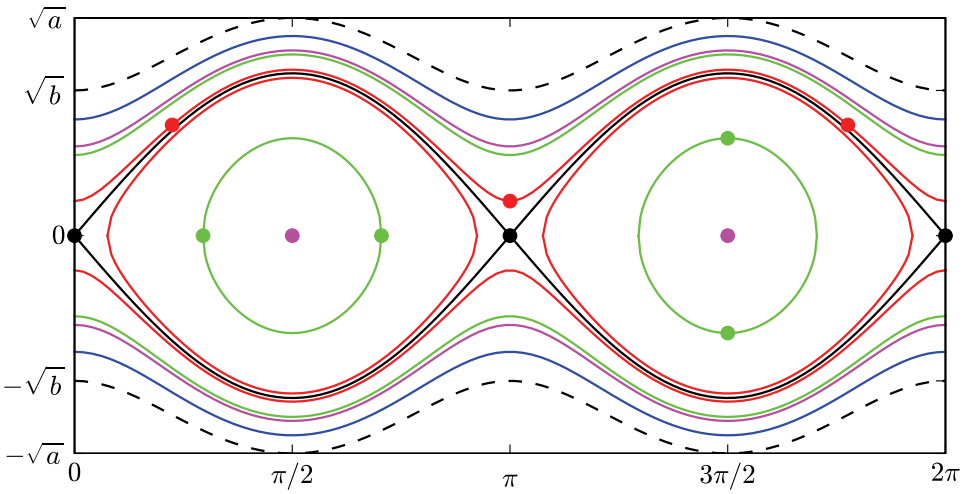

Figure 2. *Phase portrait of the billiard map in (φ, r) coordinates for $a = 1$ and $b = 4/9$. The dashed black lines enclose the phase space (11). The black points are the hyperbolic two-periodic points corresponding to the oscillation along the major axis of the ellipse. The black curves are the separatrices of these hyperbolic points. The magenta points denote the elliptic two-periodic points corresponding to the oscillation along the minor axis of the ellipse. The magenta curves are the invariant curves whose rotation number coincides with the frequency of these elliptic points. The invariant curves with rotation numbers 1/6, 1/4, and 1/3 are depicted in blue, green, and red, respectively. The red points label a three-periodic trajectory whose caustic is an ellipse. The green points label a four-periodic trajectory whose caustic is a hyperbola.*

which corresponds to the family of lines through the foci. This singular level set has rotation number 1/2; see [27, p. 428]. The cross points on this singular level represent the two-periodic trajectory along the major axis of the ellipse, and the eigenvalues of the differential of the billiard map at those points are positive but different from 1: $\mathrm{e}^{\pm h}$ with $\cosh^2 h/2 = a/b$ and $h > 0$. On the contrary, the two-periodic trajectory along the minor axis corresponds to the centers of the regions inside the ∞-shaped curve, and the eigenvalues in that case are conjugate complexes of modulus 1: $\mathrm{e}^{\pm 2\pi\theta \mathrm{i}}$ with $\cos^2 \pi\theta = b/a$ and $0 < \theta < 1/2$. Therefore, the major axis is a hyperbolic (unstable) two-periodic trajectory, and the minor axis is an elliptic (stable) one. These are the only two-periodic motions. The basic results about the stability of two-periodic billiard trajectories can be found in [29, 40].

4.3. Extension and range of the rotation number. Let $\rho(\lambda)$ be the *rotation number* of the billiard trajectories inside the ellipse Q sharing the nonsingular caustic Q_λ. From Definition 2 we get that the function $\rho : E \cup H \to \mathbb{R}$ is given by the quotients of elliptic integrals

$$\rho(\lambda) = \rho(\lambda; b, a) = \frac{\displaystyle\int_0^{\min(b,\lambda)} \frac{\mathrm{d}s}{\sqrt{(\lambda-s)(b-s)(a-s)}}}{2\displaystyle\int_{\max(b,\lambda)}^{a} \frac{\mathrm{d}s}{\sqrt{(\lambda-s)(b-s)(a-s)}}} = \frac{\displaystyle\int_\chi^\mu \frac{\mathrm{d}t}{\sqrt{t(t-1)(t-\chi)}}}{2\displaystyle\int_0^1 \frac{\mathrm{d}t}{\sqrt{t(t-1)(t-\chi)}}}, \tag{12}$$

where the parameters $1 < \chi < \mu$ are given by $\chi = (a - \underline{m})/(a - \overline{m})$ and $\mu = a/(a - \overline{m})$, with $\underline{m} = \min(b, \lambda)$ and $\overline{m} = \max(b, \lambda)$. The second equality follows from the change of variables $t = (a-s)/(a-\overline{m})$. The second quotient already appears in [13]. Other equivalent quotients of

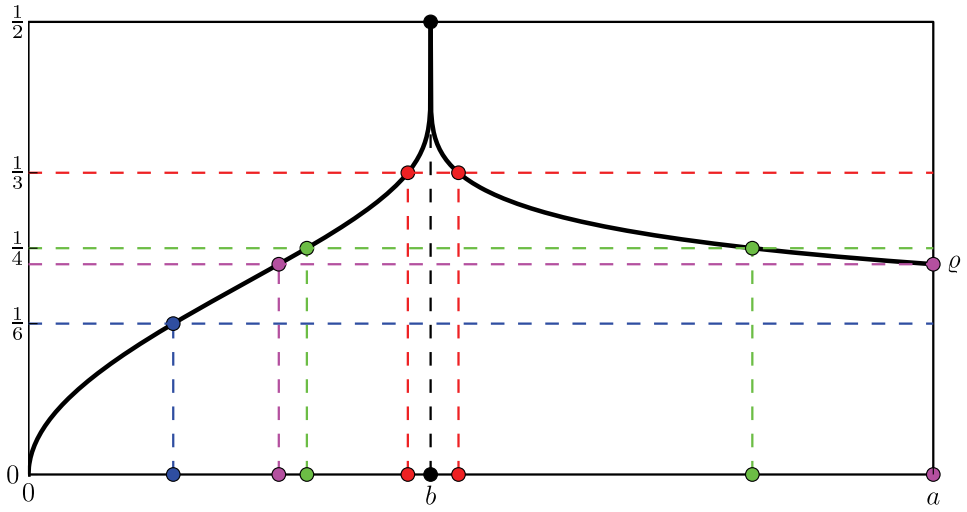

Figure 3. *The rotation function $\rho(\lambda)$ of the ellipse for $a = 1$ and $b = 4/9$. Colors are taken from Figure 2. The parameters $\lambda^0_\pm$ quickly approach b as ρ^0 tends to $1/2$.*

elliptic integrals were given in [32, 44]. We have drawn the rotation function $\rho(\lambda)$ in Figure 3; compare with [44, Fig. 2].

Proposition 10. *The rotation function $\rho : E \cup H \to \mathbb{R}$ has the following properties:*

(i) *It is analytic in $\Lambda = E \cup H$.*

(ii) *It can be continuously extended to the closed interval $\bar{\Lambda} = \Lambda \cup \partial\Lambda = [0, a]$ with*

$$\rho(0) = 0, \qquad \rho(b) = 1/2, \qquad \rho(a) = \varrho,$$

where the limit value $0 < \varrho < 1/2$ is defined by $\sin^2 \pi\varrho = b/a$.

(iii) *Let κ^G and κ^S be the positive constants given by*

$$\kappa^G = \left(\sqrt{ab} \int_b^a \frac{\mathrm{d}s}{\sqrt{s(s-b)(a-s)}} \right)^{-1}, \qquad \cosh^2 \kappa^S = \frac{a}{b}.$$

The asymptotic behavior of $\rho(\lambda)$ at the singular parameters $\lambda \in \partial\Lambda = \{0, b, a\}$ is then

1. *$\rho(\lambda) = \kappa^G \lambda^{1/2} + \mathrm{O}(\lambda^{3/2})$ as $\lambda \to 0^+$;*
2. *$\rho(\lambda) = 1/2 + \kappa^S / \log|b - \lambda| + \mathrm{O}\left(1/\log^2|b - \lambda|\right)$ as $\lambda \to b$; and*
3. *$\rho(\lambda) = \varrho + \mathrm{O}(a - \lambda)$ as $\lambda \to a^-$.*

(iv) *Given any $\rho^0 \in (\varrho, 1/2)$, let λ^0_- be the biggest parameter in E such that $\rho(\lambda^0_-) = \rho^0$, and let λ^0_+ be the smallest parameter in H such that $\rho(\lambda^0_+) = \rho^0$. Both parameters become exponentially close to the singular caustic parameter b when ρ_0 tends to $1/2$. In fact,*

$$\lambda^0_\pm = b \pm 16(a-b)\mathrm{e}^{-\kappa^S/(1/2-\rho^0)} + \mathrm{O}\left(\mathrm{e}^{-2\kappa^S/(1/2-\rho^0)}\right), \quad \rho^0 \to (1/2)^-.$$

Proof. (i) follows from Remark 1. The rest of the proof is postponed to section A.2. ∎

Remark 7. If Conjecture 1 holds, then $\rho'(\lambda)$ is positive in E and negative in H, so $\rho(\lambda)$ maps diffeomorphically E onto $(0, 1/2)$ and H onto $(\varrho, 1/2)$. In particular, the parameters λ^0_-

and λ_+^0 are unique. The conjecture remains unproven, but we shall see in Proposition 11 that $\rho(\lambda)$ is increasing in E, which suffices to check the uniqueness of λ_-^0.

Remark 8. The limit rotation number ϱ is related to the conjugate complex eigenvalues $\mathrm{e}^{\pm 2\pi\theta \mathrm{i}}$ of the elliptic two-periodic orbit. Concretely, $\theta + \varrho = 1/2$. Additionally, ϱ tends to zero when the ellipse flattens, and tends to one half when the ellipse becomes circular. That is, $\lim_{b/a\to 0^+} \varrho = 0$ and $\lim_{b/a\to 1^-} \varrho = 1/2$.

Definition 4. *The continuous extension* $\rho : [0, a] \to \mathbb{R}$ *is called the* (extended) rotation function *of the ellipse* Q.

4.4. Geometric meaning of the rotation number. Let us assume that the billiard trajectories sharing some nonsingular caustic Q_λ are m_0-periodic, so that they describe polygons with m_0 sides inscribed in the ellipse Q. Then, according to Theorem 7, (8), and Corollary 8, it turns out that $\rho(\lambda) = m_1/2m_0$ for some integers $2 \le m_1 < m_0$ such that m_1 is always even whereas m_0 can be odd only when Q_λ is an ellipse. Further, from the geometric interpretation of the frequency map presented in section 3, we know that (a) if Q_λ is an ellipse, the polygons are enclosed between Q and Q_λ and make $m_1/2$ turns around the origin; and (b) if Q_λ is a hyperbola, they are contained in the region delimited by Q and the branches of Q_λ and cross the minor axis of the ellipse m_1 times.

These interpretations can be extended to nonperiodic trajectories. Concretely,

$$\rho(\lambda) = \begin{cases} \lim_{k\to+\infty} n_k/k & \text{if } \lambda \in E, \\ \frac{1}{2}\lim_{k\to+\infty} l_k/k & \text{if } \lambda \in H, \end{cases}$$

where n_k (resp., l_k) is the number of turns around the origin (resp., crossings of the minor axis) of the first k segments of a given billiard trajectory with caustic Q_λ.

Proposition 11. *The rotation function* $\rho(\lambda)$ *is increasing in* E.

Proof. Let $\gamma : \mathbb{T} \to Q$ be a fixed parameterization of the ellipse Q. Then the billiard dynamics inside Q associated with any caustic Q_λ, $\lambda \in E$, induces a circle diffeomorphism $f_\lambda : \mathbb{T} \to \mathbb{T}$ of rotation number $\rho(\lambda)$. Let $0 < \lambda_1 < \lambda_2 < b$. The billiard trajectories sharing the small caustic Q_{λ_2} rotate faster than those sharing the big caustic Q_{λ_1}, so $F_{\lambda_1} < F_{\lambda_2}$ for any two compatible lifts F_{λ_j} of the circle diffeomorphisms f_{λ_j}. Then $\rho(\lambda_1) \le \rho(\lambda_2)$; see [27, Prop. 11.1.8]. So, $\rho(\lambda)$ is nondecreasing and, by analyticity, increasing. ∎

We have not proved that $\rho(\lambda)$ is decreasing in H because it is not easy to construct an ordered family of circle diffeomorphisms for caustic hyperbolas.

4.5. Bifurcations in parameter space. We want to determine all the ellipses $Q = \{x^2/a + y^2/b = 1\}$, $0 < b < a$, that have billiard trajectories with a prescribed rotation number $\rho^0 \in (0, 1/2)$ and with a prescribed type of caustics (ellipses or hyperbolas). We recall that the rotation function $\rho(\lambda)$ diffeomorphically maps E onto $(0, 1/2)$ and H onto $(\varrho, 1/2)$. Therefore, $\rho^0 \in \rho(E)$ for all ellipses Q, whereas

$$\rho^0 \in \rho(H) \Leftrightarrow \varrho < \rho^0 \Leftrightarrow \sin^2 \pi\varrho < \sin^2 \pi\rho^0 \Leftrightarrow b < a \sin^2 \pi\rho^0. \tag{13}$$

This shows that flat ellipses have more periodic trajectories than rounded ones. There exist similar results for triaxial ellipsoids of $\mathbb{R}^3$. See, for instance, Propositions 15 and 17.

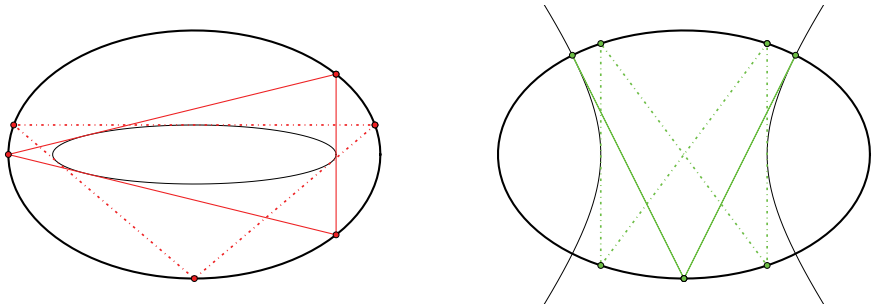

Figure 4. *Examples of symmetric nonsingular billiard trajectories with minimal periods for $a = 1$ and $b = 4/9$. Left: Period three; the caustic is an ellipse. Right: Period four; the caustic is a hyperbola. The continuous lines are reserved for the trajectories that correspond to the periodic orbits depicted in Figure 2.*

4.6. Examples of periodic trajectories with minimal periods. The billiard map associated with an ellipse has no fixed points, its only two-periodic points correspond to the oscillations along the major or minor axis, and only the trajectories with an ellipse as caustic can have odd period. Therefore, the periodic trajectories with an ellipse as caustic have period at least three, whereas those with a hyperbola as caustic have period at least four. These lower bounds are optimal; see Figure 4. To be more precise, we set

$$\lambda^*_{\mathrm{E}} = \frac{3ab}{a+b+2\sqrt{a^2-ba+b^2}}, \qquad \lambda^*_{\mathrm{H}} = \frac{ab}{a-b}. \tag{14}$$

We note that $\lambda^*_{\mathrm{E}} \in E$ for all $0 < b < a$, and $\lambda^*_{\mathrm{H}} \in H$ for all $0 < b < a/2$. The trajectories with caustic $Q_{\lambda^*_E}$ are three-periodic; the ones with caustic $Q_{\lambda^*_H}$ are four-periodic. The proof is an elementary exercise in Euclidean geometry—we leave it to the reader. Finally, we deduce from the geometric interpretation of the rotation number given before that $\rho(\lambda^*_{\mathrm{E}}) = 1/3$ and $\rho(\lambda^*_{\mathrm{H}}) = 1/4$. This second identity explains the restriction $b < a/2$; see (13).

5. Billiard inside a triaxial ellipsoid of $\mathbb{R}^3$. The previous section sets the basis of this one. Roughly speaking, we want to follow the same steps—extension of the frequency map and description of its range—in order to find the same results—bifurcations in the parameter space and minimal periodic trajectories. However, the study of ellipsoids is harder, which has two unavoidable consequences. First, statements and proofs of the analytical results are more cumbersome. Second, some results remain unproven, so we shall present numerical experiments and semianalytical arguments as support.

5.1. Confocal caustics. The caustics of a billiard inside a triaxial ellipsoid are described in several places. The representation of the caustic space shown in Figure 5 can also be found in [31, 45, 19].

We write the triaxial ellipsoid as

$$Q = \left\{ (x,y,z) \in \mathbb{R}^3 : \frac{x^2}{a} + \frac{y^2}{b} + \frac{z^2}{c} = 1 \right\}, \qquad a > b > c > 0.$$

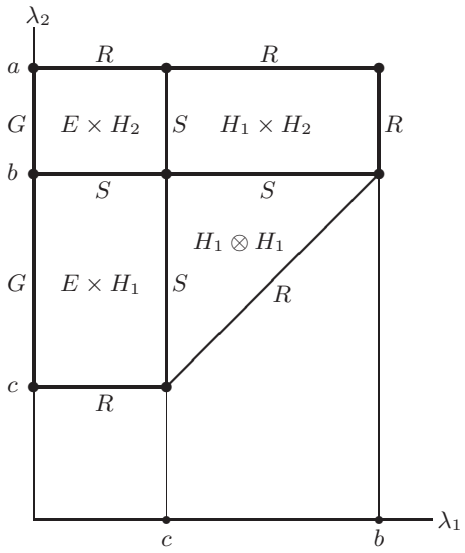

Figure 5. *The nonsingular caustic space* $\Lambda = (E \times H_1) \cup (E \times H_2) \cup (H_1 \otimes H_1) \cup (H_1 \times H_2)$ *with its border* $\partial\Lambda = G \cup R \cup S \cup \Lambda^0$.

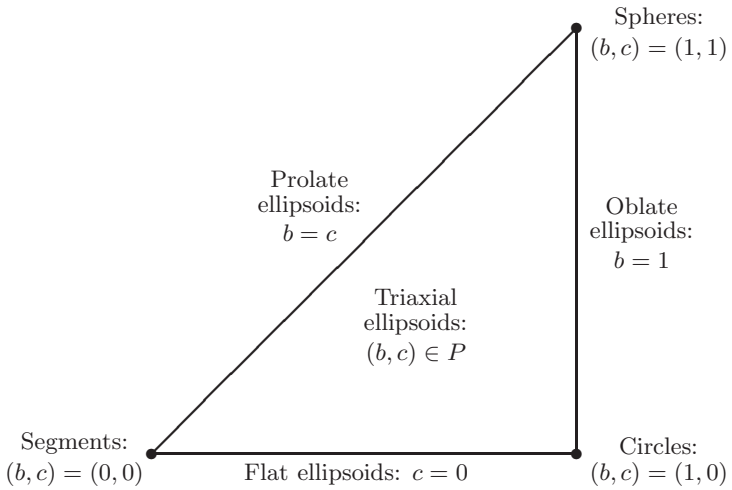

Figure 6. *The triangular parameter space* P.

We could assume, again without loss of generality, that $a = 1$. Then the parameter space of triaxial ellipsoids in $\mathbb{R}^3$ can be represented as the triangle

$$P = \left\{(b, c) \in \mathbb{R}^2 : 0 < c < b < 1\right\}, \tag{15}$$

whose edges represent ellipsoids with a symmetry of revolution (oblate and prolate ones) or flat ellipsoids, as illustrated in Figure 6. We shall write the statements of the main results for arbitrary values of a, but we shall take $a = 1$ in the pictures.

From Theorem 2, we know that any nonsingular billiard trajectory inside the ellipsoid Q

is tangent to *two* distinct nonsingular caustics of the confocal family

$$Q_\lambda = \left\{(x,y,z) \in \mathbb{R}^3 : \frac{x^2}{a-\lambda} + \frac{y^2}{b-\lambda} + \frac{z^2}{c-\lambda} = 1\right\}.$$

The caustic Q_λ is an ellipsoid for $\lambda \in E$, a one-sheet hyperboloid when $\lambda \in H_1$, and a two-sheet hyperboloid if $\lambda \in H_2$, where

$$E = (0,c), \qquad H_1 = (c,b), \qquad H_2 = (b,a).$$

In order to have a clearer picture of how these caustics change, let us explain the situation when λ approaches the singular values c, b, or a. First, when $\lambda \to c^-$ (resp., $\lambda \to c^+$), the caustic Q_λ flattens into the region of the coordinate plane $\pi_z = \{z = 0\}$ enclosed by (resp., outside) the *focal ellipse*

$$Q_c^z = \left\{(x,y,0) \in \mathbb{R}^3 : \frac{x^2}{a-c} + \frac{y^2}{b-c} = 1\right\}. \tag{16}$$

Second, when $\lambda \to b^-$ (resp., $\lambda \to b^+$), the caustic Q_λ flattens into the region of the coordinate plane $\pi_y = \{y = 0\}$ between (resp., outside) the branches of the *focal hyperbola*

$$Q_b^y = \left\{(x,0,z) \in \mathbb{R}^3 : \frac{x^2}{a-b} - \frac{z^2}{b-c} = 1\right\}.$$

Third, the caustic flattens into the whole coordinate plane $\pi_x = \{x = 0\}$ when $\lambda \to a^-$.

We recall that not all combinations of caustics can exist. For instance, both caustics cannot be ellipsoids. The four possible combinations are denoted by EH1, H1H1, EH2, and H1H2. Hence, the caustic parameter $\lambda = (\lambda_1, \lambda_2)$ belongs to the nonsingular caustic space

$$\Lambda = (E \times H_1) \cup (H_1 \otimes H_1) \cup (E \times H_2) \cup (H_1 \times H_2), \tag{17}$$

where $H_1 \otimes H_1 = \{\lambda \in H_1 \times H_1 : \lambda_1 < \lambda_2\}$. For instance, $\lambda \in E \times H_1$ for trajectories of type EH1, which means that Q_{λ_1} is an ellipsoid and Q_{λ_2} is a one-sheet hyperboloid.

5.2. The extension of the frequency map. To begin with, we extend the frequency map $\omega : \Lambda \to \mathbb{R}^2$ to the borders of the four components of the caustic space (17), in the same way that the rotation number was extended to the endpoints of the two caustic intervals (10). The extension depends strongly on the "piece" of the border under consideration. Hence, we need some notation for such pieces.

The set Λ is the union of three open rectangles and one open isosceles rectangular triangle. In total, Λ has eleven edges and eight vertexes. We consider the partitions

$$\partial\Lambda = \Lambda^0 \cup \Lambda^1, \qquad \Lambda^1 = G \cup R \cup S,$$

where Λ^1 is the set of edges, Λ^0 is the set of vertexes, and S, G, and R are the sets formed by the four inner edges, the two left edges, and the remaining five edges, respectively. See Figure 5. We shall see that the frequency map is quite singular (in fact, exponentially sharp)

at the four edges in S, quite regular at the five edges in R, and somehow related to the geodesic flow on the ellipsoid Q at the two edges in G. That motivates the notation.

Next, we shall check that the frequency map of the triaxial ellipsoid Q can be continuously extended to the borders of the caustic space in such a way that its values on the edges and vertexes can be expressed in terms of exactly six functions of one variable that "glue" well. Three of them are the extended rotation functions associated with the three ellipses obtained by sectioning Q with the coordinate planes π_{x}, π_{y}, and π_{z}. That is, they are the functions $\rho_{\mathrm{x}} : [0, b] \to \mathbb{R}$, $\rho_{\mathrm{y}} : [0, a] \to \mathbb{R}$, and $\rho_{\mathrm{z}} : [0, a] \to \mathbb{R}$ defined as

$$\rho_{\mathrm{x}}(\lambda) = \rho(\lambda; c, b), \qquad \rho_{\mathrm{y}}(\lambda) = \rho(\lambda; c, a), \qquad \rho_{\mathrm{z}}(\lambda) = \rho(\lambda; b, a),$$

using the notation in (12). The other three functions are defined in terms of the former ones as follows. Let $\underline{m} = \min(\lambda, c)$ and $\overline{m} = \max(\lambda, c)$. Let $T_{\mathrm{x}}(s) = (\lambda - s)(c - s)(b - s)$, $T_{\mathrm{y}}(s) = (c-s)(\lambda-s)(a-s)$, and $T_{\mathrm{z}}(s) = (\underline{m}-s)(b-s)(a-s)$. Then we consider the functions $\nu_{\mathrm{x}} : [0, b] \to \mathbb{R}$, $\nu_{\mathrm{y}} : [b, a] \to \mathbb{R}$, and $\nu_{\mathrm{z}} : [0, b] \to \mathbb{R}$ defined by the identities

$$\begin{aligned}
&\int_0^{\underline{m}} \frac{\mathrm{d}s}{(a-s)\sqrt{T_{\mathrm{x}}(s)}} - 2\rho_{\mathrm{x}}(\lambda) \int_{\overline{m}}^{b} \frac{\mathrm{d}s}{(a-s)\sqrt{T_{\mathrm{x}}(s)}} + \frac{2\pi\nu_{\mathrm{x}}(\lambda)}{\sqrt{-T_{\mathrm{x}}(a)}} = 0,\\
&\int_0^{c} \frac{\mathrm{d}s}{(b-s)\sqrt{T_{\mathrm{y}}(s)}} + 2\rho_{\mathrm{y}}(\lambda) \int_{\lambda}^{a} \frac{\mathrm{d}s}{(s-b)\sqrt{T_{\mathrm{y}}(s)}} - \frac{2\pi\nu_{\mathrm{y}}(\lambda)}{\sqrt{-T_{\mathrm{y}}(b)}} = 0,\\
&\int_0^{\underline{m}} \frac{\mathrm{d}s}{(\overline{m}-s)\sqrt{T_{\mathrm{z}}(s)}} + 2\rho_{\mathrm{z}}(\underline{m}) \int_{b}^{a} \frac{\mathrm{d}s}{(s-\overline{m})\sqrt{T_{\mathrm{z}}(s)}} - \frac{2\pi\nu_{\mathrm{z}}(\lambda)}{\sqrt{-T_{\mathrm{z}}(\overline{m})}} = 0.
\end{aligned}$$

Lemma 12. *The functions ν_{x}, ν_{y}, and ν_{z} have the following properties:*

(i) *They are analytic in $E \cup H_1$, H_2, and $E \cup H_1$, respectively.*
(ii) *They can be continuously extended to $[0, b]$, $[b, a]$, and $[0, b]$, respectively.*
(iii) *Their asymptotic behavior at the endpoints $\lambda \in \partial E \cup \partial H_1 \cup \partial H_2 = \{0, c, b, a\}$ is*
1. $\nu_{\mathrm{x}}(\lambda) = \mathrm{O}(\lambda^{1/2})$ *as* $\lambda \to 0^+$;
2. $\nu_{\mathrm{z}}(\lambda) = \mathrm{O}(\lambda^{1/2})$ *as* $\lambda \to 0^+$;
3. $\nu_{\mathrm{x}}(\lambda) = \rho_{\mathrm{z}}(a) + \mathrm{O}\left(1/\log|c - \lambda|\right)$ *as* $\lambda \to c$;
4. $\nu_{\mathrm{z}}(\lambda) = 1/2 + \mathrm{O}\left(|\lambda - c|^{1/2}\right)$ *as* $\lambda \to c$;
5. $\nu_{\mathrm{x}}(\lambda) = \rho_{\mathrm{y}}(a) + \mathrm{O}(b - \lambda)$ *as* $\lambda \to b^-$;
6. $\nu_{\mathrm{z}}(\lambda) = \rho_{\mathrm{z}}(c) + \mathrm{O}\left((b - \lambda)^{1/2}\right)$ *as* $\lambda \to b^-$;
7. $\nu_{\mathrm{y}}(\lambda) = \rho_{\mathrm{z}}(c) + \mathrm{O}\left((\lambda - b)^{1/2}\right)$ *as* $\lambda \to b^+$; *and*
8. $\nu_{\mathrm{y}}(\lambda) = \rho_{\mathrm{x}}(b) + \mathrm{O}(a - \lambda)$ *as* $\lambda \to a^-$.

Proof. We know that the function $\rho_{\mathrm{x}}(\lambda) = \rho(\lambda; c, b)$ is analytic in λ, c, and b, as long as $0 < c < b$ and $\lambda \in E \cup H_1$. Further, the integrand $(a - s)^{-1}(T_{\mathrm{x}}(s))^{-1/2}$ is analytic with respect to the variable of integration s in the intervals of integration $(0, \underline{m})$ and $(\overline{m}, b)$, and with respect to the parameters λ, c, b, and a, as long as $0 < c < b < a$ and $\lambda \in E \cup H_1$. Hence, the function $\nu_{\mathrm{x}}(\lambda) = \nu_{\mathrm{x}}(\lambda; c, b, a)$ is analytic in its four variables as long as $0 < c < b < a$ and $\lambda \in E \cup H_1$. The analyticity of ν_{y} and ν_{z} follows from similar arguments.

The study of the asymptotic behavior of the functions ν_{x}, ν_{y}, and ν_{z} has been deferred to Appendices A.9, A.10, and A.11, respectively. ∎

Remark 9. We have numerically observed that ν_{x} and ν_{z} are increasing in E and decreasing in H_1, whereas ν_{y} is increasing in H_2, but we have not been able to prove it.

Theorem 13. *The frequency map $\omega : \Lambda \to \mathbb{R}^2$ has the following properties:*

(i) *It is analytic in Λ.*

(ii) *It can be continuously extended to the border $\partial\Lambda$, and the extension has the form given as follows:*

1. $\omega(0, \lambda_2) = (0, 0)$, *for* $c \le \lambda_2 \le b$;
2. $\omega(\lambda_1, b) = (\rho_{\mathrm{y}}(\lambda_1), \rho_{\mathrm{y}}(\lambda_1))$, *for* $0 \le \lambda_1 \le b$;
3. $\omega(c, \lambda_2) = (1/2, \rho_{\mathrm{z}}(\lambda_2))$, *for* $c \le \lambda_2 \le a$;
4. $\omega(\lambda_1, a) = (\rho_{\mathrm{x}}(\lambda_1), \nu_{\mathrm{x}}(\lambda_1))$, *for* $0 \le \lambda_1 \le b$;
5. $\omega(b, \lambda_2) = (\nu_{\mathrm{y}}(\lambda_2), \rho_{\mathrm{y}}(\lambda_2))$, *for* $b \le \lambda_2 \le a$;
6. $\omega(\lambda_1, c) = (\nu_{\mathrm{z}}(\lambda_1), \rho_{\mathrm{z}}(\lambda_1))$, *for* $0 \le \lambda_1 \le c$; *and*
7. $\omega(\lambda_1, \lambda_1) = (\nu_{\mathrm{z}}(\lambda_1), \rho_{\mathrm{z}}(c))$, *for* $c \le \lambda_1 \le b$.

(iii) *Its asymptotic behavior at the eleven edges in $\Lambda^1 = G \cup S \cup R$ is as follows:*

1. $\omega(\lambda_1, \lambda_2) = \kappa^G(\lambda_2)\lambda_1^{1/2} + \mathrm{O}(\lambda_1^{3/2})$ *as* $\lambda_1 \to 0^+$;
2. $\omega(\lambda_1, \lambda_2) - \omega(c, \lambda_2) \asymp \kappa^S(c, \lambda_2)/\log|c - \lambda_1|$ *as* $\lambda_1 \to c$;
3. $\omega(\lambda_1, \lambda_2) - \omega(\lambda_1, b) \asymp \kappa^S(\lambda_1, b)/\log|b - \lambda_2|$ *as* $\lambda_2 \to b$; *and*
4. $\omega(\lambda) - \omega(\lambda^R) = \mathrm{O}(\lambda - \lambda^R)$ *as* $\lambda \to \lambda^R \in R$

for some analytic functions $\kappa^G : H_1 \cup H_2 \to \mathbb{R}^2_+$ and $\kappa^S : S \to \mathbb{R}^2$.

(iv) *Its asymptotic behavior at the eight vertexes in Λ^0 is as follows:*

1. $\omega(\lambda_1, \lambda_2) = \mathrm{O}(\lambda_1^{1/2})$ *as* $(\lambda_1, \lambda_2) \to (0^+, c^+)$;
2. $\omega(\lambda_1, \lambda_2) = \mathrm{O}(\lambda_1^{1/2})$ *as* $(\lambda_1, \lambda_2) \to (0^+, b)$;
3. $\omega(\lambda_1, \lambda_2) = \mathrm{O}(\lambda_1^{1/2})$ *as* $(\lambda_1, \lambda_2) \to (0^+, a^-)$;
4. $\omega(\lambda_1, \lambda_2) = (1/2, \rho_{\mathrm{z}}(c)) + \mathrm{O}(1/\log|c - \lambda_1|, \lambda_2 - c)$ *as* $(\lambda_1, \lambda_2) \to (c, c^+)$;
5. $\omega(\lambda_1, \lambda_2) = (1/2, 1/2) + \mathrm{O}(1/\log|c - \lambda_1|, 1/\log|b - \lambda_2|)$ *as* $(\lambda_1, \lambda_2) \to (c, b)$;
6. $\omega(\lambda_1, \lambda_2) = (1/2, \rho_{\mathrm{z}}(a)) + \mathrm{O}(1/\log|c - \lambda_1|, a - \lambda_2)$ *as* $(\lambda_1, \lambda_2) \to (c, a^-)$;
7. $\omega(\lambda_1, \lambda_2) = (\rho_{\mathrm{y}}(b), \rho_{\mathrm{y}}(b)) + \mathrm{O}(b - \lambda_1, 1/\log|b - \lambda_2|)$ *as* $(\lambda_1, \lambda_2) \to (b^-, b)$; *and*
8. $\omega(\lambda_1, \lambda_2) = (\rho_{\mathrm{x}}(b), \rho_{\mathrm{y}}(a)) + \mathrm{O}(b - \lambda_1, a - \lambda_2)$ *as* $(\lambda_1, \lambda_2) \to (b^-, a^-)$.

Proof. Once we have fixed the parameters $a > b > c > 0$ of the ellipsoid and the pair of caustic parameters λ_1 and λ_2, we set

$$\{c_1, \dots, c_5\} = \{a, b, c\} \cup \{\lambda_1, \lambda_2\}, \qquad c_0 := 0 < c_1 < \cdots < c_5.$$

Four configurations are possible; see Figure 7. We said in Remark 1 that the frequency is analytic in $c_1, \dots, c_5$, provided that $0 < c_1 < \cdots < c_5$. In particular, this implies that the frequency is analytic in the caustic parameter, provided that it belongs to Λ.

The frequency map is expressed in terms of six hyperelliptic integrals over the intervals $(0, c_1)$, (c_2, c_3), and (c_4, c_5)—represented in thick lines in Figure 7; see Definition 2. We face its asymptotic behavior at the border $\partial\Lambda = \Lambda^0 \cup \Lambda^1$, which requires the study of the asymptotic behavior of the six hyperelliptic integrals when some interval defined by the ordered sequence $0 < c_1 < \cdots < c_5$ collapses to a point. Therefore, there are exactly five simple collapses. The collapse of the first interval is called the *geodesic flow limit*, $c_1 \to 0^+$; the collapse of the second or fourth intervals is called *singular*, $c_2 - c_1 \to 0^+$ or $c_4 - c_3 \to 0^+$; and the collapse of the third or fifth intervals is called *regular*, $c_3 - c_2 \to 0^+$ or $c_5 - c_4 \to 0^+$. Thus, regular collapses imply that the interval of integration of a couple of hyperelliptic integrals collapses to a point, whereas singular collapses imply the connection of two consecutive intervals of integration.

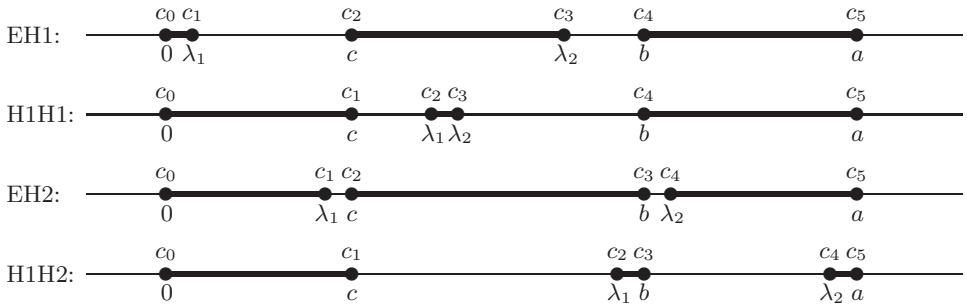

Figure 7. *The four possible configurations of the ordered sequence* $0 < c_1 < \cdots < c_5$. *Thick lines denote intervals of integration. Each one of the displayed configurations illustrates some collapse: geodesic flow limit (and type EH1), simple regular collapse (and type H1H1), double singular collapse (and type EH2), and double regular collapse (and type H1H2).*

See Figure 7. It is immediate to check that this terminology agrees with the partition $\Lambda^1 = G \cup R \cup S$, whereas double collapses—that is, two simultaneous simple collapses—correspond to the eight vertexes in Λ^0.

The asymptotic behavior of the frequency map at the eleven edges in $\Lambda^1 = G \cup R \cup S$ is deduced from several results described in Appendix A. In short, some technical lemmas are listed in Appendix A.1, some notation is introduced in Appendix A.3, the geodesic flow limit is studied in Appendix A.4, simple regular collapses are analyzed in Appendix A.5, and simple singular collapses are computed in Appendix A.6. For instance, one can trace the definition of the functions ν_{x}, ν_{y}, and ν_{z} to (23). The reader is encouraged to consult the appendix; here, we just note that Appendix A deals with the general high-dimensional setup, since the computations do not become substantially more involved when the dimension is increased.

The computations regarding the vertexes have also been relegated to Appendix A, although for the sake of brevity we have written out only the computations for two vertexes: vertex $\lambda = (c, b)$ in Appendix A.8—which corresponds to the unique double singular collapse—and vertex $\lambda = (b, a)$ in Appendix A.7—which corresponds to the unique double regular collapse. The study of the remaining six vertexes does not require additional ideas. For instance, the three vertexes related to the geodesic flow limit can be simultaneously dealt with simply by using Lemma 22, which ensures that the hyperelliptic integrals over $(c_0, c_1) = (0, \lambda_1)$ are $\mathrm{O}(\lambda_1^{1/2})$ as $\lambda_1 \to 0^+$.

Finally, we realize that the extended frequency map $\omega : \bar{\Lambda} \to \mathbb{R}^2$ is continuous because the extensions "glue" well at the eight vertexes; see Lemma 12. For instance, let us consider the vertex (b, b). We obtain from the three statements of Theorem 13 regarding this vertex that

$$\omega(b, b) = (\rho_{\mathrm{y}}(b), \rho_{\mathrm{y}}(b)) = (\nu_{\mathrm{y}}(b), \rho_{\mathrm{y}}(b)) = (\nu_{\mathrm{z}}(b), \rho_{\mathrm{z}}(c)),$$

which is consistent: $\nu_{\mathrm{y}}(b) = \nu_{\mathrm{z}}(b) = \rho_{\mathrm{z}}(c) = \rho(c; b, a) = \rho(b; c, a) = \rho_{\mathrm{y}}(b)$. ∎

Definition 5. *The continuous extension* $\omega : \bar{\Lambda} \to \mathbb{R}^2$ *is called the* (extended) frequency map *of the ellipsoid* Q.

The origin of the terminology "geodesic flow limit" can be explained as follows. The phase space of the geodesic flow on an triaxial ellipsoid $Q \subset \mathbb{R}^3$ was completely described by Knörrer [30]. Any nonsingular geodesic on Q oscillates between two symmetric curvature lines

obtained by intersecting Q with some hyperboloid Q_λ, $\lambda \in H_1 \cup H_2$. The rotation number of those oscillations is the quotient

$$\rho^G(\lambda) = \frac{\int_c^{\min(b,\lambda)} \frac{s\mathrm{d}s}{\sqrt{T^G(s)}}}{\int_{\max(b,\lambda)}^a \frac{s\mathrm{d}s}{\sqrt{T^G(s)}}}, \qquad T^G(s) = -s(\lambda - s)(c - s)(b - s)(a - s);$$

see [19, sect. 4.1]. This rotation number $\rho^G(\lambda)$ can be continuously extended to the closed interval $[c, a]$ with $\rho^G(b) = 1$. On the other hand, the geodesic flow on the ellipsoid Q with caustic lines $Q \cap Q_{\lambda_2}$ can be obtained as a limit of the billiard dynamics inside Q when its first caustic Q_{λ_1} approaches Q, that is, when $\lambda_1 \to 0^+$, so that $(\lambda_1, \lambda_2) \to G$. Therefore, it is natural to look for a relation between the function $\kappa^G = (\kappa_1^G, \kappa_2^G) : H_1 \cup H_2 \to \mathbb{R}_+^2$ and the rotation number $\rho^G : H_1 \cup H_2 \to \mathbb{R}_+$.

Lemma 14. *$\rho^G = \kappa_2^G/\kappa_1^G$, so $\omega_2(\lambda_1, \lambda_2)/\omega_1(\lambda_1, \lambda_2) = \rho^G(\lambda_2) + \mathrm{O}(\lambda_1)$ as $\lambda_1 \to 0^+$.*

Proof. In Appendix A.4 we will check that κ^G is the unique solution of the linear system

$$2 \begin{pmatrix} K_{01}^G & -K_{02}^G \\ K_{11}^G & -K_{12}^G \end{pmatrix} \begin{pmatrix} \kappa_1^G \\ \kappa_2^G \end{pmatrix} = \begin{pmatrix} K_{00}^G \\ 0 \end{pmatrix},$$

where $K_{ij}^G = \int_{c_{2j}}^{c_{2j+1}} (T^G(s))^{-1/2} s^i \mathrm{d}s$, $K_{00}^G = 2(abc\lambda)^{-1/2}$, and $\{c_2, c_3, c_4, c_5\} = \{a, b, c, \lambda\}$ with $c_2 < c_3 < c_4 < c_5$. Therefore, since $\lambda \in H_1 \cup H_2$, it turns out that $c_2 = c$, $c_3 = \min(b, \lambda)$, $c_4 = \max(b, \lambda)$, and $c_5 = a$. Finally, $\kappa_2^G/\kappa_1^G = K_{11}^G/K_{12}^G = \rho^G$. ∎

5.3. On the Jacobian of the frequency map. We present the numerical experiments on Conjecture 1. We have computed the Jacobian of the frequency map

$$J : \Lambda \to \mathbb{R}, \qquad J(\lambda) := \det \left(\frac{\partial \omega_j}{\partial \lambda_i}(\lambda) \right)_{i,j=1,2}$$

for several ellipsoids, in order to check that it never vanishes. Its visualization close to the four inner edges labelled with the letter S in Figure 5 has a technical difficulty. To understand this fact, one can look at the graph of the rotation number $\rho(\lambda)$ shown in Figure 3. The derivative $\rho'(\lambda)$ explodes at $\lambda = b$, which would make its visual representation difficult. The problem is worse in the spatial case, because the frequency map has the same kind of "inverse logarithm" singularity at the four inner edges instead of at a single point.

We overcome the visualization problem by representing the normalized Jacobian:

$$J_* : \Lambda \to [0, 1], \qquad J_*(\lambda) = (1 - \exp(-|J(\lambda)|))^{1/4}.$$

The exponential function is intended to cancel the exponentially sharp behavior of the Jacobian at the inner edges. The exponent $1/4$ has been chosen by trial and error to obtain more informative plots. The normalized Jacobian ranges over the interval $[0, 1]$. We note that $J_* = 0 \Leftrightarrow J = 0$ and $J_* = 1 \Leftrightarrow |J| = \infty$. The results are shown in Figure 8. In the upper left corner, we have displayed the parameter space P, introduced in (15) and sketched in Figure 6. We study the eight ellipsoids that correspond to the eight points in P labelled from 1 to 8. In particular, we have chosen at least one sample of each "kind" of ellipsoid: 1. standard, 2.

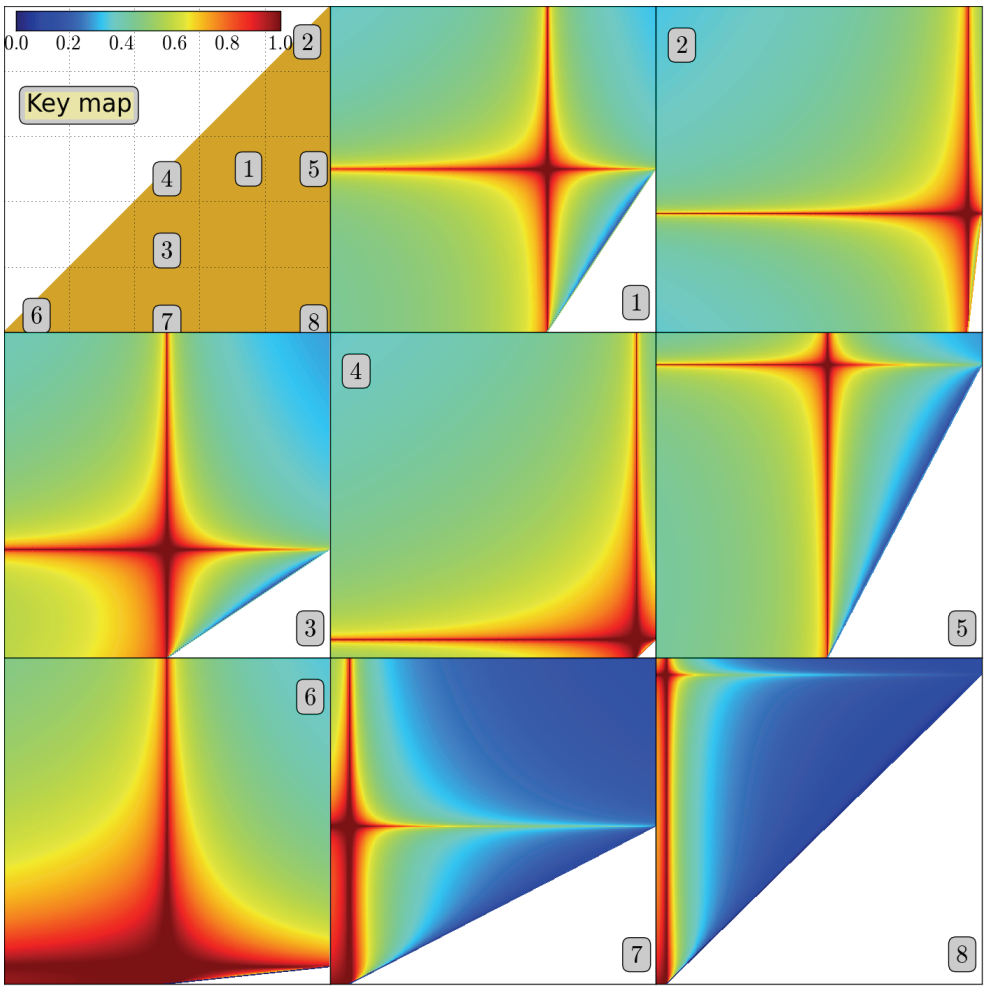

Figure 8. *The normalized Jacobian $J_* : \Lambda \to [0,1]$ of the frequency map for eight different ellipsoids.*

almost spheric, 3. standard, 4. almost prolate, 5. almost oblate, 6. close to a segment, 7. close to a flat solid ellipse, and 8. close to a flat circle. The color palette is a classical one: cold colors represent low values, hot colors represent high values. The neighborhood of the inner edges is always a "hot" region; that is, the Jacobian is always big on that region. In contrast, the Jacobian tends to zero close to the hypotenuse of the $H_1 \otimes H_1$ region. This can be seen from a symmetry reasoning. Furthermore, the Jacobian never vanishes, not even in the cases 7 and 8, which correspond to almost flat ellipsoids.

5.4. The range of the frequency map. We recall that if the two conjectures stated in section 3.2 hold, then the components of the frequency map are ordered as stated in (9). Thus, the range of the frequency map should be a subset of the frequency space

$$\Omega = \left\{(\omega_1, \omega_2) \in \mathbb{R}^2 : 0 < \omega_2 < \omega_1 < 1/2\right\}.$$

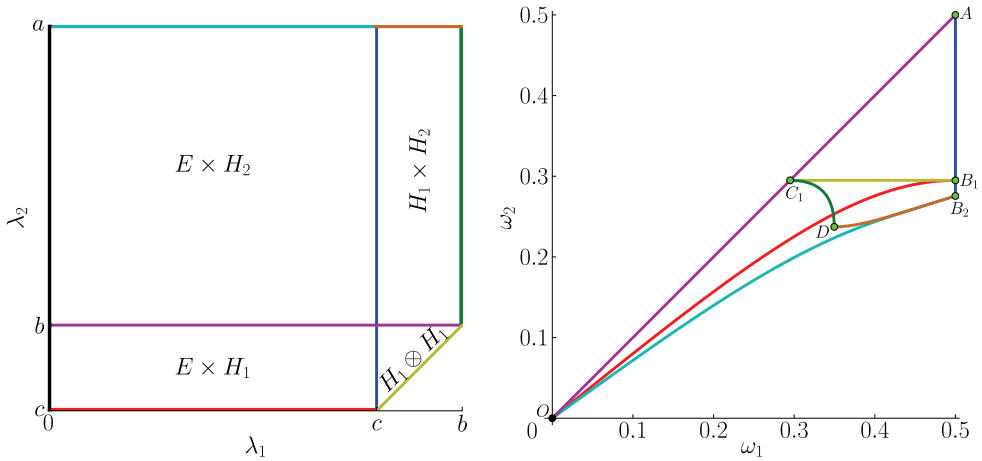

Figure 9. *The extended frequency map* $\omega : \bar{\Lambda} \to \bar{\Omega}$ *on the edges of the caustic space for* $a = 1$, $b = 0.58$, *and* $c = 0.46$. *Left: Caustic space. Right: Frequency space.*

We visualize in Figure 9 how each edge of the caustic space is mapped onto the frequency space. All the depicted curves have been numerically computed from exact formulae given in Theorem 13. We have represented the caustic space Λ in the left panel, and the frequency space Ω in the right panel. Each colored segment in the caustic space is mapped onto the curve of the same color in the frequency space. The black segment in Λ—which represents the geodesic flow limit—is mapped onto the origin $O = (0, 0)$. The point (c, b) is mapped onto $A = (1/2, 1/2)$. The images of the magenta and blue segments are folded at this point A. Henceforth, $[AB]$ stands for the segment with endpoints A and B, and $\triangle[ABC]$ stands for the interior of the triangle with vertexes A, B, C. We see that $\omega(E \times H_1)$ is enclosed by the magenta segment $[OA]$, the blue segment $[AB_1]$, and a red smooth curve from B_1 to O; $\omega(H_1 \otimes H_1) = \triangle[AB_1C_1]$; $\omega(E \times H_2)$ is enclosed by the magenta segment $[OA]$, the blue segment $[AB_2]$, and a cyan smooth curve from B_2 to O; and $\omega(H_1 \times H_2)$ is enclosed by the magenta segment $[C_1A]$, the blue segment $[AB_2]$, a brown smooth curve from B_2 to D, and a green smooth curve from D to C_1.

The points A, B_1, B_2, C_1, and D can be explicitly expressed in terms of the parameters of the ellipsoid Q. Let $0 < \varrho_x, \varrho_y, \varrho_z, \varrho_* < 1/2$ be the quantities defined by

$$\sin^2 \pi\varrho_x = c/b, \quad \sin^2 \pi\varrho_y = c/a, \quad \sin^2 \pi\varrho_z = b/a, \quad \varrho_* = \rho(c; b, a), \tag{18}$$

where $\rho(\lambda; b, a)$ is the rotation number (12). From the formulae contained in Theorem 13, we get that $A = (1/2, 1/2)$, $B_1 = (1/2, \varrho_*)$, $B_2 = (1/2, \varrho_z)$, $C_1 = (\varrho_*, \varrho_*)$, and $D = (\varrho_x, \varrho_y)$. We note that $D \in \Omega$, since $\varrho_y < \varrho_x$. In fact, $\varrho_y < \varrho_z$ and $\varrho_y < \varrho_* < \varrho_x$, although we do not have a rigorous proof of the inequalities involving ϱ_*. The four quantities defined in (18) can be interpreted in terms of the restriction of the billiard dynamics to suitable planar sections of the original ellipsoid. For instance, ϱ_* is the rotation number of the trajectories contained in the section by the plane π_z whose caustic is the focal ellipse (16).

We now give some numerical estimates on the size and the shape of the four ranges.

Numerical Result 2. *Let* $0 < \varrho_x, \varrho_y, \varrho_z, \varrho_* < 1/2$ *be the quantities defined in* (18). *Let*

$\varrho = \max(\varrho_*, \varrho_z)$. *Let* $O = (0,0)$, $A = (1/2, 1/2)$, $B_1 = (1/2, \varrho_*)$, $B_2 = (1/2, \varrho_z)$, $B = (1/2, \varrho)$, $C_1 = (\varrho_*, \varrho_*)$, $C_2 = (\varrho_z, \varrho_z)$, $C = (\varrho, \varrho)$, *and* $D = (\varrho_x, \varrho_y)$. *Then we have the following:*

(i) $\triangle[AB_jC_j] \subsetneq \omega(E \times H_j) \subsetneq \triangle[AB_jO]$ *for* $j = 1, 2$*;*

(ii) $\omega(H_1 \otimes H_1) = \triangle[AB_1C_1]$*; and*

(iii) $\triangle[ABC] \subsetneq \omega(H_1 \times H_2) \subsetneq \omega(E \times H_2) \cap \{(\omega_1, \omega_2) \in \Omega : \omega_1 > \varrho_*, \omega_2 > \varrho_y\}$.

Next, we investigate some practical consequences of these estimates. To begin with, let us present four simple criteria for deciding whether the ellipsoid has billiard trajectories of frequency $\omega^0 = (\omega_1^0, \omega_2^0) \in \Omega$ and of caustic type EH1, H1H1, EH2, or H1H2. Compare with the criterion for the existence of billiard trajectories inside an ellipse with rotation number $\rho^0 \in (0, 1/2)$ and a caustic hyperbola given in (13).

Proposition 15. *If Numerical Result 2 holds, the following criteria can be applied:*

(i) *If* $\omega_2^0 > \rho(c; b, a)$, $\omega^0 \in \omega(E \times H_1)$. *If* $\omega_2^0/2\omega_1^0 \le \rho(c; b, a)$, $\omega^0 \notin \omega(E \times H_1)$.

(ii) $\omega^0 \in \omega(H_1 \otimes H_1)$ *if and only if* $\omega_2^0 > \rho(c; b, a)$.

(iii) *If* $b < a \sin^2 \pi\omega_2^0$, $\omega^0 \in \omega(E \times H_2)$. *If* $b \ge a \sin^2(\pi\omega_2^0/2\omega_1^0)$, $\omega^0 \notin \omega(E \times H_2)$.

(iv) *If* $\omega_2^0 > \rho(c; b, a)$ *and* $b < a \sin^2 \pi\omega_2^0$, *then* $\omega^0 \in \omega(H_1 \times H_2)$. *If* $\omega_1^0 \le \rho(c; b, a)$ *or* $c \ge a \sin^2 \pi\omega_2^0$ *or* $b \ge a \sin^2(\pi\omega_2^0/2\omega_1^0)$, *then* $\omega^0 \notin \omega(H_1 \times H_2)$.

Hence, there exist billiard trajectories of the four caustic types when ω_2^0 *is big enough:* $\omega_2^0 > \rho(c; b, a)$ *and* $\sin^2 \pi\omega_2^0 > b/a$. *In contrast, there do not exist any such trajectories when* ω_2^0/ω_1^0 *is small enough:* $\omega_2^0/\omega_1^0 \le 2\rho(c; b, a)$ *and* $\sin^2(\pi\omega_2^0/2\omega_1^0) \le b/a$.

Proof. Criteria (i) and (iii) follow from $\triangle[AB_jC_j] \subset \omega(E \times H_j) \subset \triangle[AB_jO]$, $j = 1, 2$. (ii) follows from the identity $\omega(H_1 \otimes H_1) = \triangle[AB_1C_1]$. Finally, (iv) follows from Numerical Result 2(iii). ∎

We can also understand how the range of the frequency map depends on the shape of the ellipsoid. It suffices to see how the quantities ϱ_x, ϱ_y, ϱ_z, and ϱ_* depend on the parameters $0 < c < b < a$. On the one hand, if the ellipsoid flattens—that is, if c decreases, but a and b remain fixed—then ϱ_* decreases, so $\omega(E \times H_1)$ and $\omega(H_1 \otimes H_1)$ expand. Indeed, both ranges tend to cover the whole space Ω for flat ellipsoids, $c \to 0^+$, whereas they collapse to the empty set for prolate ellipsoids, $c \to b^-$. On the other hand, if the ellipsoid becomes more oblate—that is, if b increases, but a and c remain fixed—then ϱ_z increases, so $\omega(E \times H_2)$ contracts. Indeed, $\omega(E \times H_2)$ tends to cover Ω for "segments," $b \to 0^+$, but collapses to the empty set for oblate ellipsoids, $b \to a^-$. The behavior of $\omega(H_1 \times H_2)$ is more complicated, because its vertex $D = (\varrho_x, \varrho_y)$ can be at any point of the frequency space Ω; see (18). Anyway, if the ellipsoid becomes spheric—that is, c and b approach a—then ϱ_z and ϱ_* tend to one half, so B_j tends to A, and the four ranges collapse to the empty set. This means that *the more spheric is an ellipsoid, the poorer are its four types of nonsingular billiard dynamics.* Some of the criteria stated in Propositions 15 and 17 quantify this general principle.

The ranges of the frequency map for eight different ellipsoids are shown in Figure 10. In the upper left picture, we have again marked the ellipsoids as points in the parameter space (15). The image sets $\omega(E \times H_1)$, $\omega(H_1 \otimes H_1)$, $\omega(E \times H_2)$, and $\omega(H_1 \times H_2)$ are depicted in yellow, green, magenta, and blue, respectively. The transparency allows us to visualize all four sets simultaneously. We can check all their properties as stated in Numerical Result 2, together with those regarding their dependence on the shape of the ellipsoids. Blue dots correspond to rational frequencies with small common denominators.

In the previous paragraphs the range of the frequency map has been described by mixing

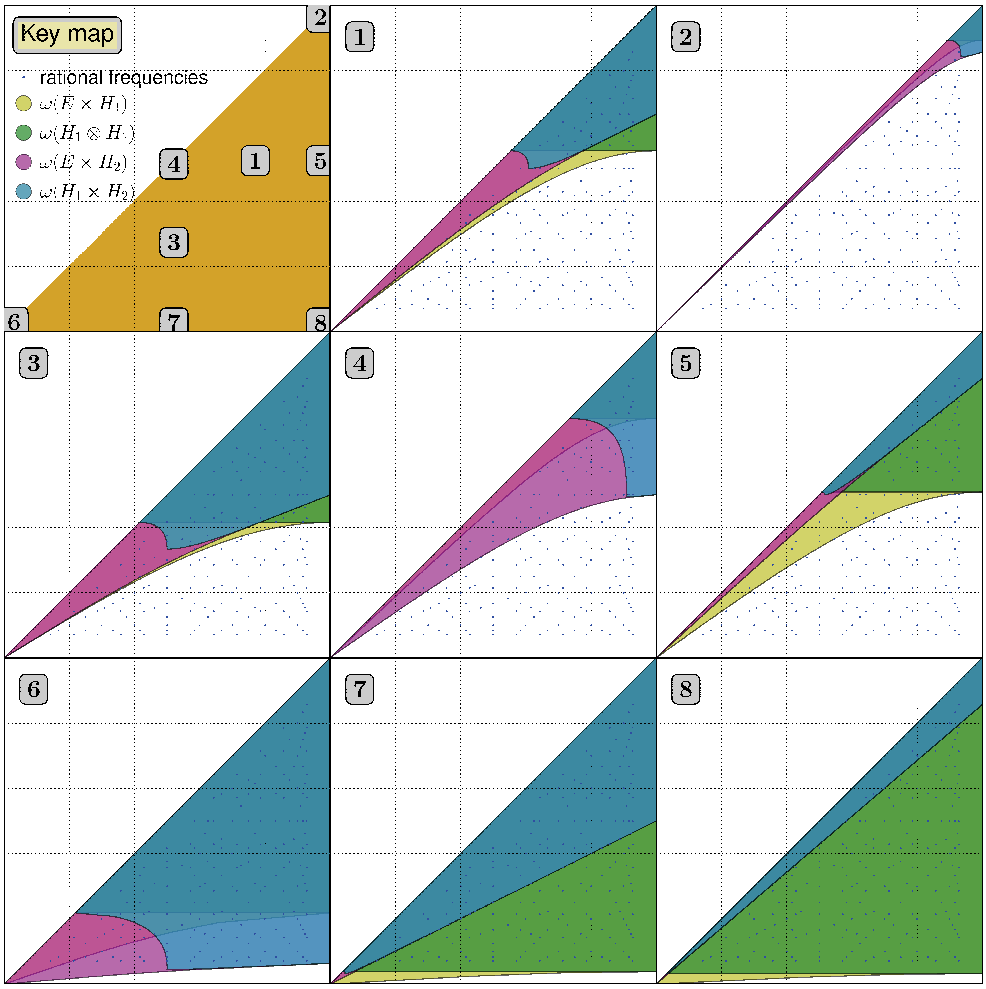

Figure 10. *Ranges of the frequency map for eight different ellipsoids.*

analytic formulae and numerical computations, but some properties can be justified. The following proposition is an example.

Proposition 16. *If Conjecture 1 holds, then* $\omega(H_1 \otimes H_1) = \triangle[AB_1C_1] \subsetneq \omega(E \times H_1)$, *and* $\omega : H_1 \otimes H_1 \to \triangle[AB_1C_1]$ *is a global diffeomorphism. Further,* $\omega^0 \in \omega(H_1 \otimes H_1)$ *if and only if* $\omega_2^0 > \varrho_* := \rho(c; b, a)$. *Finally,* $\lim_{c\to 0} \triangle[AB_1C_1] = \Omega$ *and* $\lim_{c\to b} \triangle[AB_1C_1] = \emptyset$.

Proof. If $U = H_1 \otimes H_1$, then $X = \partial U$ is the triangle with vertexes $\tilde{A} = (c, b)$, $\tilde{B}_1 = (c, c)$, $\tilde{C}_1 = (b, b)$. Using the formulae for the extended frequency map established in Theorem 13, we get that $\omega([\tilde{A}\tilde{B}_1]) = [AB_1]$, $\omega([\tilde{B}_1\tilde{C}_1]) = [B_1C_1]$, and $\omega([\tilde{C}_1\tilde{A}]) = [C_1A]$. Thus, $Y = \omega(X)$ is the triangle with vertexes A, B_1, C_1. In particular, X and Y are Jordan curves, so the frequency map $\omega : U \to \mathbb{R}^2$ verifies the hypotheses of Lemma 27 in Appendix B. Hence, $\omega(U) = \triangle[AB_1C_1]$ and $\omega : U \to \omega(U)$ is a global diffeomorphism.

In order to prove the strict inclusion $\triangle[AB_1C_1] \subsetneq \omega(E \times H_1)$, it suffices to see that the red curve from O to B_1 in Figure 9(right) is strictly below the yellow segment $[B_1C_1]$. This

Table 1
Geometric meaning of the winding numbers and the frequency vector when $Q \subset \mathbb{R}^3$.

Type	m_1	m_2	ω_1	ω_2
EH1	Crossings of π_z	Half-turns around a_z	z-oscillation	z-rotation
EH2	Half-turns around a_x	Crossings of π_x	x-rotation	x-oscillation
H1H1	Touches of Q_{λ_j}	Half-turns around a_z	(H1-oscillation)/2	z-rotation
H1H2	Crossings of π_y	Crossings of π_x	y-oscillation	x-oscillation

is equivalent to proving the inequality

$$\rho_z(\lambda_1) < \rho_z(c) \qquad \forall \lambda_1 \in (0, c),$$

due to the formulae for the extended frequency map contained in Theorem 13. This inequality was proved in Proposition 11. Finally, we note that $\lim_{c\to 0^+} \varrho_* = 0$ and $\lim_{c\to b^-} \varrho_* = 1/2$; see the second item of Proposition 10. ∎

5.5. Geometric meaning of the frequency map. Let m_0, m_1, m_2 be the winding numbers of a periodic billiard trajectory of type EH1. Then m_0 is the period. Furthermore, according to Remark 2, m_1 and $m_2/2$ are the number of times along one period that the trajectory crosses the coordinate plane $\pi_z = \{z = 0\}$ and the number of times along one period that it rotates around the coordinate axis $a_z = \{x = y = 0\}$, respectively. Therefore, the components of the frequency map have the following geometric meaning: $\omega_1 = m_1/2m_0$ is the number of oscillations around π_z per period, whereas $\omega_2 = m_2/2m_0$ is the number of rotations around a_z per period. Thus, it is quite natural to say that ω_1 is the z-*oscillation number* and ω_2 is the z-*rotation number* of the trajectory.

As in the planar case, these interpretations are extended to quasi-periodic trajectories. If $\lambda = (\lambda_1, \lambda_2) \in E \times H_1$, then Q_{λ_1} is an ellipsoid, Q_{λ_2} is a one-sheet hyperboloid, and

$$\omega(\lambda) = \lim_{k\to+\infty} (n_k, l_k)/k,$$

where n_k (resp., l_k) is the number of oscillations around π_z (resp., number of rotations around a_z) of the first k segments of *any* given trajectory with caustics Q_{λ_1} and Q_{λ_2}.

The billiard trajectories of other types can be analyzed by following similar arguments. The results are listed in Table 1 and can be checked by visual inspection; see Figure 13.

Finally, we stress a point already noted in Remark 3. If the trajectory is of type H1H1—that is, if both caustics are one-sheet hyperboloids—then the winding number m_1 is the number of (alternate) tangential touches with the caustics, so $\omega_1 = m_1/2m_0$ is half the number of oscillations between the one-sheet hyperboloids per period. In that situation, we call $2\omega_1$ the $H1$-*oscillation number* of the trajectory. In particular, it can happen that $m_0\omega \notin \mathbb{Z}^2$. For instance, if the winding numbers are $m_0 = 4$, $m_1 = 3$, and $m_2 = 2$, the period is four, but $\omega = (3/8, 1/4)$.

5.6. Bifurcations in parameter space. We want to determine the ellipsoids that have billiard trajectories with a prescribed frequency and with a prescribed caustic type. We recall that each ellipsoid is represented by a point in $P = \{(b, c) \in \mathbb{R}^2 : 0 < c < b < 1\}$, because $a = 1$. Let P_1^0, P_2^0, P_3^0, and P_4^0 be the four regions of P that correspond to ellipsoids with

billiard trajectories of frequency ω^0 and caustic type EH1, H1H1, EH2, and H1H2, respectively. Their shapes are described below.

Numerical Result 3. *Once we have fixed any frequency vector $\omega^0 = (\omega_1^0, \omega_2^0) \in \Omega$, let $b_1^0 = b_2^0 = 1$, $b_3^0 = b_4^0 = \sin^2(\pi\omega_2^0/2\omega_1^0)$, $c_1^0 = c_3^0 = \beta_4^0 = \sin^2 \pi\omega_2^0 / \sin^2 \pi\omega_1^0$, and $c_2^0 = c_4^0 = \sin^2 \pi\omega_2^0$. Then*

$$P_j^0 = \left\{(b,c) \in P : b < b_j^0,\ c < g_j^0(b)\right\}, \quad 1 \le j \le 4,$$

for some continuous functions $g_j^0 : [0, b_j^0] \to \mathbb{R}$ such that

(i) *g_1^0 is concave increasing in $[0,1]$, $0 < g_1^0(b) < b$ for all $b \in (0,1)$, and $g_1^0(1) = c_1^0$;*
(ii) *g_2^0 is concave increasing in $[0,1]$, $0 < g_2^0(b) < g_1^0(b)$ for all $b \in (0,1)$, and $g_2^0(1) = c_2^0$;*
(iii) *g_3^0 is the identity in $[0, c_3^0]$, concave decreasing in $[c_3^0, b_3^0]$, and $g_3^0(b_3^0) = 0$; and*
(iv) *g_4^0 is increasing in $[0, \beta_4^0]$, concave decreasing in $[\beta_4^0, b_4^0]$, $c_4^0 b/\beta_4^0 < g_4^0(b) < b$ for all $b \in (0, \beta_4^0)$, $0 < g_4^0(b) < g_3^0(b)$ for all $b \in (\beta_4^0, b_4^0)$, $g_4^0(\beta_4^0) = c_4^0$, and $g_4^0(b_4^0) = 0$.*

Remark 10. Numerical Result 1 follows from Numerical Result 3 just by choosing suitable rational frequency vectors: $\omega^0 = (2/5, 1/5)$ in the cases EH1 and EH2, $\omega^0 = (3/8, 1/4)$ in the case H1H1, and $\omega^0 = (1/3, 1/6)$ in the case H1H2. We stress that inequality $g_1^* < g_2^*$ in Numerical Result 1 and inequality $g_2^0 < g_1^0$ in Numerical Result 3 are not contradictory, because the first one refers to two different frequency vectors: $(2/5, 1/5)$ and $(3/8, 1/4)$.

Remark 11. We have numerically checked that g_4^0 is not concave in $[0, \beta_4^0]$.

Remark 12. Inclusions $P_2^0 \subset P_1^0$ and $P_4^0 \subset P_3^0$—and so, inequalities $g_2^0(b) < g_1^0(b)$ and $g_4^0(b) < g_3^0(b)$—are in direct agreement with inclusions $\omega(H_1 \otimes H_1) \subset \omega(E \times H_1)$ and $\omega(H_1 \times H_2) \subset \omega(E \times H_2)$ mentioned in Numerical Result 2.

Some bifurcation curves corresponding to the graphs of the functions $g_j^0 : [0, b_j^0] \to \mathbb{R}$ are presented in Figure 11. At the top of this figure we consider the eight rational frequencies with the smallest denominators. The inclusions $P_2^0 \subset P_1^0$ and $P_4^0 \subset P_3^0$ can be easily visualized, since all dashed curves are below their continuous pairs. At the bottom, we depict the bifurcation curves associated with the rational frequencies marked with blue dots in Figure 10. We needed multiple precision arithmetic to compute the bifurcation curves close to some of the endpoints, since the involved root-finding problems become quite singular at them. The programs were written using the PARI system [5].

Next, we describe four more criteria for deciding whether an ellipsoid has billiard trajectories of a given frequency. They are similar to the four established in Proposition 15.

Proposition 17. *If Numerical Result 3 holds, the following criteria can be applied:*

(i) *If $c < c_1^0 b$, then $\omega^0 \in \omega(E \times H_1)$. If $c \ge c_1^0 a$, then $\omega^0 \notin \omega(E \times H_1)$.*
(ii) *If $c < c_2^0 b$, then $\omega^0 \in \omega(H_1 \otimes H_1)$. If $c \ge c_2^0 a$, then $\omega^0 \notin \omega(H_1 \otimes H_1)$.*
(iii) *If $(b_3^0 - c_3^0)c < c_3^0(b_3^0 a - b)$, then $\omega^0 \in \omega(E \times H_2)$. If $b \ge b_3^0 a$, $\omega^0 \notin \omega(E \times H_2)$.*
(iv) *If $\beta_4^0 c < \min(c_4^0 b, \beta_4^0 b_4^0 a + (c_4^0 - b_4^0)b)$, then $\omega^0 \in \omega(H_1 \times H_2)$. If $b \ge b_4^0 a$ or $c \ge c_4^0 a$, then $\omega^0 \notin \omega(H_1 \times H_2)$.*

Proof. From Numerical Result 3, we get that $T_j^0 := \triangle[O\Gamma_j^0\Delta_j^0] \subset P_j^0$, where $O = (0,0)$, $\Gamma_1^0 = \Gamma_2^0 = (1,0)$, $\Gamma_3^0 = (b_3^0, 0)$, $\Gamma_4^0 = (b_4^0, 0)$, $\Delta_1^0 = (1, c_1^0)$, $\Delta_2^0 = (1, c_2^0)$, $\Delta_3^0 = (c_3^0, c_3^0)$, and $\Delta_4^0 = (\beta_4^0, c_4^0)$. It is straightforward to check that a point $(b,c) \in P$ belongs to the triangles T_1^0, T_2^0, T_3^0, and T_4^0 if and only if $c < c_1^0 b$, $c < c_2^0 b$, $(b_3^0 - c_3^0)c < c_3^0(b_3^0 - b)$, and $\beta_4^0 c < \min(c_4^0 b, \beta_4^0 b_4^0 + (c_4^0 - b_4^0)b)$, respectively. This proves the first part of each criterion for $a = 1$. To prove the general case, it suffices to take into account that its formulae are

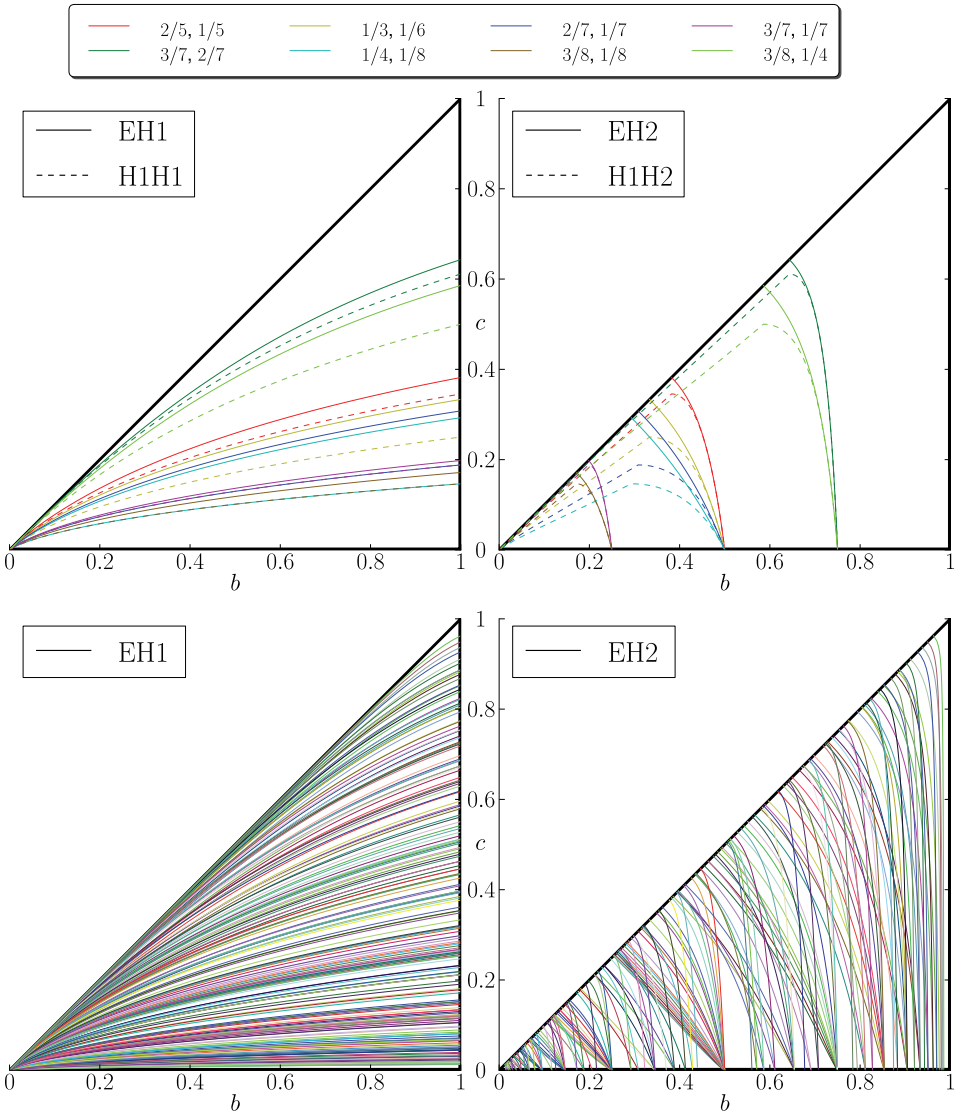

Figure 11. *Some bifurcation curves in the parameter space P.*

homogeneous in the parameters a, b, c.

The second parts follow from similar arguments. For instance, $P_j^0 \cap \{c \geq c_j^0\} = \emptyset$ for $j = 1, 2$, since $g_j^0(b)$ are increasing in $[0, 1]$ and $g_j^0(1) = c_j^0$. ■

Remark 13. Proposition 15 was obtained by fixing the ellipsoid and looking at the frequency space. In contrast, Proposition 17 was derived by fixing the frequency vector and looking at the parameter space. Of course, both approaches are equivalent, but their criteria are slightly different. The second ones are computationally simpler, because they do not involve any elliptic integral.

Although the description of the regions P_j^0 has a strong numerical component, some results can be proved. The following proposition is an example.

Proposition 18. *Let $\omega^0 = (\omega_1^0, \omega_2^0)$ be a fixed frequency vector. If Conjecture 1 holds, then $P_2^0 \subset P_1^0$, P_2^0 depends only on ω_2^0, and $P_2^0 = \{(b,c) \in P : 0 < b < 1,\ c < g_2^0(b)\}$ for some increasing analytic function $g_2^0 : (0,1) \to \mathbb{R}$ such that $0 < g_2^0(b) < b$ for all $b \in (0,1)$. Further, $\lim_{b\to 1^-} g_2^0(b) = \sin^2 \pi\omega_2^0$. Finally,*

$$g_2^0(b) = \begin{cases} 3b/\big(1+b+2\sqrt{1-b+b^2}\big) & \text{for } \omega_2^0 = 1/3, \\ b/(1+b) & \text{for } \omega_2^0 = 1/4. \end{cases}$$

Proof. If Conjecture 1 holds, then $\omega(H_1 \otimes H_1) = \triangle(AB_1C_1) \subset \omega(E \times H_1)$; see Proposition 16. Therefore, $P_2^0 \subset P_1^0$, because

$$(b,c) \in P_2^0 \Rightarrow \omega^0 \in \omega(H_1 \otimes H_1) \subset \omega(E \times H_1) \Rightarrow (b,c) \in P_1^0.$$

On the other hand, since $A = (1/2, 1/2)$, $B_1 = (1/2, \varrho_*)$, and $C_1 = (\varrho_*, \varrho_*)$, we deduce that

$$(b,c) \in P_2^0 \Leftrightarrow \omega^0 \in \omega(H_1 \otimes H_1) = \triangle(AB_1C_1) \Leftrightarrow \omega_2^0 > \varrho_* := \rho(c; b, a).$$

We know that the rotation function $\rho(\lambda) = \rho(\lambda; b, a)$ is increasing in $(0, b)$, $\rho(0) = 0$, and $\rho(b) = 1/2$. Hence, the function $g_2^0 : (0,1) \to \mathbb{R}$, $0 < g_2^0(b) < b$, is implicitly defined by

$$\rho(g_2^0(b); b, a) = \omega_2^0, \tag{19}$$

where $\omega_2^0 \in (0, 1/2)$ and $a = 1$ are fixed parameters. Analyticity of g_2^0 follows from the implicit function theorem, since Conjecture 1 also implies that $\partial_1\rho(\lambda; b, a) \neq 0$ for all $\lambda \in (0, b) \cup (b, a)$. Indeed, this derivative is positive in $(0, b)$ and negative in (b, a), because $\rho(\cdot; b, a)$ is increasing in $(0, b)$ and decreasing in (b, a). Additionally, we know that $\partial_2\rho(\lambda; b, a) = \partial_1\rho(b; \lambda, a)$ from the symmetry $\rho(\lambda; b, a) = \rho(b; \lambda, a)$; see (12). Hence, by differentiating (19) with respect to b and setting $c = g_2^0(b) \in (0, b)$, we get that

$$\big(g_2^0\big)'(b) = -\partial_2\rho(c; b, a)/\partial_1\rho(c; b, a) = -\partial_1\rho(b; c, a)/\partial_1\rho(c; b, a) > 0.$$

Using Proposition 10, we know that $\lim_{b\to a^-} \sin^2 \pi\rho(c; b, a) = \lim_{b\to a^-} \sin^2 \pi\rho(b; c, a) = c/a$. Thus, we deduce $\lim_{b\to 1^-} g_2^0(b) = \sin^2 \pi\omega_2^0$, since $a = 1$.

Finally, we must find the values $c \in (0, b)$ such that $\rho(c; b, a)$ is equal to $1/3$ or $1/4$. That is, we must find the values of $c \in (0, b)$ such that the billiard trajectories inside the ellipse $\{x^2/a + y^2/b = 1\}$ with caustic $\{x^2/(a-c) + y^2/(b-c) = 1\}$ have period three or four. This is an old result that goes back to Cayley [9]. For instance, $c = ab/(a+b)$ in the four-periodic case. The value for the three-periodic case was given in (14). ∎

The fact that P_2^0 depends only on ω_2^0 can be visualized in the upper left panel of Figure 11. The two dashed curves with $\omega_2^0 = 1/8$ coincide, as well as the two with $\omega_2^0 = 1/7$.

5.7. On the ubiquity of almost singular trajectories. In Figure 12 we have superposed the edges and borders (drawn in light colors) already displayed in Figure 9 and some new segments and curves (drawn in heavy colors). In the caustic space, these new segments are close to the original edges. To be precise, the distance between the segments and the edges is equal to $c/100 = 4.6 \cdot 10^{-3}$. Nevertheless, the images of the black, magenta, and blue

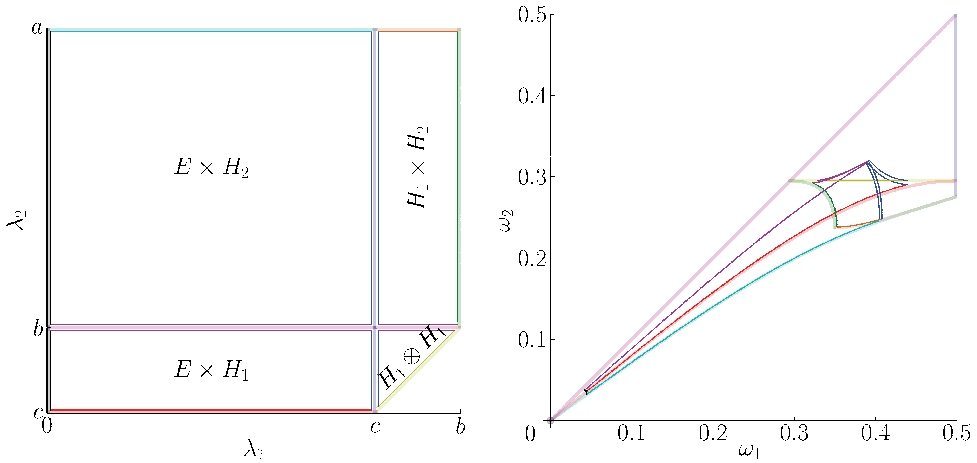

Figure 12. *The extended frequency map* $\omega : \bar{\Lambda} \to \bar{\Omega}$ close to *the edges of the caustic space for* $a = 1$, $b = 0.58$, *and* $c = 0.46$. *(Compare with Figure 9.)*

segments are far from their corresponding borders in the frequency space. This phenomenon seems stronger on the magenta and blue borders. It has to do with the fact that, as stated in Theorem 13, the frequency map has an *inverse logarithm* singularity at the blue and magenta edges of the caustic space. Therefore, one must be *exponentially close* to them just to be close to their images. On the other hand, the frequency map has a *square root* singularity at the black edges of the caustic space. Thus, one must be *quadratically close* to them just to be close to the origin in the frequency space.

We deduce from this phenomenon that *billiard trajectories with some almost singular caustic are ubiquitous.* Let us describe a quantitative sample of this principle using Figure 12. Let T be the triangle delimited by the yellow, blue and magenta thin segments that are close to the edges of $H_1 \otimes H_1$. It turns out that the area of $\omega(H_1 \otimes H_1)$ is approximately 16 times the area of $\omega(T)$. Hence, if we look for billiard trajectories of type H1H1 inside Q with a random frequency in $\omega(H_1 \otimes H_1)$, their caustic parameter $\lambda = (\lambda_1, \lambda_2)$ shall verify $\min(|\lambda_1 - c|, |\lambda_2 - b|) < 4.6 \cdot 10^{-3}$ with a probability approximately equal to 94%. It suffices to note that $15/16 = 0.9375$.

5.8. Examples of periodic trajectories with minimal periods. We have numerically computed some symmetric periodic trajectories to check that the lower bounds stated in Theorem 1 are optimal; see Figure 13. All these trajectories are almost singular. Concretely, $c - \lambda_1 \simeq 5 \cdot 10^{-4}$ in the case EH2; $\lambda_1 - c \simeq 2 \cdot 10^{-2}$ in the case H1H2; $c - \lambda_1 \simeq 2 \cdot 10^{-2}$ and $\lambda_2 - c \simeq 10^{-2}$ in the case EH1; and $\lambda_1 - c \simeq 10^{-2}$ in the case H1H1. Of course, we did not look for almost singular trajectories, but we got them anyway.

Considering the values given in Figure 13, and bearing in mind Table 1, we have that $(m_1, m_2) = (4, 2)$ for the EH2 trajectory, so it performs two turns around the coordinate axis a_{x} and crosses the coordinate plane π_{x} twice. As well, $(m_1, m_2) = (4, 2)$ for the EH1 trajectory, meaning four crossings with π_{z} and just one turn around a_{z}. Again, we have $(m_1, m_2) = (4, 2)$ for the H1H2 trajectory, meaning four crossings with π_{y} and two crossings with π_{x}. Finally, $(m_1, m_2) = (3, 2)$ for the H1H1 trajectory, which corresponds to three tangential touches with

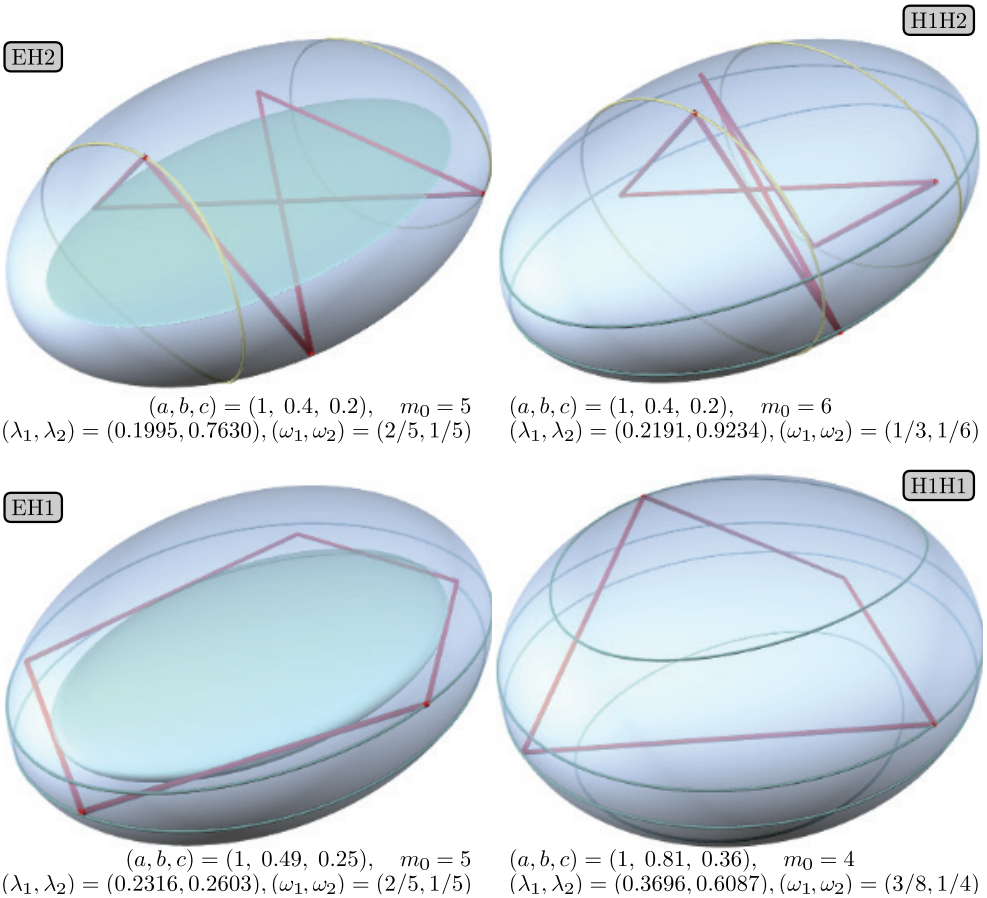

Figure 13. *Examples of symmetric nonsingular billiard trajectories with minimal periods. Lines in red represent the particle's trajectory. Lines in green and yellow correspond to the intersections of the original ellipsoid with the caustic one-sheet and two-sheet hyperboloids, respectively. In the cases EH*1 *and EH*2*, the caustic ellipsoid is also depicted.*

each of the caustics and a single turn around a_z. Each of those geometric interpretations has been verified on the corresponding trajectory.

6. Billiard inside a nondegenerate ellipsoid of $\mathbb{R}^{n+1}$. We describe briefly the high-dimensional version of some of the analytical results already shown in the spatial case. We denote again the nondegenerate ellipsoid as in (1) and the nonsingular caustic space as in (2).

By analogy with the spatial case, we consider three disjoint partitions:

$$\partial\Lambda = \bigcup_{k=0}^{n-1} \Lambda^k, \qquad \Lambda^{n-1} = G \cup R \cup S, \qquad S = \bigcup_{j=1}^{n} S_j.$$

With regard to the first partition, Λ^k is the k-dimensional border of Λ. That is, Λ^0 is the set of vertexes, Λ^1 is the set of edges, Λ^2 is the set of faces, and so on. The second partition mimics the distinction among geodesic flow limits, simple regular collapses, and simple singular

collapses already seen in the previous section. For instance, $G = \{\lambda \in \Lambda^{n-1} : \lambda_1 = 0\}$. The asymptotic behavior of the frequency map in each one of these three situations is expected to be dramatically different; see the theorem below. The last partition labels the component of the caustic parameter that becomes singular: $S_j = \{\lambda \in \Lambda^{n-1} : \lambda_j = a_j\}$. Further, given any caustic parameter $\lambda \in \Lambda$, we shall denote by $\lambda^{S_j} \in S_j$ the caustic parameter obtained from λ by substituting its jth component with a_j. Finally, we introduce the $(n-1)$-dimensional set

$$G_* = \{(\lambda_2, \dots, \lambda_n) \in \mathbb{R}^{n-1} : (0, \lambda_2, \dots, \lambda_n) \in G\},$$

which turns out to be the nonsingular caustic space for the geodesic flow on the ellipsoid. We note that $S_1 = \{c\} \times (H_1 \cup H_2)$, $S_2 = (E \cup H_1) \times \{b\}$, and $G_* = H_1 \cup H_2$ with the notation used in the previous section for triaxial ellipsoids of $\mathbb{R}^3$.

Theorem 19. *The frequency map $\omega : \Lambda \to \mathbb{R}^n$ has the following properties:*

(i) *It is analytic in Λ.*

(ii) *It can be continuously extended to $\partial\Lambda$, the extended map being as follows:*

1. *It vanishes at $\bar{G}$.*
2. *One of its components can be explicitly written as a function of the rest at $\bar{R}$.*
3. *Its first component is equal to $1/2$ at $\bar{S}_1$.*
4. *Its lth component is equal to the $(l-1)$th component at $\bar{S}_l$ for $2 \le l \le n$.*
5. *Its "free" components are an $(n-1)$-dimensional frequency of the billiard inside the section of the original ellipsoid by a suitable coordinate hyperplane at $\bar{R} \cup \bar{S}$.*

Furthermore, the restriction of the continuous extended map to any of the k-dimensional connected components of Λ^k, $1 \le k \le n-1$, is analytic.

(iii) *Its asymptotic behavior at $\Lambda^{n-1} = G \cup S \cup R$ is*

1. $\omega(\lambda) = \kappa^G(\lambda_2, \dots, \lambda_n)\lambda_1^{1/2} + \mathrm{O}(\lambda_1^{3/2})$ *as* $\lambda_1 \to 0^+$;
2. $\omega(\lambda) - \omega(\lambda^{S_j}) \asymp \kappa^S(\lambda^{S_j})/\log|a_j - \lambda_j|$ *as* $\lambda_j \to a_j$; *and*
3. $\omega(\lambda) - \omega(\lambda^R) = \mathrm{O}(\lambda - \lambda^R)$ *as* $\lambda \to \lambda^R \in R$

for some analytic functions $\kappa^G : G_* \to \mathbb{R}^n_+$ and $\kappa^S : S \to \mathbb{R}^n$.

Proof. The proof follows from the same arguments and computations used in the spatial case. The arguments are not repeated. The computations with hyperelliptic integrals have been relegated to Appendix A. ∎

We recall that, once we have fixed the parameters $a_1, \dots, a_{n+1}$ of the ellipsoid and the caustic parameters $\lambda_1, \dots, \lambda_n$, we write the $2n+1$ positive numbers

$$\{c_1, \dots, c_{2n+1}\} = \{a_1, \dots, a_{n+1}\} \cup \{\lambda_1, \dots, \lambda_n\}$$

in an ordered way: $c_0 := 0 < c_1 < \cdots < c_{2n+1}$. Then the frequency $\omega(\lambda)$ is defined in terms of some hyperelliptic integrals over the intervals (c_{2j}, c_{2j+1}). If two consecutive elements of $\{c_0, \dots, c_{2n+1}\}$ collide, then $\omega(\lambda)$ is, a priori, not well defined. Thus, it is natural to ask: How does $\omega(\lambda)$ behave at these collisions?

In the previous theorem we have solved this question at the set $\Lambda^{n-1} = G \cup R \cup S$, which covers just the geodesic flow limit, $c_1 \to 0^+$; the n simple regular collapses, $c_{2l+1}, c_{2l} \to c^*$ for some l; and the n simple singular collapses, $c_{2l-1}, c_{2l} \to c^*$ for some l. But there are many more (multiple) collapses, from double ones to total ones. Double collapses correspond to the set Λ^{n-2}. Total collapses have multiplicity n, so they correspond to set of vertexes Λ^0.

We believe that it does not make sense to describe the asymptotic behavior of the frequency map at all the collapses, since the behavior in each case must be the expected one. In order to convince the reader of the validity of this claim, we end the paper with a couple of extreme cases.

As a first example, let us consider the vertex $\hat{\lambda} = (a_1, \dots, a_n) \in \Lambda^0$. This represents the unique total singular collapse, because it is the unique common vertex of the 2^n open connected components of the caustic space:

$$\bigcap_{\sigma \in \{0,1\}^n} \bar{\Lambda}_\sigma = \{\hat{\lambda}\} = \bigcap_{j=1}^{n} \bar{S}_j.$$

Using that the point $\hat{\lambda}$ belongs to all the closures $\bar{S}_j$, from Theorem 19 we get that $\omega(\hat{\lambda}) = (1/2, \dots, 1/2)$. Which is the asymptotic behavior of ω at this vertex? In Appendix A.8 it is proved that

$$\omega(\lambda) = \omega(\hat{\lambda}) + \mathrm{O}\big(1/\log|a_1 - \lambda_1|, \dots, 1/\log|a_n - \lambda_n|\big), \qquad \lambda \to \hat{\lambda}.$$

This behavior is singular in the n caustic coordinates, as expected.

In contrast, the vertex $\tilde{\lambda} = (a_2, \dots, a_{n+1}) \in \Lambda^0$ represents the unique total regular collapse, so we predict a regular behavior in the n caustic coordinates. In Appendix A.7 we show that $\omega(\tilde{\lambda}) = (\widetilde{\omega}_1, \dots, \widetilde{\omega}_n)$, where the limit frequencies $0 < \widetilde{\omega}_j < 1/2$ are defined as $\sin^2 \pi\widetilde{\omega}_j = a_1/a_{j+1}$, and the asymptotic behavior is

$$\omega(\lambda) = \omega(\tilde{\lambda}) + \mathrm{O}(\tilde{\lambda} - \lambda), \qquad \lambda \to \tilde{\lambda}^-.$$

Once more, the frequency map has the expected behavior.

7. Conclusion and further questions. We have studied periodic trajectories of billiards inside nondegenerate ellipsoids of $\mathbb{R}^{n+1}$. First, we trivially extended the definition of the frequency map ω to any dimension, presented two conjectures about ω based on numerical computations, and deduced from the second conjecture some lower bounds on the periods. Next, we proved that ω can be continuously extended to any singular value of the caustic parameters, although it is exponentially sharp at the "inner" singular caustic parameters. Finally, we focused on ellipses and triaxial ellipsoids, where we found examples of trajectories whose periods coincide with the previous lower bounds. We also computed several bifurcation curves. Despite these results, many unsolved questions remain. We note just four.

The most obvious challenge is to tackle any of the conjectures, although it does not look easy. We have already devoted some effort to this without success. We believe that the proof of any of these conjectures requires either a deep use of algebraic geometry or to rewrite the frequency map as the gradient of a "Hamiltonian"; see [46, sect. 4].

Another interesting question is to describe completely the phase space of billiards inside ellipsoids in $\mathbb{R}^{n+1}$ for $n \geq 2$. A rich hierarchy of invariant objects appears in these billiards: Liouville maximal tori, low-dimensional tori, normally hyperbolic manifolds whose stable and unstable manifolds are doubled, etc. For instance, the stable and unstable invariant manifolds of the two-periodic hyperbolic trajectory corresponding to an oscillation along the major axis of the ellipsoid were fully described in [14].

Third, we plan to give a complete classification of the symmetric periodic trajectories inside generic ellipsoids [10]. To present the problem, let us consider the symmetric periodic trajectories inside an ellipse displayed in Figure 4. On the one hand, the three-periodic trajectory drawn in a continuous red line has an impact point on (and is symmetric with respect to) the x-axis. On the other hand, the four-periodic trajectory drawn in a dashed green line has a couple of segments passing through (and is symmetric with respect to) the origin. It is immediate to realize that there exists neither a trajectory with a hyperbola as caustic as the first one nor a trajectory with an ellipse as caustic as the second one. The problem consists of describing all possible kinds of symmetric periodic trajectories once the type of the n caustics for ellipsoids in $\mathbb{R}^{n+1}$ is fixed. Once these trajectories were well understood, we could study their persistence under small symmetric perturbations of the ellipsoid and the break-up of the Liouville tori on which they live. Similar results have already been found in other billiard frameworks: homoclinic trajectories inside ellipsoids of $\mathbb{R}^{n+1}$ with a unique major axis [8] and periodic trajectories inside circumferences of the plane [37].

Finally, we look for simple formulae to express the caustic parameters $\lambda_1, \dots, \lambda_n$ that give rise to periodic trajectories of small periods in terms of the parameters $a_1, \dots, a_{n+1}$ of the ellipsoid. As a byproduct of those formulae, one can find algebraic expressions for the functions $g_j^*(b)$ that appear in Numerical Result 1. This is a work in progress [38].

Appendix A. Computations with hyperelliptic integrals.

A.1. Technical lemmas.

Lemma 20. *Let $f_\epsilon \in C^0([\alpha,\beta])$ be a family of functions such that $f_\epsilon = f_0 + \mathrm{O}(\epsilon)$ in the C^0-topology. Then*

$$I_\epsilon = \int_\alpha^\beta \frac{f_\epsilon(s)\mathrm{d}s}{\sqrt{(s-\alpha)(\beta-s)}} = \int_\alpha^\beta \frac{f_0(s)\mathrm{d}s}{\sqrt{(s-\alpha)(\beta-s)}} + \mathrm{O}(\epsilon).$$

Proof. $|I_\epsilon - I_0| \leq |f_\epsilon - f_0|_{C^0([\alpha,\beta])} \int_\alpha^\beta ((s-\alpha)(\beta-s))^{-1/2}\mathrm{d}s = \pi |f_\epsilon - f_0|_{C^0([\alpha,\beta])} = \mathrm{O}(\epsilon)$. ∎

Lemma 21. *Let $f \in C^1([m,M])$ with $m < \alpha < \beta < M$ and $\epsilon = \beta - \alpha$. Then*

$$\int_\alpha^\beta \frac{f(s)\mathrm{d}s}{\sqrt{(s-\alpha)(\beta-s)}} = \pi f(\alpha) + \mathrm{O}(\epsilon) = \pi f(\beta) + \mathrm{O}(\epsilon), \qquad \epsilon \to 0^+.$$

Proof. Using the mean value theorem for integrals, we get that there exists some $s_0 \in [\alpha,\beta]$ such that the integral is equal to $f(s_0)\int_\alpha^\beta ((s-\alpha)(\beta-s))^{-1/2}\mathrm{d}s = \pi f(s_0)$. ∎

Lemma 22. *Let $f \in C^1([0,M])$ with $0 < \epsilon < M$. Then*

$$I_\epsilon = \int_0^\epsilon \frac{f(s)\mathrm{d}s}{\sqrt{\epsilon - s}} = 2f(0)\epsilon^{1/2} + \mathrm{O}(\epsilon^{3/2}), \qquad \epsilon \to 0^+.$$

Proof. $I_\epsilon = \left[-2\sqrt{\epsilon - s}f(s)\right]_{s=0}^{s=\epsilon} + 2\int_0^\epsilon \sqrt{\epsilon - s}f'(s)\mathrm{d}s = 2f(0)\epsilon^{1/2} + \mathrm{O}(\epsilon^{3/2})$. ∎

Lemma 23. *Let $f \in C^1([\alpha,\beta])$. Set $\xi = \int_\alpha^\beta (s-\alpha)^{-3/2}(f(s)-f(\alpha))\mathrm{d}s$, $\eta = f(\alpha)\log(4\beta - 4\alpha) + \int_\alpha^\beta (s-\alpha)^{-1}(f(s)-f(\alpha))\mathrm{d}s$, $\psi = \int_\alpha^\beta (\beta-s)^{-3/2}(f(s)-f(\beta))\mathrm{d}s$, and $\mu = f(\beta)\log(4\beta -$*

$4\alpha) + \int_\alpha^\beta (\beta - s)^{-1}(f(s) - f(\beta))\mathrm{d}s$. *Then*

$$\int_\alpha^\beta \frac{f(s)\mathrm{d}s}{\sqrt{(s+\epsilon-\alpha)(s-\alpha)}} = -f(\alpha)\log\epsilon + \eta + \mathrm{O}(\epsilon\log\epsilon), \qquad \epsilon \to 0^+,$$
$$\int_\alpha^\beta \frac{f(s)\mathrm{d}s}{(s+\epsilon-\alpha)\sqrt{s-\alpha}} = \pi f(\alpha)\epsilon^{-1/2} + \xi + \mathrm{O}(\epsilon^{1/2}), \qquad \epsilon \to 0^+,$$
$$\int_\alpha^\beta \frac{f(s)\mathrm{d}s}{\sqrt{(\beta+\epsilon-s)(\beta-s)}} = -f(\beta)\log\epsilon + \mu + \mathrm{O}(\epsilon\log\epsilon), \qquad \epsilon \to 0^+,$$
$$\int_\alpha^\beta \frac{f(s)\mathrm{d}s}{(\beta+\epsilon-s)\sqrt{\beta-s}} = \pi f(\beta)\epsilon^{-1/2} + \psi + \mathrm{O}(\epsilon^{1/2}), \qquad \epsilon \to 0^+.$$

The first (resp., last) two estimates also hold when f has a singularity at $s = \beta$ (resp., at $s = \alpha$), provided $f \in L^1([\alpha, \beta])$.

Proof. We split the first integral as $I_\epsilon = \tilde\eta + \hat I_\epsilon - \tilde I_\epsilon$, where $\tilde\eta = \int_\alpha^\beta (s-\alpha)^{-1}(f(s)-f(\alpha))\mathrm{d}s$ is a constant, and

$$\hat I_\epsilon = \int_\alpha^\beta \frac{f(\alpha)\mathrm{d}s}{\sqrt{(s+\epsilon-\alpha)(s-\alpha)}}, \qquad \tilde I_\epsilon = \int_\alpha^\beta \frac{f(s)-f(\alpha)}{s-\alpha}\left(1 - \sqrt{\frac{s-\alpha}{s+\epsilon-\alpha}}\right)\mathrm{d}s.$$

By performing the change $x^2 = s - \alpha$ in the integral $\hat I_\epsilon$, we get that

$$\hat I_\epsilon = 2\int_0^{\sqrt{\beta-\alpha}} \frac{f(\alpha)\mathrm{d}x}{\sqrt{x^2+\epsilon}} = 2f(\alpha)\left[\log\left(x + \sqrt{x^2+\epsilon}\right)\right]_{x=0}^{x=\sqrt{\beta-\alpha}} = -f(\alpha)\log\epsilon + \hat\eta + \mathrm{O}(\epsilon),$$

where $\hat\eta = f(\alpha)\log(4\beta - 4\alpha)$ is another constant. Thus, to get the first formula with constant $\eta = \hat\eta + \tilde\eta$ it suffices to see that $\tilde I_\epsilon = \mathrm{O}(\epsilon\log\epsilon)$.

Once we have fixed some $\gamma \in (\alpha, \beta)$, we decompose the integral $\tilde I_\epsilon$ as the sum $\tilde J_\epsilon + \tilde K_\epsilon$, where $\tilde J_\epsilon = \int_\alpha^\gamma \tilde f(s) r_\epsilon(s)\mathrm{d}s$, $\tilde K_\epsilon = \int_\gamma^\beta \tilde f(s) r_\epsilon(s)\mathrm{d}s$, and

$$\tilde f(s) = \frac{f(s)-f(\alpha)}{s-\alpha}, \qquad r_\epsilon(s) = 1 - \sqrt{\frac{s-\alpha}{s+\epsilon-\alpha}}.$$

First, we consider the interval $[\alpha, \gamma]$. Then $|\tilde f|_\infty = \max\{|\tilde f(s)| : \alpha \le s \le \gamma\} < \infty$, and $r_\epsilon(s)$ is positive in $[\alpha, \gamma]$. Set $\delta = \gamma - \alpha$. Using again the change $x^2 = s - \alpha$, we see that

$$|\tilde f|_\infty^{-1}|\tilde J_\epsilon| \le \int_\alpha^\gamma r_\epsilon(s)\mathrm{d}s = \delta - \int_\alpha^\gamma \sqrt{\frac{s-\alpha}{s+\epsilon-\alpha}}\mathrm{d}s = \delta - 2\int_0^{\sqrt\delta} \frac{x^2\mathrm{d}x}{\sqrt{x^2+\epsilon}}$$
$$= \delta - \left[x\sqrt{x^2+\epsilon} + \epsilon\log\left(x + \sqrt{x^2+\epsilon}\right)\right]_{x=0}^{x=\sqrt\delta} = -\frac{\epsilon}{2}\log\epsilon + \mathrm{O}(\epsilon).$$

Concerning the other interval, we note that $r_\epsilon(s)$ is positive and decreasing in $[\gamma, \beta]$. Hence, $\max\{|r_\epsilon(s)| : \gamma \le s \le \beta\} = r_\epsilon(\gamma)$, and so $|\tilde K_\epsilon| \le r_\epsilon(\gamma)\int_\gamma^\beta |\tilde f(s)|\mathrm{d}s = \mathrm{O}(\epsilon)$. This ends the proof of the first formula.

We split the second integral as $L_\epsilon = \xi + \hat{L}_\epsilon - \tilde{L}_\epsilon$, where ξ is the constant given in the statement of the lemma, and

$$\hat{L}_\epsilon = \int_\alpha^\beta \frac{f(\alpha)\mathrm{d}s}{(s+\epsilon-\alpha)\sqrt{s-\alpha}}, \qquad \tilde{L}_\epsilon = \int_\alpha^\beta \frac{f(s)-f(\alpha)}{(s-\alpha)^{3/2}}\left(1-\frac{s-\alpha}{s+\epsilon-\alpha}\right)\mathrm{d}s.$$

By performing the change $x = s-\alpha$ in the integral $\hat{L}_\epsilon$, we get that

$$\hat{L}_\epsilon = \int_0^{\beta-\alpha} \frac{f(\alpha)\mathrm{d}x}{(x+\epsilon)\sqrt{x}} = 2f(\alpha)\epsilon^{-1/2}\left[\operatorname{atan}\left(\frac{x}{\epsilon}\right)^{1/2}\right]_{x=0}^{x=\beta-\alpha} = \pi f(\alpha)\epsilon^{-1/2} + \mathrm{O}(\epsilon^{1/2}).$$

Thus, to get the second formula it suffices to see that $\tilde{L}_\epsilon = \mathrm{O}(\epsilon^{1/2})$, which follows from computations similar to the ones above.

The last formulae are obtained by performing the change of variables $s-\alpha = \beta - t$ in the earlier ones. ∎

Corollary 24. *Let $f \in C^1([m,M])$ with $m < \alpha_- < \alpha_+ < \beta_- < \beta_+ < M$, and*

$$I = I(\alpha_-,\alpha_+,\beta_-,\beta_+) = \int_{\alpha_+}^{\beta_-} \frac{f(s)\mathrm{d}s}{\sqrt{(s-\alpha_-)(s-\alpha_+)(\beta_- - s)(\beta_+ - s)}}.$$

Let α_* and β_* be two reals such that $m < \alpha_* < \beta_* < M$. Let $\epsilon = (\epsilon_1,\epsilon_2) \in \mathbb{R}^2_+$ with $\epsilon_1 = \alpha_+ - \alpha_-$ and $\epsilon_2 = \beta_+ - \beta_-$. Then there exists a constant $\zeta \in \mathbb{R}$ such that

$$I = -\frac{f(\alpha_*)(1+\mathrm{O}(\epsilon_2))\log\epsilon_1 + f(\beta_*)(1+\mathrm{O}(\epsilon_1))\log\epsilon_2}{\beta_* - \alpha_*} + \zeta + \mathrm{O}(\epsilon_1\log\epsilon_1, \epsilon_2\log\epsilon_2)$$

as $\alpha_\pm \to \alpha_*$ and $\beta_\pm \to \beta_*$, so that $\epsilon = (\epsilon_1,\epsilon_2) \to (0^+,0^+)$.

Proof. The corollary follows by applying the first and third estimates of Lemma 23 to the integrals $\int_{\alpha_+}^{\gamma}$ and $\int_{\gamma}^{\beta_-}$ for some point $\gamma \in (\alpha_+,\beta_-)$, although before we must fix the lower limit of the first integral with the change $x-\alpha_* = s-\alpha_+$, and the upper limit of the second integral with the change $x-\beta_* = s-\beta_-$. ∎

Lemma 25. *Let $\mathbf{K}_\epsilon\omega_\epsilon = \tau_\epsilon$ be a family of square linear systems defined for $\epsilon > 0$.*

(i) *If the limits $\mathbf{K} = \lim_{\epsilon\to 0^+}\mathbf{K}_\epsilon$ and $\tau = \lim_{\epsilon\to 0^+}\tau_\epsilon$ exist and $\mathbf{K}$ is nonsingular, then*

$$\omega_\epsilon = \omega + \mathrm{O}(|\mathbf{K}_\epsilon - \mathbf{K}|, |\tau_\epsilon - \tau|), \qquad \epsilon \to 0^+,$$

where $\omega = \mathbf{K}^{-1}\tau$ is the unique solution of the nonsingular limit system $\mathbf{K}\omega = \tau$.

(ii) *If, in addition, the matrix $\mathbf{K}_\epsilon$ and the vector τ_ϵ are differentiable at $\epsilon = 0$, then the solution ω_ϵ also is differentiable at $\epsilon = 0$. To be more precise, if*

$$\mathbf{K}_\epsilon = \mathbf{K} + \epsilon\mathbf{L} + \mathrm{o}(\epsilon), \qquad \tau_\epsilon = \tau + \epsilon\zeta + \mathrm{o}(\epsilon), \qquad \epsilon \to 0^+,$$

for some square matrix $\mathbf{L}$ and some vector ζ, then

$$\omega_\epsilon = \omega + \epsilon\kappa + \mathrm{o}(\epsilon), \qquad \epsilon \to 0^+,$$

where $\omega = \mathbf{K}^{-1}\tau$ and $\kappa = \mathbf{K}^{-1}(\zeta - \mathbf{L}\omega)$.

Proof. Both results follow directly from classical error bounds in numerical linear algebra. See, for instance, [25, sect. 2.7]. ∎

A.2. Properties of the rotation number. Let us write the rotation number as the quotient $\rho(\lambda) = \Delta(\lambda)/2K(\lambda)$, where

$$\Delta(\lambda) = \int_0^{\min(b,\lambda)} \frac{\mathrm{d}s}{\sqrt{T(s)}}, \qquad K(\lambda) = \int_{\max(b,\lambda)}^{a} \frac{\mathrm{d}s}{\sqrt{T(s)}},$$

and $T(s) = (\lambda - s)(b - s)(a - s)$.

The study of the limit $\lambda \to 0^+$ is easy. From Lemma 22 we get the estimate $\Delta(\lambda) = 2(ab)^{-1/2}\lambda^{1/2} + \mathrm{O}(\lambda^{3/2})$ as $\lambda \to 0^+$, whereas from Lemma 20 we get that

$$K(\lambda) = \int_b^a \frac{\mathrm{d}s}{\sqrt{s(s-b)(a-s)}} + \mathrm{O}(\lambda), \qquad \lambda \to 0^+.$$

By combining both estimates, we get that $\rho(\lambda) = \kappa^G \lambda^{1/2} + \mathrm{O}(\lambda^{3/2})$, so $\lim_{\lambda\to 0^+} \rho(\lambda) = 0$.

Next, we consider $\lambda \to b^-$. After some computations based on Lemma 23, we get

$$\begin{aligned} K(b-\epsilon) &= -c^{-1/2}\log\epsilon + \eta + \mathrm{O}(\epsilon\log\epsilon), \qquad \epsilon \to 0^+, \\ \Delta(b-\epsilon) &= -c^{-1/2}\log\epsilon + \mu + \mathrm{O}(\epsilon\log\epsilon), \qquad \epsilon \to 0^+, \end{aligned}$$

where $c = a - b$, $\eta = \hat\eta + \tilde\eta$, $\mu = \hat\mu + \tilde\mu$, with $\hat\eta = c^{-1/2}\log 4c$, $\hat\mu = c^{-1/2}\log 4b$, and

$$\begin{aligned} \tilde\eta &= \int_b^a \left(\frac{1}{\sqrt{a-s}} - \frac{1}{\sqrt{a-b}}\right)\frac{\mathrm{d}s}{s-b} = \frac{2}{\sqrt{c}}\int_0^{\sqrt{c}} \frac{\mathrm{d}x}{x+\sqrt{c}} = \frac{\log 4}{\sqrt{c}}, \\ \tilde\mu &= \int_0^b \left(\frac{1}{\sqrt{a-s}} - \frac{1}{\sqrt{a-b}}\right)\frac{\mathrm{d}s}{b-s} = -\frac{2}{\sqrt{c}}\int_{\sqrt{c}}^{\sqrt{a}} \frac{\mathrm{d}x}{x+\sqrt{c}} = \frac{1}{\sqrt{c}}\log\frac{4c}{(\sqrt{a}+\sqrt{c})^2}. \end{aligned}$$

We have used the change $x^2 = a - s$ in both integrals. Let $\eta_* = c^{1/2}\eta = \log 16c$ and $\mu_* = c^{1/2}\mu = \log 16bc(a^{1/2} + c^{1/2})^{-2}$. Then we have the estimate

$$2\rho(b-\epsilon) = \frac{\Delta(b-\epsilon)}{K(b-\epsilon)} = \frac{1 - c^{1/2}\mu\log^{-1}\epsilon + \mathrm{O}(\epsilon)}{1 - c^{1/2}\eta\log^{-1}\epsilon + \mathrm{O}(\epsilon)} = \frac{1 - \mu_*\log^{-1}\epsilon}{1 - \eta_*\log^{-1}\epsilon} + \mathrm{O}(\epsilon) \tag{20}$$

as $\epsilon \to 0^+$. So, $\kappa^S = (\eta_* - \mu_*)/2 = \log\left((a/b)^{1/2} + (c/b)^{1/2}\right) = \log\left(d + (d^2-1)^{1/2}\right) = \operatorname{acosh} d$, where $d = (a/b)^{1/2}$. This implies that $\cosh^2\kappa^S = a/b$. Further, estimate (20) is the key to proving that the caustic parameter λ_-^0 is exponentially close to b. Once we have fixed $\rho^0 \lesssim 1/2$, let $\lambda_-^0 \in E$ be the unique caustic parameter such that $\rho(\lambda_-^0) = \rho^0$, $0 < \epsilon = b - \lambda_-^0 \ll 1$, and $\delta = \log^{-1}\epsilon$. By finding $\delta^{-1} = \log\epsilon$ in estimate (20), we get

$$\log\epsilon = \frac{1}{\delta} = \eta_* + \frac{\mu_* - \eta_*}{1 - 2\rho^0} + \mathrm{O}(\epsilon).$$

Using that $\kappa^S = (\eta_* - \mu_*)/2$ and $\eta_* = \log 16c$, we check that $\lambda_-^0 = b - \epsilon$, with

$$\epsilon = \mathrm{e}^{1/\delta} = \mathrm{e}^{\eta_* - 2\kappa^S/(1-2\rho^0) + \mathrm{O}(\epsilon)} = 16c\mathrm{e}^{-\kappa^S/(1/2-\rho^0)} + \mathrm{O}\left(\mathrm{e}^{-2\kappa^S/(1/2-\rho^0)}\right)$$

as $\rho^0 \to (1/2)^-$. The limit $\lambda \to b^+$ is completely analogous; we omit the computations.

With respect to the limit $\lambda \to a^-$, we note that $T(s) = (b-s)(a-s)^2 + \mathrm{O}(a-\lambda)$ uniformly in the interval $[0, b]$. Hence,

$$\Delta(\lambda) = \int_0^b \frac{\mathrm{d}s}{(a-s)\sqrt{b-s}} + \mathrm{O}(a-\lambda) = \frac{2}{\sqrt{a-b}} \operatorname{atan} \sqrt{\frac{b}{a-b}} + \mathrm{O}(a-\lambda), \quad \lambda \to a^-.$$

Furthermore, from Lemma 21 we get the estimate $K(\lambda) = \pi(a-b)^{-1/2} + \mathrm{O}(a-\lambda)$ as $\lambda \to a^-$. Therefore, $\rho(\lambda) = \varrho + \mathrm{O}(a-\lambda)$ as $\lambda \to a^-$, where the limit value $\varrho \in (0, 1/2)$ is defined by $\tan^2 \pi\varrho = b/(a-b)$. That is, $\sin^2 \pi\varrho = b/a$.

A.3. Another characterization of the frequency. We associate a "frequency vector" $\omega = \varpi(c) \in \mathbb{R}^n$ with any $c = (c_1, \dots, c_{2n+1}) \in \mathbb{R}^{2n+1}$ such that $c_0 := 0 < c_1 < \cdots < c_{2n+1}$ in the way described next. First, we consider the following:

- the polynomial $T(s) = \prod_{i=1}^{2n+1}(c_i - s) \in \mathbb{R}_{2n+1}[s]$, which is positive in the $n+1$ intervals of the form (c_{2j}, c_{2j+1}),
- the $n+1$ linear functionals $P(s) \mapsto \mathcal{K}_j[P(s)] = \int_{c_{2j}}^{c_{2j+1}} (T(s))^{-1/2} P(s)\mathrm{d}s$,
- the $n+1$ column vectors $K_j = (\mathcal{K}_j[1], \mathcal{K}_j[s], \dots, \mathcal{K}_j[s^{n-1}])^t \in \mathbb{R}^n$,
- the $n \times n$ nonsingular matrix $\mathbf{K} = (-K_1, \dots, (-1)^n K_n)$, and
- the linear functionals $P(s) \mapsto \mathcal{K}[P(s); \omega] = \mathcal{K}_0[P(s)] + 2\sum_{j=1}^n (-1)^j \omega_j \mathcal{K}_j[P(s)]$ for $\omega \in \mathbb{R}^n$.

The hypothesis $c_1 > 0$ is not essential for getting a nonsingular matrix $\mathbf{K}$, but it suffices to assume the strict inequalities $c_1 < \cdots < c_{2n+1}$; see [26, sect. III.3].

Lemma 26. *There exists an unique $\omega \in \mathbb{R}^n$ such that*

$$\mathcal{K}[P(s); \omega] = 0 \qquad \forall P(s) \in \mathbb{R}_{n-1}[s] \tag{21}$$

or, equivalently, such that $K_0 + 2\mathbf{K}\omega = 0$, which is the matricial form of the linear system given in (7).

Proof. By taking the basis $\{1, s, \dots, s^{n-1}\}$ of $\mathbb{R}_{n-1}[s]$, we see that condition (21) is equivalent to the linear system $K_0 + 2\mathbf{K}\omega = 0$. ∎

Therefore, condition (21) is an equivalent characterization of the frequency. From now on, $\omega = \varpi(c)$ stands for the frequency computed through the previous steps.

A.4. Geodesic flow limit: $c_1 \to 0^+$. Let $K_0^G = (K_{00}^G, 0, \dots, 0) \in \mathbb{R}^n$ with $K_{00}^G = 2(\prod_{i=2}^n c_i)^{-1/2}$, and $T^G(s) = -s\prod_{i=2}^{2n+1}(c_i - s)$. Let $\mathbf{K}^G$ be the $n \times n$ nonsingular matrix associated with the vector $c^G = (0, c_2, \dots, c_{2n+1})$. Let $\kappa^G \in \mathbb{R}^n$ be the unique solution of the linear system $K_0^G + 2\mathbf{K}^G\kappa^G = 0$. Then

$$\omega = \kappa^G c_1^{1/2} + \mathrm{O}(c_1^{3/2}), \qquad c_1 \to 0^+. \tag{22}$$

The proof is short. First, we note that $T = T^G + \mathrm{O}(c_1)$ uniformly in $[0, c_{2n+1}]$. Thus, using Lemma 20, we get that $\mathbf{K} = \mathbf{K}^G + \mathrm{O}(c_1)$ as $c_1 \to 0^+$. And, using Lemma 22, we see that $K_0 = K_0^G c_1^{1/2} + \mathrm{O}(c_1^{3/2})$ as $c_1 \to 0^+$. Therefore, the linear systems $K_0^G + 2\mathbf{K}^G\kappa^G = 0$ and $c_1^{-1/2}K_0 + 2\mathbf{K}(c_1^{-1/2}\omega) = 0$ are $\mathrm{O}(c_1)$-close, $\mathbf{K}^G$ being nonsingular, so (22) follows from Lemma 25(i).

A.5. Simple regular collapse: $c_{2l+1}, c_{2l} \to c^*$ for some $l = 1, \dots, n$. Set $c^R = (c_1, \dots, c_{2l-1}, c_{2l+2}, \dots, c_{2n+1}) \in \mathbb{R}^{2n-1}$. Let $T^R(s) = \prod_{i \neq 2l, 2l+1}(c_i - s)$ be the polynomial associated with c^R. Let $\mathcal{K}^R_j$ and $\mathcal{K}^R$ be the functionals associated with c^R. Let $\omega^R = (\omega^R_1, \dots, \omega^R_n) \in \mathbb{R}^n$, where $\omega^R_{\neq l} := (\omega^R_1, \dots, \omega^R_{l-1}, \omega^R_{l+1}, \dots, \omega^R_n) = \varpi(c^R) \in \mathbb{R}^{n-1}$ is the frequency associated with c^R, and where $\omega^R_l \in \mathbb{R}$ is determined by

$$\int_0^{c_1} \frac{\mathrm{d}s}{|c^* - s|\sqrt{T^R(s)}} + 2\sum_{j \neq l} \int_{c_{2j}}^{c_{2j+1}} \frac{(-1)^j \omega^R_j \mathrm{d}s}{|c^* - s|\sqrt{T^R(s)}} + \frac{(-1)^l 2\pi \omega^R_l}{\sqrt{-T^R(c^*)}} = 0. \tag{23}$$

Let $\epsilon = c_{2l+1} - c_{2l}$. Then

$$\omega = \omega^R + \mathrm{O}(\epsilon), \qquad c_{2l+1}, c_{2l} \to c^*. \tag{24}$$

In order to prove this claim, we first observe that characterization (21) is equivalent to the system of n linear equations

$$\begin{cases} \mathcal{K}[(c^* - s)s^i; \omega] = 0 & \text{for } i = 0, \dots, n-2, \\ \mathcal{K}[1; \omega] = 0, \end{cases} \tag{25}$$

because $\{1, c^* - s, \dots, (c^* - s)s^{n-2}\}$ is a basis of $\mathbb{R}_{n-1}[s]$. Now, using Lemmas 20 and 21, we deduce the estimates

$$\mathcal{K}_j[(c^* - s)s^i] = \int_{c_{2j}}^{c_{2j+1}} \frac{(c^* - s)s^i \mathrm{d}s}{|c^* - s|\sqrt{T^S(s)} + \mathrm{O}(\epsilon)} = \begin{cases} \mathcal{K}^R_j[s^i] + \mathrm{O}(\epsilon) & \text{if } j < l, \\ \mathrm{O}(\epsilon) & \text{if } j = l, \\ -\mathcal{K}^R_{j-1}[s^i] + \mathrm{O}(\epsilon) & \text{if } j > l \end{cases}$$

and

$$\mathcal{K}_j[1] = \begin{cases} \pi \left(-T^R(c^*)\right)^{-1/2} + \mathrm{O}(\epsilon) & \text{if } j = l, \\ \int_{c_{2j}}^{c_{2j+1}} \frac{\mathrm{d}s}{|c^* - s|\sqrt{T^R(s)}} + \mathrm{O}(\epsilon) & \text{otherwise.} \end{cases}$$

Therefore, the linear system (25) is $\mathrm{O}(\epsilon)$-close to the nonsingular linear system

$$\begin{cases} \mathcal{K}^R[s^i; \omega^R_{\neq l}] = 0 & \text{for } i = 0, \dots, n-2, \\ \text{condition (23)}, \end{cases}$$

and the asymptotic formula (24) follows from Lemma 25(i).

A.6. Simple singular collapse: $c_{2l-1}, c_{2l} \to c^*$ for some $l = 1, \dots, n$. Set $c^S = (c_1, \dots, c_{2l-2}, c_{2l+1}, \dots, c_{2n+1}) \in \mathbb{R}^{2n-1}$. Let $T^S(s) = \prod_{i \neq 2l-1, 2l}(c_i - s)$ be the polynomial associated with c^S. Let $\mathcal{K}^S_j$ and $\mathcal{K}^S$ be the functionals associated with c^S. Let $\omega^S = (\omega^S_1, \dots, \omega^S_n) \in \mathbb{R}^n$, where $\omega^S_{\neq l} := (\omega^S_1, \dots, \omega^S_{l-1}, \omega^S_{l+1}, \dots, \omega^S_n) = \varpi(c^S) \in \mathbb{R}^{n-1}$ and

$$\omega^S_l = \begin{cases} 1/2 & \text{if } l = 1, \\ \omega^S_{l-1} & \text{otherwise.} \end{cases}$$

Let $\epsilon = c_{2l} - c_{2l-1} > 0$ and $\delta = |\log \epsilon|^{-1} > 0$. Then there exists $\kappa^S \in \mathbb{R}^n$ such that

$$\omega = \omega^S + \delta \kappa^S + \mathrm{o}(\delta), \qquad c_{2l-1}, c_{2l} \to c^*. \tag{26}$$

To prove this claim, we set $d = \sqrt{T^S(c^*)} > 0$. We know that characterization (21) is equivalent to the system of n linear equations

$$\left\{ \begin{array}{l} \mathcal{K}[\delta d; \omega] = 0, \\ \mathcal{K}[(c^* - s)s^i; \omega] = 0 \quad \text{for } i = 0, \dots, n-2, \end{array} \right. \tag{27}$$

because $\{\delta d, c^* - s, \dots, (c^* - s)s^{n-2}\}$ is a basis of $\mathbb{R}_{n-1}[s]$. Now, using Lemmas 20 and 23, we deduce the following asymptotic estimates. On the one hand, there exist some constants $\zeta_0, \zeta_1, \dots, \zeta_n \in \mathbb{R}$ such that

$$\mathcal{K}_j[\delta d] = \delta d \mathcal{K}_j[1] = \left\{ \begin{array}{ll} 1 + \zeta_j \delta + \mathrm{O}(\epsilon) & \text{if } j = l-1, l, \\ \zeta_j \delta + \mathrm{O}(\epsilon\delta) & \text{otherwise.} \end{array} \right.$$

On the other hand,

$$\mathcal{K}_j[(c^* - s)s^i] = \int_{c_{2j}}^{c_{2j+1}} \frac{(c^* - s)s^i \mathrm{d}s}{|c^* - s|\sqrt{T^S(s)} + \mathrm{O}(\epsilon)} = \left\{ \begin{array}{ll} \mathcal{K}_j^S[s^i] + \mathrm{O}(\epsilon) & \text{if } j < l-1, \\ \int_{c_{2l-2}}^{c^*} \frac{s^i \mathrm{d}s}{\sqrt{T^S(s)}} + \mathrm{O}(\epsilon) & \text{if } j = l-1, \\ -\int_{c^*}^{c_{2l+1}} \frac{s^i \mathrm{d}s}{\sqrt{T^S(s)}} + \mathrm{O}(\epsilon) & \text{if } j = l, \\ -\mathcal{K}_{j-1}^S[s^i] + \mathrm{O}(\epsilon) & \text{if } j > l. \end{array} \right.$$

In particular, $\mathcal{K}_{l-1}[(c^* - s)s^i] - \mathcal{K}_l[(c^* - s)s^i] = \int_{c_{2l-2}}^{c_{2l+1}} \frac{s^i \mathrm{d}s}{\sqrt{T^S(s)}} + \mathrm{O}(\epsilon) = \mathcal{K}_{l-1}^S[s^i] + \mathrm{O}(\epsilon)$.

We assume now that $l \neq 1$. (The case $l = 1$ is studied later on.) Since $\epsilon \ll \delta$, the linear system (27) is $\mathrm{O}(\delta)$-close to the nonsingular linear system

$$\left\{ \begin{array}{l} 2(-1)^{l-1}(\omega_{l-1}^S - \omega_l^S) = 0, \\ \mathcal{K}^S[s^i; \omega_{\neq l}^S] = 2(-1)^l(\omega_l^S - \omega_{l-1}^S) \int_{c^*}^{c_{2l+1}} \frac{s^i \mathrm{d}s}{\sqrt{T^S(s)}} \quad \text{for } i = 0, \dots, n-2, \end{array} \right.$$

which in its turn is equivalent to the linear system

$$\left\{ \begin{array}{l} \omega_l^S = \omega_{l-1}^S, \\ \mathcal{K}^S[s^i; \omega_{\neq l}^S] = 0 \quad \text{for } i = 0, \dots, n-2, \end{array} \right. \tag{28}$$

whose unique solution is $\omega_{\neq l}^S = \varpi(c^S)$ and $\omega_l^S = \omega_{l-1}^S$.

Thus, the asymptotic formula $\omega = \omega^S + \mathrm{O}(\delta)$ follows from the first item in Lemma 25. In fact, this result can be improved using the second item in Lemma 25. It suffices to note that the linear system (27) is not only $\mathrm{O}(\delta)$-equivalent to (28), but also differentiable at $\delta = 0$. Hence, (26) holds for some vector κ^S that could be explicitly computed in terms of the limit system and the constants $\zeta_0, \dots, \zeta_n$.

If $l = 1$, the linear system (27) is $\mathrm{O}(\delta)$-equivalent to the nonsingular linear system

$$\left\{ \begin{array}{l} \omega_1^S = 1/2, \\ \mathcal{K}^S[s^i; \omega_{\neq 1}^S] = 0 \quad \text{for } i = 0, \dots, n-2, \end{array} \right.$$

and the proof ends with just the same arguments as for $l \neq 1$. We omit the details.

A.7. Total regular collapse: $c_{2l+1}, c_{2l} \to c_l^*$ for all $l = 1, \dots, n$. Let us study the case of n simultaneous collapses, all of them regular. That is, once we have fixed a vector $c^* = (c_1^*, \dots, c_n^*) \in \mathbb{R}^n$ such that $0 < c_1 < c_1^* < \cdots < c_n^*$, we study the asymptotic behavior of the frequency $\omega = \varpi(c)$ when $c_{2l+1}, c_{2l} \to c_l^*$ for all $l = 1, \dots, n$. Let $\widetilde{\omega} = (\widetilde{\omega}_1, \dots, \widetilde{\omega}_n) \in \mathbb{R}^n$ be the vector whose components verify that $0 < \widetilde{\omega}_l < 1/2$ and $\sin^2 \pi\widetilde{\omega}_l = c_1/c_l^*$. Let $\epsilon = (\epsilon_1, \dots, \epsilon_n) \in \mathbb{R}^n_+$ with $\epsilon_l = c_{2l+1} - c_{2l}$. Then

$$\omega = \widetilde{\omega} + \mathrm{O}(\epsilon), \qquad \epsilon \to (0^+, \dots, 0^+). \tag{29}$$

Let $Q_l = \sqrt{c_l^* - c_1} \prod_{i \neq l} |c_i^* - c_l^*| > 0$. Let $\{P_1(s), \dots, P_n(s)\}$ be the basis of $\mathbb{R}_{n-1}[s]$ univocally determined by the interpolating conditions

$$P_l(c_j^*) = \begin{cases} Q_l & \text{if } j = l, \\ 0 & \text{otherwise.} \end{cases}$$

That is, $P_l(s) = (-1)^{l-1} \sqrt{c_l^* - c_1} \prod_{i \neq l} (c_i^* - s)$. Using Lemma 21, we get the estimates

$$\mathcal{K}_0[P_l(s)] = \int_0^{c_1} \left(\frac{(-1)^{l-1} \sqrt{c_l^* - c_1}}{(c_l^* - s)\sqrt{c_1 - s}} + \mathrm{O}(\epsilon) \right) \mathrm{d}s = 2(-1)^{l-1} \operatorname{atan} \sqrt{\frac{c_1}{c_l^* - c_1}} + \mathrm{O}(\epsilon),$$

$\mathcal{K}_l[P_l(s)] = \pi + \mathrm{O}(\epsilon)$, and $\mathcal{K}_j[P_l(s)] = \mathrm{O}(\epsilon)$ for $j \neq 0, l$. Thus, the $n \times n$ linear system

$$\mathcal{K}[P_l(s); \omega] = 0 \quad \text{for } l = 1, \dots, n$$

is $\mathrm{O}(\epsilon)$-close to the nonsingular decoupled linear system

$$2(-1)^{l-1} \left(\operatorname{atan} \sqrt{\frac{c_1}{c_l^* - c_1}} - \pi\widetilde{\omega}_l \right) = 0 \quad \text{for } l = 1, \dots, n,$$

whose unique solution is given by $\tan^2 \pi\widetilde{\omega}_l = c_1/(c_l^* - c_1)$, and so, by $\sin^2 \pi\widetilde{\omega}_l = c_1/c_l^*$. Hence, the asymptotic formula (29) follows from the first item in Lemma 25.

A.8. Total singular collapse: $c_{2l-1}, c_{2l} \to c_l^*$ for all $l = 1, \dots, n$. Let us study the case of n simultaneous singular collapses. Let $\widehat{\omega} = (1/2, \dots, 1/2) \in \mathbb{R}^n$, $\epsilon = (\epsilon_1, \dots, \epsilon_n) \in \mathbb{R}^n_+$, and $\delta = (\delta_1, \dots, \delta_n) \in \mathbb{R}^n_+$, where $\epsilon_l = c_{2l} - c_{2l-1}$ and $\delta_l = |\log \epsilon_l|^{-1}$. Then

$$\omega = \widehat{\omega} + \mathrm{O}(\delta), \qquad \epsilon \to (0^+, \dots, 0^+). \tag{30}$$

Remark 14. By repeatedly applying the result on simple singular collapses, we see that

$$\lim_{\epsilon_n \to 0^+} \left(\cdots \lim_{\epsilon_2 \to 0^+} \left(\lim_{\epsilon_1 \to 0^+} \omega \right) \right) = \widehat{\omega}.$$

In fact, these repeated limits can be taken in any order. Nevertheless, this result is weaker than estimate (30), so we need a formal proof of the estimate.

We consider the constants $Q_l = \sqrt{c_{2n+1} - c_l^*} \prod_{i \neq l} |c_i^* - c_l^*|$. Let $\{P_1(s), \dots, P_n(s)\}$ be the basis of $\mathbb{R}_{n-1}[s]$ univocally determined by

$$P_l(c_j^*) = \begin{cases} Q_l & \text{if } j = l, \\ 0 & \text{otherwise.} \end{cases}$$

Now, using Corollary 24, we get that there exist some constants $\zeta_{jl} \in \mathbb{R}$ such that

$$\mathcal{K}_j[\delta_l P_l(s)] = \delta_l \mathcal{K}_j[P_l(s)] = \begin{cases} 1 + \zeta_{ll}\delta_l + \mathrm{o}(\delta) & \text{if } j = l, \\ \zeta_{jl}\delta_l + \mathrm{o}(\delta) & \text{otherwise,} \end{cases}$$

where $0 \le j \le n$ and $1 \le l \le n$. Therefore, the $n \times n$ linear system

$$\delta_l \mathcal{K}[P_l(s); \omega] = 0 \quad \text{for } l = 1, \dots, n$$

is $\mathrm{O}(\delta)$-close to the nonsingular linear system

$$\begin{cases} 1 - 2\widehat{\omega}_1 = 0, \\ 2(-1)^{l-1}(\widehat{\omega}_{l-1} - \widehat{\omega}_l) = 0 \quad \text{for } l = 2, \dots, n, \end{cases}$$

whose unique solution is $\widehat{\omega} = (1/2, \dots, 1/2)$. Thus, the asymptotic formula (30) follows from Lemma 25(i).

Remark 15. The vectorial estimate (30) can be refined in several ways. For instance, one can get the componentwise estimates $\omega_1 = 1/2 + \mathrm{O}(\delta_1)$ and $\omega_l = \omega_{l-1} + \mathrm{O}(\delta_l)$ for $l > 1$. In particular, $\omega_l = 1/2 + \mathrm{O}(\delta_1, \dots, \delta_l)$. Even more, there exists a $n \times n$ constant *lower triangular* matrix $\mathbf{L}$ such that

$$\omega = \widehat{\omega} + \mathbf{L}\delta + \mathrm{o}(\delta), \qquad \epsilon \to (0^+, \dots, 0^+).$$

We omit the proof, since we do not need this result and the computations are cumbersome.

A.9. Asymptotic behavior of the function ν_{x}. The function $\nu_{\mathrm{x}} : (0, c) \cup (c, b) \to \mathbb{R}$ verifies that $I(\lambda) + J(\lambda)\rho_{\mathrm{x}}(\lambda) + K(\lambda)\nu_{\mathrm{x}}(\lambda) = 0$, where the coefficients $I, J, K : (0, c) \cup (c, b) \to \mathbb{R}$ were given by

$$I(\lambda) = \int_0^{\underline{m}} \frac{\mathrm{d}s}{(a-s)\sqrt{T_{\mathrm{x}}(s)}}, \quad J(\lambda) = -2\int_{\overline{m}}^{b} \frac{\mathrm{d}s}{(a-s)\sqrt{T_{\mathrm{x}}(s)}}, \quad K(\lambda) = \frac{2\pi}{\sqrt{-T_{\mathrm{x}}(a)}},$$

with $T_{\mathrm{x}}(s) = (\lambda - s)(c - s)(b - s)$, $\underline{m} = \min(\lambda, c)$, and $\overline{m} = \max(\lambda, c)$. Here, $\rho_{\mathrm{x}}(\lambda) = \rho(\lambda; c, b)$ is the rotation function of the ellipse obtained by sectioning the ellipsoid Q with the coordinate plane $\{x = 0\}$. The asymptotic properties of rotation functions of billiards inside ellipses were established in Proposition 10.

First, let us consider the case $\epsilon := \lambda \to 0^+$. Using Lemmas 20 and 22, we get the following:

- $I(\epsilon) = I_0\epsilon^{1/2} + \mathrm{O}(\epsilon^{3/2})$, where $I_0 = 2a^{-1}(bc)^{-1/2}$;
- $J(\epsilon) = J_0 + \mathrm{O}(\epsilon)$, where $J_0 = -2\int_c^b (a-s)^{-1}(s(s-c)(b-s))^{-1/2}\mathrm{d}s$;
- $K(\epsilon) = K_0 + \mathrm{O}(\epsilon)$, where $K_0 = 2\pi(a(a-c)(a-b))^{-1/2}$;
- $\rho_{\mathrm{x}}(\epsilon) = \kappa^G\epsilon^{1/2} + \mathrm{O}(\epsilon^{3/2})$, where $\kappa^G = \kappa^G(b, c)$ can be found in Proposition 10;
- $\nu_{\mathrm{x}}(\epsilon) = -(I_0 + J_0\kappa^G)K_0^{-1}\epsilon^{1/2} + \mathrm{O}(\epsilon^{3/2}) = \mathrm{O}(\epsilon^{1/2})$. It is possible to check that $(I_0 + J_0\kappa^G)K_0^{-1} < 0$, but we do not need it.

Next, let us consider the case $\epsilon := b - \lambda \to 0^+$. We begin by computing the integral

$$r(\beta, \alpha) := \int_0^{\beta} \frac{\mathrm{d}s}{(\alpha - s)\sqrt{\beta - s}} = \frac{2}{\sqrt{\alpha - \beta}} \operatorname{atan}\sqrt{\beta/(\alpha - \beta)}$$

for any $0 < \beta < \alpha$. Then it is immediate to check that

$$\int_0^\beta \frac{\mathrm{d}s}{(\alpha_+ - s)(\alpha_- - s)\sqrt{\beta - s}} = \frac{r(\beta, \alpha_-) - r(\beta, \alpha_+)}{\alpha_+ - \alpha_-}$$

for any $0 < \beta < \alpha_- < \alpha_+$. We also need the formula $r(\beta, \alpha) = 2\pi(\alpha - \beta)^{-1/2}\varrho(\beta, \alpha)$, where $\varrho(\beta, \alpha) := \lim_{\gamma \to \alpha^-} \rho(\gamma; \beta, \alpha)$ is one of the limits of the rotation number described in Proposition 10. Using these formulae, jointly with Lemmas 20 and 21, we see the following:

- $I(b - \epsilon) = I_* + \mathrm{O}(\epsilon)$, $I_* = 2\pi(a - b)^{-1}\left((b - c)^{-1/2}\varrho(c, b) - (a - c)^{-1/2}\varrho(c, a)\right)$;
- $J(b - \epsilon) = J_* + \mathrm{O}(\epsilon)$, where $J_* = -2\pi(a - b)^{-1}(b - c)^{-1/2}$;
- $K(b - \epsilon) = K_* + \mathrm{O}(\epsilon)$, where $K_* = 2\pi(a - b)^{-1}(a - c)^{-1/2}$;
- $\rho_{\mathrm{x}}(b - \epsilon) = \rho_{\mathrm{x}}(b) + \mathrm{O}(\epsilon) = \rho(b; c, b) + \mathrm{O}(\epsilon) = \varrho(c, b) + \mathrm{O}(\epsilon)$; and
- $\nu_{\mathrm{x}}(b - \epsilon) = \varrho(c, a) + \mathrm{O}(\epsilon) = \rho(a; c, a) + \mathrm{O}(\epsilon) = \rho_{\mathrm{y}}(a) + \mathrm{O}(\epsilon)$.

The estimates in the limit $\epsilon := \overline{m} - \underline{m} \to 0^+$, which means $\lambda \to c$, are

- $I(c \pm \epsilon) = -(a - c)^{-1}(b - c)^{-1/2}\log\epsilon + \mu + \mathrm{O}(\epsilon\log\epsilon)$, where μ is a constant that can be exactly computed from Lemma 23;
- $J(c \pm \epsilon) = -(a - c)^{-1}(b - c)^{-1/2}\log\epsilon + \eta + \mathrm{O}(\epsilon\log\epsilon)$, where η is a constant that can be exactly computed from Lemma 23;
- $K(c \pm \epsilon) = 2\pi(a - c)^{-1}(a - b)^{-1/2} + \mathrm{O}(\epsilon)$;
- $\rho_{\mathrm{x}}(c \pm \epsilon) = 1/2 + \kappa^S \log^{-1}\epsilon + \mathrm{O}(\log^{-2}\epsilon)$, where $\kappa^S = \kappa^S(c, b) = \operatorname{acosh}(b/c)^{1/2}$ according to Proposition 10; and
- $\nu_{\mathrm{x}}(c \pm \epsilon) = (a - b)^{1/2}\left((a - c)(\eta - \mu) - 2(b - c)^{-1/2}\kappa^S\right)/2\pi + \mathrm{O}(\log^{-1}\epsilon)$. After some tedious but simple computations, one gets that $\nu_{\mathrm{x}}(c) = \varrho(b, a) = \rho(a; b, a) = \rho_{\mathrm{z}}(a)$.

A.10. Asymptotic behavior of the function ν_{y}. The function $\nu_{\mathrm{y}} : (b, a) \to \mathbb{R}$ verifies that $I(\lambda) + J(\lambda)\rho_{\mathrm{y}}(\lambda) + K(\lambda)\nu_{\mathrm{y}}(\lambda) = 0$, where the coefficients $I, J, K : (b, a) \to \mathbb{R}$ were given by

$$I(\lambda) = \int_0^c \frac{\mathrm{d}s}{(b - s)\sqrt{T_{\mathrm{y}}(s)}}, \quad J(\lambda) = 2\int_\lambda^a \frac{\mathrm{d}s}{(s - b)\sqrt{T_{\mathrm{y}}(s)}}, \quad K(\lambda) = -\frac{2\pi}{\sqrt{-T_{\mathrm{y}}(b)}},$$

with $T_{\mathrm{y}}(s) = (c - s)(\lambda - s)(a - s)$. Here, $\rho_{\mathrm{y}}(\lambda) = \rho(\lambda; c, a)$ is the rotation function of the ellipse obtained by sectioning the ellipsoid Q with the coordinate plane $\{y = 0\}$.

We begin with the limit $\epsilon := \lambda - b \to 0^+$. Using Lemmas 20 and 23, we see the following:

- $I(b + \epsilon) = I_0 + \mathrm{O}(\epsilon)$, where $I_0 = \int_0^c (b - s)^{-3/2}(c - s)^{-1/2}(a - s)^{-1/2}\mathrm{d}s$;
- $J(b + \epsilon) = 2\pi(a - b)^{-1/2}(b - c)^{-1/2}\epsilon^{-1/2} + \mathrm{O}(1)$;
- $K(b + \epsilon) = -2\pi(a - b)^{-1/2}(b - c)^{-1/2}\epsilon^{-1/2}$;
- $\rho_{\mathrm{y}}(b + \epsilon) = \rho_{\mathrm{y}}(b) + \mathrm{O}(\epsilon)$; and
- $\nu_{\mathrm{y}}(b + \epsilon) = \rho_{\mathrm{z}}(c) + \mathrm{O}(\epsilon^{1/2})$, since $\rho_{\mathrm{y}}(b) = \rho(b; c, a) = \rho(c; b, a) = \rho_{\mathrm{z}}(c)$.

Next, let us consider the case $\epsilon := a - \lambda \to 0^+$, which is similar to the limit $\lim_{\epsilon \to 0^+} \nu_{\mathrm{x}}(b - \epsilon)$ studied in the previous subsection, so we need the same simple integrals. Using them, jointly with Lemmas 20 and 21, we get the following:

- $I(a - \epsilon) = I_* + \mathrm{O}(\epsilon)$, $I_* = 2\pi(a - b)^{-1}\left((b - c)^{-1/2}\varrho(c, b) - (a - c)^{-1/2}\varrho(c, a)\right)$;
- $J(a - \epsilon) = J_* + \mathrm{O}(\epsilon)$, where $J_* = 2\pi(a - b)^{-1}(a - c)^{-1/2}$;
- $K(a - \epsilon) = K_* + \mathrm{O}(\epsilon)$, where $K_* = -2\pi(a - b)^{-1}(b - c)^{-1/2}$;
- $\rho_{\mathrm{y}}(a - \epsilon) = \varrho(c, a) + \mathrm{O}(\epsilon)$; and
- $\nu_{\mathrm{y}}(a - \epsilon) = \varrho(c, b) + \mathrm{O}(\epsilon) = \rho(b; c, b) + \mathrm{O}(\epsilon) = \rho_{\mathrm{x}}(b) + \mathrm{O}(\epsilon)$.

A.11. Asymptotic behavior of the function ν_z. The function $\nu_z : (0,c) \cup (c,b) \to \mathbb{R}$ verifies that

$$I(\lambda) + J(\lambda)\rho_z(\underline{m}) + K(\lambda)\nu_z(\lambda) = 0, \tag{31}$$

where the coefficients $I, J, K : (0,c) \cup (c,b) \to \mathbb{R}$ were given by

$$I(\lambda) = \int_0^{\underline{m}} \frac{\mathrm{d}s}{(\overline{m}-s)\sqrt{T_z(s)}}, \quad J(\lambda) = 2\int_b^a \frac{\mathrm{d}s}{(s-\overline{m})\sqrt{T_z(s)}}, \quad K(\lambda) = -\frac{2\pi}{\sqrt{-T_z(\overline{m})}},$$

with $T_z(s) = (\underline{m}-s)(b-s)(a-s)$, $\underline{m} = \min(\lambda, c)$, and $\overline{m} = \max(\lambda, c)$. Here, $\rho_z(\lambda) = \rho(\lambda; b, a)$ is the rotation function of the ellipse obtained by sectioning the ellipsoid Q with the coordinate plane $\{z = 0\}$.

Let us consider the case $\epsilon := \lambda \to 0^+$. Using Lemmas 20 and 22, we see the following:

- $I(\epsilon) = I_0\epsilon^{1/2} + \mathrm{O}(\epsilon^{3/2})$, where $I_0 = 2c^{-1}(ab)^{-1/2}$;
- $J(\epsilon) = J_0 + \mathrm{O}(\epsilon)$, where $J_0 = 2\int_b^a (s-c)^{-1}(s(s-b)(a-s))^{-1/2}\mathrm{d}s$;
- $K(\epsilon) = K_0 + \mathrm{O}(\epsilon)$, where $K_0 = -2\pi(c(b-c)(a-c))^{-1/2}$;
- $\rho_z(\underline{m}) = \rho_z(\min(\epsilon, c)) = \rho_z(\epsilon) = \kappa^G\epsilon^{1/2} + \mathrm{O}(\epsilon^{3/2})$, where the constant $\kappa^G = \kappa^G(b,a)$ can be found in Proposition 10; and
- $\nu_z(\epsilon) = -(I_0 + J_0\kappa^G)K_0^{-1}\epsilon^{1/2} + \mathrm{O}(\epsilon^{3/2}) = \mathrm{O}(\epsilon^{1/2})$, with $(I_0 + J_0\kappa^G)K_0^{-1} < 0$.

The estimates in the limit $\epsilon := \overline{m} - \underline{m} \to 0^+$, which means $\lambda \to c$, are

- $I(c \pm \epsilon) = \pi(a-c)^{-1/2}(b-c)^{-1/2}\epsilon^{-1/2} + \mathrm{O}(1)$ (see Lemma 23);
- $J(c \pm \epsilon) = \mathrm{O}(1)$;
- $K(c \pm \epsilon) = -2\pi(a-c)^{-1/2}(b-c)^{-1/2}\epsilon^{-1/2} + \mathrm{O}(\epsilon^{1/2})$;
- $\rho_z(\underline{m}) = \rho_z(\min(c \pm \epsilon, c)) = \rho_z(c) + \mathrm{O}(\epsilon)$, since $\rho_z(\lambda)$ is analytic at $\lambda = c$; and
- $\nu_z(c \pm \epsilon) = 1/2 + \mathrm{O}(\epsilon^{1/2})$.

Next, we consider the case $\epsilon := b - \lambda \to 0^+$. Using Lemmas 20 and 21, we get

- $I(b-\epsilon) = \mathrm{O}(1)$;
- $J(b-\epsilon) = J_*\epsilon^{-1/2} + \mathrm{O}(1)$, where $J_* = 2\pi(a-b)^{-1/2}(b-c)^{-1/2}$;
- $K(b-\epsilon) = K_*\epsilon^{-1/2} + \mathrm{O}(\epsilon^{1/2})$, where $K_* = -2\pi(a-b)^{-1/2}(b-c)^{-1/2}$;
- $\rho_z(\underline{m}) = \rho_z(\min(b-\epsilon, c)) = \rho_z(c)$; and
- $\nu_z(b-\epsilon) = \rho_z(c) + \mathrm{O}(\epsilon^{1/2})$.

Appendix B. A topological lemma. We recall that the complement of any Jordan curve X in the plane $\mathbb{R}^2$ has two distinct connected components. One of them is bounded and simply connected (the interior, denoted by $\mathcal{B}_X$), and the other is unbounded (the exterior, denoted by $\mathcal{U}_X$).

Lemma 27. *Let X and Y be two Jordan curves of $\mathbb{R}^2$. If $f : \mathcal{B}_X \to \mathbb{R}^2$ is a bounded local homeomorphism that has a continuous extension to the boundary X such that $f(X) \subset Y$, then $f : \mathcal{B}_X \to \mathcal{B}_Y$ is a global homeomorphism.*

Proof. We note that $W = f(\mathcal{B}_X)$ is a nonempty open bounded subset of $\mathbb{R}^2$ such that

$$\partial W = \partial f(\mathcal{B}_X) \subset f(\partial\mathcal{B}_X) = f(X) \subset Y.$$

Next, we are going to prove that $W = \mathcal{B}_Y$. Using that $\partial W \subset Y$, we deduce that the intersection $W \cap \mathcal{B}_Y$ (resp., $W \cap \mathcal{U}_Y$) is open and closed in $\mathcal{B}_Y$ (resp., in $\mathcal{U}_Y$), so it is either the

empty set or the whole interior (resp., exterior). Therefore, we deduce that 1. $W \cap \mathcal{U}_Y = \emptyset$, because W is bounded; 2. $W \cap Y = \emptyset$, because W is open; and 3. $W \cap \mathcal{B}_Y = \mathcal{B}_Y$, because W is open and nonempty. That is, $f(\mathcal{B}_X) = W = \mathcal{B}_Y$.

Once we know that $f : \mathcal{B}_X \to \mathcal{B}_Y$ is a surjective local homeomorphism, we deduce from covering space theory that it is a global homeomorphism. It suffices to realize that $\mathcal{B}_X$ is connected and open and $\mathcal{B}_Y$ is simply connected. ■

In particular, if $f : \mathcal{B}_X \to \mathbb{R}^2$ is smooth or analytic, then its inverse is also smooth or analytic. This means that if f is a local diffeomorphism whose image is bounded and that has a continuous extension to the boundary X such that $f(X) \subset Y$, then $f : \mathcal{B}_X \to \mathcal{B}_Y$ is a global diffeomorphism.

Acknowledgments. We acknowledge useful conversations with Jaume Amorós, Yuri Fedorov, Àlex Haro, and Carles Simó.

REFERENCES

[1] S. Abenda and Yu. Fedorov, *Closed geodesics and billiards on quadrics related to elliptic KdV solutions*, Lett. Math. Phys., 76 (2006), pp. 111–134.
[2] M. Audin, *Courbes algébriques et sistèmes intégrables: Géodésiques des quadriques*, Expo. Math., 12 (1994), pp. 193–226.
[3] M. Audin, *Topologie des systèmes de Moser en dimension quatre*, in The Floer Memorial Volume, Progr. Math. 133, Birkhäuser-Verlag, Basel, 1995, pp. 109–122.
[4] I. Babenko, *Periodic trajectories in three-dimensional Birkhoff billiards*, Math. USSR-Sb., 71 (1992), pp. 1–13.
[5] C. Batut, K. Belabas, D. Bernardi, H. Cohen, and M. Olivier, *Users Guide to PARI/GP*, available online from http://www.parigp-home.de/.
[6] M. Berger, *Seules les quadriques admettent des caustiques*, Bull. Soc. Math. France, 123 (1995), pp. 107–116.
[7] G. D. Birkhoff, *Dynamical Systems*, Amer. Math. Soc. Colloq. Publ. IX, AMS, Providence, RI, 1966.
[8] S. Bolotin, A. Delshams, and R. Ramírez-Ros, *Persistence of homoclinic orbits for billiards and twist maps*, Nonlinearity, 17 (2004), pp. 1153–1177.
[9] A. Cayley, *Developments on the porism of the in-and-circumscribed polygon*, Philos. Mag., 7 (1854), pp. 339–345.
[10] P. S. Casas and R. Ramírez-Ros, *Classification of Symmetric Periodic Billiard Trajectories inside Ellipsoids*, manuscript.
[11] S.-J. Chang and R. Friedberg, *Elliptical billiards and Poncelet's theorem*, J. Math. Phys., 29 (1988), pp. 1537–1550.
[12] S.-J. Chang, B. Crespi, and K.-J. Shi, *Elliptical billiard systems and the full Poncelet's theorem in n dimensions*, J. Math. Phys., 34 (1993), pp. 2242–2256.
[13] S.-J. Chang, B. Crespi, and K.-J. Shi, *Elliptical billiards and hyperelliptic functions*, J. Math. Phys., 34 (1993), pp. 2257–2289.
[14] A. Delshams, Yu. Fedorov, and R. Ramírez-Ros, *Homoclinic billiard orbits inside symmetrically perturbed ellipsoids*, Nonlinearity, 14 (2001), pp. 1141–1195.
[15] V. Dragović and M. Radnović, *Conditions of Cayley's type for ellipsoidal billiard*, J. Math. Phys., 39 (1998), pp. 355–362.
[16] V. Dragović and M. Radnović, *On periodical trajectories of the billiard systems within an ellipsoid in $\mathbb{R}^d$ and generalized Cayley's condition*, J. Math. Phys., 39 (1998), pp. 5866–5869.
[17] V. Dragović and M. Radnović, *Geometry of integrable billiards and pencils of quadrics*, J. Math. Pures Appl., 85 (2006), pp. 758–790.
[18] V. Dragović and M. Radnović, *Hyperelliptic Jacobians as billiard algebra of pencils of quadrics: Beyond Poncelet porisms*, Adv. Math., 219 (2008), pp. 1577–1607.

[19] V. Dragović and M. Radnović, *Bifurcations of Liouville tori in elliptical billiards*, Regul. Chaotic Dyn., 14 (2009), pp. 479–494.
[20] M. Farber, *Topology of billiard problems* (I), Duke Math. J., 115 (2002), pp. 559–585.
[21] M. Farber, *Topology of billiard problems* (II), Duke Math. J., 115 (2002), pp. 587–621.
[22] M. Farber and S. Tabachnikov, *Periodic trajectories in* 3*-dimensional convex billiards*, Manuscripta Math., 108 (2002), pp. 431–437.
[23] Yu. Fedorov, *Classical integrable systems and billiards related to generalized Jacobians*, Acta Appl. Math., 55 (1999), pp. 251–301.
[24] Yu. Fedorov, *Algebraic closed geodesics on a triaxial ellipsoid*, Regul. Chaotic Dyn., 10 (2005), pp. 463–485.
[25] G. H. Golub and C. F. Van Loan, *Matrix Computations*, Johns Hopkins University Press, Baltimore, MD, 1996.
[26] P. A. Griffiths, *Introduction to Algebraic Curves*, Transl. Math. Monogr. 76, AMS, Providence, RI, 1989.
[27] A. Katok and B. Hasselblatt, *Introduction to the Modern Theory of Dynamical Systems*, Cambridge University Press, Cambridge, UK, 1995.
[28] O. Knill, *On nonconvex caustics of convex billiards*, Elem. Math., 53 (1998), pp. 89–106.
[29] V. V. Kozlov and D. V. Treshchëv, *Billiards: A Genetic Introduction to the Dynamics of Systems with Impacts*, Transl. Math. Monogr. 89, AMS, Providence, RI, 1991.
[30] H. Knörrer, *Geodesics on the ellipsoid*, Inv. Math., 59 (1980), pp. 119–143.
[31] H. Knörrer, *Singular fibres of the momentum mapping for integrable Hamiltonian systems*, J. Math., 355 (1985), pp. 67–107.
[32] R. Kolodziej, *The rotation number of some transformation related to billiards in an ellipse*, Studia Math., 81 (1985), pp. 293–302.
[33] J. K. Moser, *Geometry of quadrics and spectral theory*, in The Chern Symposium, Springer-Verlag, New York, Berlin, 1980, pp. 147–188.
[34] J. V. Poncelet, *Traité des Propriétés Projectives des Figures*, Bachelier, Paris, 1822.
[35] G. Popov and P. Topalov, *On the integral geometry of Liouville billiard tables*, Comm. Math. Phys., to appear.
[36] E. Previato, *Poncelet theorem in space*, Proc. Amer. Math. Soc., 127 (1999), pp. 2547–2556.
[37] R. Ramírez-Ros, *Break-up of resonant invariant curves in billiards and dual billiards associated to perturbed circular tables*, Phys. D, 214 (2006), pp. 78–87.
[38] R. Ramírez-Ros, *On Cayley-Like Conditions for Elliptic Billiards*, manuscript.
[39] H. Rüssmann, *Invariant tori in non-degenerate nearly integrable Hamiltonian systems*, Regul. Chaotic Dyn., 6 (2001), pp. 119–204.
[40] S. Tabachnikov, *Billiards*, Panoramas et Syntheses 1, Société Mathématique de France, Paris, 1995.
[41] M. B. Tabanov, *Separatrices splitting for Birkhoffs billiard in symmetric convex domain, closed to an ellipse*, Chaos, 4 (1994), pp. 595–606.
[42] A. P. Veselov, *Integrable systems with discrete time and difference operators*, Funct. Anal. Appl., 22 (1988), pp. 83–93.
[43] A. P. Veselov, *Integrable maps*, Russian Math. Surveys, 46 (1991), pp. 3–45.
[44] H. Waalkens, J. Wiersig, and H. R. Dullin, *The elliptic quantum billiard*, Ann. Phys. (NY), 260 (1997), pp. 50–90.
[45] H. Waalkens, J. Wiersig, and H. R. Dullin, *Triaxial ellipsoidal quantum billiards*, Ann. Phys. (NY), 276 (1999), pp. 64–110.
[46] H. Waalkens and H. R. Dullin, *Quantum monodromy in prolate ellipsoidal billiards*, Ann. Phys. (NY), 295 (2002), pp. 81–112.